University College of London

Department of Mathematics

Doctoral Thesis

Numerical computation of resonances and pseudospectra in acoustic scattering

Author:
Jacopo Lanzoni

Supervisor:
Dr. Timo Betcke

Thesis submitted in fulfilment of the requirements for the degree of Doctor of Philosophy

January 2016

Declaration of Authorship

I, Jacopo Lanzoni, confirm that the work presented in this thesis, titled 'Numerical computation of resonances and pseudospectra in acoustic scattering', is my own. Where information has been derived from other sources, I confirm that this has been indicated in the thesis.

Signed: _____

Date: _____

UNIVERSITY COLLEGE OF LONDON

Abstract

Faculty of Mathematical and Physical Sciences

Department of Mathematics

Doctor of Philosophy

Numerical computation of resonances and pseudospectra in acoustic scattering

by Jacopo Lanzoni

Acoustic scattering is a well-known physical phenomenon which arises in a wide range of fields: when acoustic waves propagating in a medium impinge on a localised non-uniformity, such as a density fluctuation or an external obstacle, their trajectories are deviated and scattered waves are generated. A key role in scattering theory is played by resonances; these are particular scatterer-dependent non-physical 'complex' frequencies at which acoustic scattering exhibits exceptional behaviour. The study of acoustic resonances for a particular scatterer provides an insight in the behaviour that the acoustic scattering assumes at the near physical 'real' frequencies, and it is a fundamental step in many applications. Yet, the numerical computation of resonances and pseudospectra - a mathematical tool which can be used to study the influence of resonances on physical frequencies - remains very expensive. With the present Thesis we want to address this particular problem, by proposing numerical algorithms based on the Boundary Element Method (BEM) for computing resonances and pseudospectra and by analysing their efficiency and performance. Finally, we apply such algorithms to half a dozen of physically relevant scatterer, inspired from different fields where acoustic scattering plays a relevant role.

Contents

List of Figures

List of Tables

Introduction

The mathematical description of acoustic scattering is based on the Helmholtz equation $-\Delta u - k^2 u = f$, a linear second-order partial differential equation. The Helmholtz equation describes time-harmonic solutions $\mathcal{U}(x,t) = e^{-i\omega t}u(x)$ of the wave equation $c^2\Delta\mathcal{U} - \partial_{tt}\mathcal{U} = \mathcal{F}$. The wave-number $k = \omega/c$ is defined as the ratio between the angular frequency ω and the speed c of sound in the medium. The formal setting of acoustic scattering problems on unbounded domain is completed by the Sommerfeld radiation condition $\partial_{|x|}u - iku = o(|x|^{-(d-1)/2})$, $x \in \mathbb{R}^d$, which translates in mathematical terms the fact that no waves are reflected from infinity. Apart from few special cases, e.g. scattering by a sphere, the analytical solution of boundary value problems involving the Helmholtz equation is not possible. Yet, a class of mathematical techniques called integral equation methods, which has a long tradition in scattering theory [Colton and Kress, 2013a], can be used to investigate such boundary value problems. The fortune of these methods lies in the fact that problems defined on unbounded three-dimensional domains can be rewritten as boundary integral equations defined on bounded two-dimensional surfaces, i.e. the border of the scatterers. This is a major advantage from a numerical point of view. Moreover, integral equation methods can be used to study resonances and to prove many important results about them. Resonances are non-physical complex values of the wave-number k for which there exist solutions to the homogenous Helmholtz equation which are 'outgoing'. Although they represent complex frequencies, resonances may influence physically-relevant 'real' wave-numbers k and the behaviour of boundary integral operators for such frequencies. In particular, a great deal of attention has been paid recently to the influence of resonances on the normality properties of the boundary integral operators arising from the application of integral

equation methods [Betcke and Spence, 2011].

As 'complex' resonances influence close 'real' wave-numbers, an instrument is needed to quantify and investigate such influence. The ideal tool to describe such a situation turns out to be pseudospectra. Pseudospectra, which are defined as the level set of the resolvent norm of an operator, arise from the investigation of standard eigenvalue problems $Ax = \lambda x$, when one is interested in the behaviour of the operator norm $\|(A-\lambda I)^{-1}\|$. In the last decades pseudospectra have been used to investigate many different problems: from the analysis of differential operators to the investigation of transient effects and non-normal dynamics, from fluid mechanics to matrix iterations, from the numerical solution of differential equations to random matrices. An extensive review about linear pseudospectra can be found in the popular monograph by Trefethen and Embree [2005]. In recent years the notion of pseudospectra has been extended to the case of operator pencils and analytic families, where one considers resolvent norms of the form $\|(A-\lambda B)^{-1}\|$, $B \neq I$, and $\|A(\lambda)^{-1}\|$ respectively. Although a smaller number of results is available for these extended definition of pseudospectra, we are mainly interested in these two extended definition of pseudospectra because they are the ones which can be applied to the numerical discretisation of acoustic scattering problems using FEM and BEM respectively.

Finite and Boundary Element Methods (BEM and FEM respectively) are the main techniques used for the numerical solution of acoustic scattering problems. The application of FEM to acoustic scattering problem faces the issue of truncating the unbounded domain and introducing an appropriate artificial boundary condition to reduce the reflection of incident waves. The standard choice for such a treatment has become the application of a Perfectly Matched Layer (PML) [Berenger, 1994, 1996], where the wave is absorbed and decays exponentially. The PML can be viewed as a complex change of variables [Collino and Monk, 1998], and it turns out to be the translation in acoustic scattering of the well-known technique called complex scalings in spectral theory [Hislop and Sigal, 1996, Reed and Simon, 1980]. Once applied the PML, the unbounded domain can be truncated and FEM applied to get a linear system of the form $(K - k^2M)x = f$, and pseudospectra can be computed by approximating the

norm $\|(K-k^2M)^{-1}\|$ on some complex grid of nodes k. Even for simple one- and two-dimensional examples, such matrices can be very large and the calculation of pseudospectra becomes computationally expensive. The efficient computation of pseudospectra has been widely studied [Kressner and Vandereycken, 2014, Lui, 1997, Reddy et al., 1993, Toh and Trefethen, 1996], and many approximation tricks are available. In particular, when an eigenvalue decomposition is affordable, much may be gained by projecting matrix discretisations onto the subspace spanned by certain eigenvectors. In the present thesis we extend to the case of matrix pencils an eigenspace projection method proposed by Reddy et al. [1993] for standard pseudospectra and we apply it to a simple two-dimensional case.

An alternative strategy to the application of PML and FEM is represented by BEM. In a BEM, one solves not the original differential operators but an equivalent boundary integral equation. As a result, BEM inherits the advantages deriving from integral equation methods: three-dimensional problems defined on unbounded domains become two-dimensional problems on bounded surfaces [Sauter and Schwab, 2011]. The resulting discretisation matrices are much smaller than their FEM analogues; yet, BEM require the numerical integration of complex function and the possible regularisation of those equations which are not always uniquely solvable due to interior eigenvalues. The computation of pseudospectra of the boundary integral operators arising in acoustic scattering is quite new, and the development of efficient algorithms for these particular pseudospectra is at the initial stage. This is where the present thesis has its main target: we develop here efficient algorithms tailored for the computation of resonances and pseudospectra of boundary integral operators arising in scattering theory. These new tools will provide further insight about the spectral properties of the integral operators and their relation with the nearest resonances, which is a topic of recent and strong interest in the scientific community [Betcke and Spence, 2011, Betcke et al., 2011, 2014, Chandler-Wilde et al., 2009].

In particular, a great deal of attention is paid to the class of trapping domains, which can 'trap' acoustic waves and exhibit scattering poles close to the real axis. The properties of boundary integral operators defined on trapping obstacles are known to be rather peculiar, and many recent papers compare their behaviour

with that of acoustic scattering by convex scatterers [Betcke and Spence, 2011, Chandler-Wilde et al., 2009]. The study of acoustic scattering by this class of obstacles is not new. Indeed, the investigation of the link between the geometry of a generic obstacle K and the scattering poles has a long tradition. The well-known Lax-Phillips conjecture [Lax and Phillips, 1967], according to which trapping obstacles admit an infinite sequence of eigenvalues asymptotically close to the real axis, has attracted large attention for a long time, and many authors have tried either to prove it or to show counterexamples [Ikawa, 1983, 1985, Stefanov, 1999, Stefanov and Vodev, 1995, 1996, Tang and Zworski, 1998]. In this context, the computation of resonances and pseudospectra of boundary integral operators on trapping obstacles is particularly relevant, and it represents another target of the present work.

The structure of the thesis is as follows. In Chapter 1 we introduce the setting of acoustic scattering theory, describing the mathematical representation of acoustic waves by the Helmholtz equation, the wave-number and the Sommerfeld radiation condition; moreover, we describe the special case of scattering by a sphere and its analytical solution; finally, we introduce integral equation methods and acoustic resonances. In Chapter 2 we define the notion of pseudospectra, both in its original linear version and in its matrix pencil and analytic extensions, and we highlight the link with the notion of normality of an operator. In Chapter 3 we give an overview of the computation of resonances and pseudospectra by the use of PML and FEM; moreover, we discuss some numerical techniques necessary for an efficient computation of those quantities (weighted norms and subspace projection methods); the Chapter finishes with the numerical computation of pseudospectra and resonances for a two-dimensional rectangular cavity. Chapter 4 is devoted to BEM and to the computation of resonances and pseudospectra of boundary integral operators: we start by providing further information about boundary integral equations and by introducing Galerkin BEM; after this, we describe two numerical algorithm to compute pseudospectra: the first one uses direct methods, while the second adopts iterative techniques and advanced approximation strategies as the Fast Multiple Methods (FMM) and the Adaptive Cross Approximation (ACA); we then perform a detailed analysis of the efficiency and the performance of the two algorithms, and investigate further some

parameters involved in the computation. Chapter 4 represents the most original part of the thesis and contains the main scientific contributions of this work. In Chapter 5 we discuss the notion of 'trapping' obstacle and we apply the algorithms developed in the previous Chapter to half a dozen different scatterers, some of which have already appeared in the scientific literature, while others are inspired from the different fields where acoustic scattering plays a relevant role. In Chapter 6 we draw a few conclusion from the work contained in the present thesis, and we highlight some topics for possible future researches.

Chapter 1

Acoustic Scattering

Scattering theory investigates the propagation of different types of waves (e.g., acoustic, electromagnetic, elastic, quantum waves) in one medium, or more media. In acoustic scattering theory the attention is focused on acoustic waves, which propagate by successive compression and decompression of the medium and travel with the sound speed typical of that medium. The mathematical description of acoustic scattering is based on the Helmholtz equation, a linear second-order partial differential equation.

The structure of the present Chapter is the following: In Section 1.1 we review the mathematical description of acoustic scattering by the Helmholtz equation, while in Section 1.2 we discuss the Sommerfeld radiation condition, a particular boundary condition 'at infinity' that needs to be required in boundary value problems on unbounded domains. In Section 1.3 we describe the special case of scattering by a sphere, where solutions can be written in term of special functions, while in Section 1.4 we introduce integral equation methods for the treatment of boundary value problems in acoustic scattering. Finally, in Section 1.5, we discuss the notion of scattering poles, or resonances.

1.1 Acoustic Waves

Acoustic waves are oscillations of a fluid pressure and their governing equations are obtained from the fundamental laws of fluid dynamics. In this Section, we

review the origin of the Helmholtz equation (Subsection 1.1.1) and we discuss the fundamental role of the parameter k, known as the wave number (Subsection 1.1.2).

1.1.1 The Helmholtz Equation

Vibrations in a fluid are represented by the pressure $\mathcal{U}(x,t)$ and the density $\rho(x,t)$ that depend on the position $x \in \mathbb{R}^3$ and the time $t \in \mathbb{R}$. Pressure and density are related by the law $\mathcal{U} = c^2\rho$, where the constant c is the speed of sound in the vibrating medium. By considering the mass conservation law $\partial_t\rho + \nabla\cdot(\rho V) = 0$, where V is the particle velocity, and the equation of motion $\rho\partial_t V = -\nabla\mathcal{U}$, we obtain

$$\Delta\mathcal{U} - \frac{1}{c^2}\frac{\partial^2\mathcal{U}}{\partial t^2} = 0, \tag{1.1}$$

where $\Delta = \nabla\cdot\nabla$ is the Laplacian in the spatial coordinates. If we assume for $\mathcal{U}(x,t)$ a time-harmonic dependence of the form $u(x)e^{-i\omega t}$, where ω is the angular frequency, from (1.1) we obtain the Helmholtz equation

$$\Delta u + k^2 u = 0, \tag{1.2}$$

with $k^2 = \omega^2/c^2$. The parameter k is known as the wave number and has a fundamental role in acoustic scattering theory.

1.1.2 The Wave Number

Strictly speaking, the relation $k^2 = \omega^2/c^2$ is not enough to define the wave number k as we need a branch cut for the square root. We choose the sign of k in (1.2) such that

$$\text{Im } k \geq 0. \tag{1.3}$$

In order to show the role of the parameter k, let us consider the one-dimensional version of the Helmholtz equation (1.2), i.e. the ordinary differential equation $u'' + k^2 u = 0$. The general solution

$$u(x) = Ae^{ikx} + Be^{-ikx} \tag{1.4}$$

is periodic, with period

$$\lambda = \frac{2\pi}{k}.$$

The parameter λ is the wavelength of u, while k measures the number of waves in a 2π-length and is expressed as m^{-1}.

From (1.4) we can write the solution of the corresponding one-dimensional wave equation as

$$\mathcal{U}(x,t) = Ae^{i(kx-\omega t)} + Be^{-i(kx+\omega t)}. \tag{1.5}$$

Such a solution depends on k and ω only by the quantities $kx \pm \omega t$. Computing the phase velocities $v_{\text{ph}} := dx/dt$, we see that the first term on the right-hand side of (1.5) represents an outgoing wave (traveling to the right with $v_{\text{ph}} = c$), while the second term is an incoming wave (traveling to the left with $v_{\text{ph}} = -c$). In this one-dimensional case, the incoming wave can be eliminated by applying at any point $x = x_0$ a boundary condition of the form

$$c\,\frac{\partial \mathcal{U}(x,t)}{\partial x}\bigg|_{x=x_0} + \frac{\partial \mathcal{U}(x,t)}{\partial t}\bigg|_{x=x_0} = 0, \tag{1.6}$$

which acts as a nonreflecting boundary condition. Nonreflecting boundary conditions as (1.6) have great importance in the treatment of boundary value problems on unbounded domains in any dimensions.

1.2 The Sommerfeld Radiation Condition

When we consider acoustic scattering in an unbounded domain, we suppose that no waves are reflected from infinity. The mathematical expression for this far-field condition is obtained by using integral equation methods. As we treat such methods in more depth in Section 1.4, we introduce here only what is necessary in order to obtain the Sommerfeld conditions.

We set here the notation which we use throughout the whole thesis. Let $K \subset \mathbb{R}^3$ be a compact obstacle, $\Gamma := \partial K$ its Lipschitz boundary and $\Omega := \mathbb{R}^3 \setminus K$ be the unbounded connected complement. If one considers the Helmholtz equation (1.2) on Ω, it is often required that $u(x)$ satisfies the Green's representation

formula

$$u(x) = \int_\Gamma \left(u(y) \frac{\partial E_k(x,y)}{\partial n(y)} - E_k(x,y) \frac{\partial u}{\partial n}(y) \right) \, dS(y), \quad x \in \Omega, \tag{1.7}$$

where

$$E_k(x,y) = \frac{e^{ik|x-y|}}{4\pi|x-y|} \tag{1.8}$$

is the fundamental solution of the Helmholtz equation in three dimensions [Ihlenburg, 1998].

Remark 1.1. In two dimensions, the fundamental solution of the Helmholtz equation is

$$E_k(x,y) = \frac{iH_0^{(1)}(k|x-y|)}{4}, \tag{1.9}$$

where $H_0^{(1)}(x)$ is the Hankel function of the first kind of order 0, which has a logarithmic singularity at the origin [NIST, Formula 10.7.2].

If we truncate Ω at an artificial boundary $S_R := \{|x| = R\}$ with $R \gg 1$ such that $K \subset\subset B_R := \{|x| \leq R\}$, then $\partial\Omega = \Gamma \cup S_R$ and we require

$$\int_{S_R} \left(u(y) \frac{\partial E_k(x,y)}{\partial n(y)} - E_k(x,y) \frac{\partial u}{\partial n}(y) \right) \, dS(y) \to 0 \quad \text{as } R \to \infty. \tag{1.10}$$

If we assume that for $x \in \Omega$ the sphere S_R is sufficiently large such that $R = |x-y| \approx |y|$, and $\partial/\partial n(y) \approx \partial/\partial R$, then the integral in (1.10) becomes

$$\int_{S_R} \left(iku - \frac{u}{R} - \frac{du}{dR} \right) \frac{e^{ikR}}{4\pi R} \, dS.$$

As $dS \sim R^2$, waves are then absorbed at infinity if

$$u = O(R^{-1}) \quad \text{and} \quad iku - \frac{\partial u}{\partial R} = o(R^{-1}), \quad \text{as } R \to \infty. \tag{1.11}$$

Equations (1.11) are known as the Sommerfeld conditions. Assuming $k \in \mathbb{R}_+$, the Sommerfeld conditions select solutions of exterior Helmholtz problems that are outgoing (in Section 1.3 we see that for complex wave numbers $k \in \mathbb{C}$ outgoing solutions are defined in a different way).

It is otherwise possible to show [Colton and Kress, 2013a] that the Sommerfeld radiation conditions (1.11) imply the Green representation formula (1.7). Indeed, the two expressions are equivalent for wave numbers $k > 0$ [McLean, 2000, Nedelec, 2001].

Similar considerations lead to the Sommerfeld conditions in $\mathbb{R}^n$ for any n

$$u = O(R^{-(n-1)/2}), \quad iku - \frac{du}{dR} = o(R^{-(n-1)/2}), \quad \text{as } R \to \infty. \tag{1.12}$$

The Sommerfeld conditions (1.11) (and (1.12)) consist of two equations, one for the far-field decay of the solution and one for that of its normal derivative. It can be shown [Colton and Kress, 2013b] that any function that satisfies both the Helmholtz equation (1.2) and the Sommerfeld radiation condition (i.e., the second equation in the Sommerfeld conditions (1.12)) automatically satisfies the Sommerfeld decay condition (i.e. the first equation). Therefore, only the Sommerfeld radiation condition is usually assumed.

1.3 The Special Case of Scattering by a Sphere

In general, solutions to boundary value problems involving the Helmholtz equation (1.2) can not be written in closed form. Yet, in the special case when the obstacle K is a sphere, we can use spherical coordinates and separation of variables to write solutions in terms of special functions. In this Section we consider different boundary value problems for this special case (Subsection 1.3.1), and we take into consideration the corresponding eigenvalue problems (Subsection 1.3.2).

1.3.1 Spherical Solutions

Let K be the compact ball B_R, let Γ be its boundary and let $\Omega := \mathbb{R}^3 \setminus K$ be its unbounded complement. We look for a function $u = u(x, y, z)$ satisfying

$$\begin{aligned} \Delta u + k^2 u &= 0, \quad \text{in } \Omega, && (1.13) \\ \frac{\partial u}{\partial r} - iku &= o(r^{-1}), \quad \text{as } r \to \infty, && (1.14) \end{aligned}$$

where $r = \sqrt{x^2 + y^2 + z^2}$ is the radial coordinate.

In the spherical coordinates r, $\theta := \arccos(z/\sqrt{x^2 + y^2 + z^2})$ and $\phi := \arctan(y/x)$, the Laplacian is written as

$$\Delta u(r, \theta, \phi) = \frac{1}{r^2}\left[\frac{\partial}{\partial r}\left(r^2 \frac{\partial u}{\partial r}\right) + \frac{1}{\sin\theta}\frac{\partial}{\partial \theta}\left(\sin\theta \frac{\partial u}{\partial \theta}\right) + \frac{1}{\sin^2\theta}\frac{\partial^2 u}{\partial \phi^2}\right].$$

Looking for a solution of the form $u = \Re(r)\Theta(\theta)\Phi(\phi)$, we obtain from (1.13) the three separated ordinary differential equations

$$\begin{aligned} \frac{d}{dr}\left(r^2 \frac{d\Re(r)}{dr}\right) + (k^2 r^2 - \lambda)\Re(r) &= 0, && (1.15) \\ \sin\theta \frac{d}{d\theta}\left(\sin\theta \frac{d\Theta(\theta)}{d\theta}\right) + (\lambda \sin^2\theta - \nu)\Theta(\theta) &= 0, && (1.16) \\ \frac{d^2\Phi(\phi)}{d\phi^2} + \nu\Phi(\phi) &= 0, && (1.17) \end{aligned}$$

where λ and ν are constants. The function $\Re$ is defined on the unbounded domain $[R, \infty)$ and has to satisfy the Sommerfeld radiation condition, while Θ and Φ are defined on $[-\pi/2, \pi/2)$ and $[0, 2\pi)$, respectively.

Equation (1.17) is solved by the 2π-periodic real functions $\sin(m\phi)$ and $\cos(m\phi)$ where $m \in \mathbb{N} \cup \{0\}$ and $\nu = m^2$.

Equation (1.16) can be transformed via $t := \cos\theta$ in

$$(1 - t^2)\frac{d^2\Theta}{dt^2} - 2t\frac{d\Theta}{dt} + \left(\lambda - \frac{m^2}{1 - t^2}\right)\Theta(t) = 0.$$

For $\lambda = n(n + 1)$, with $n \in \mathbb{N} \cup \{0\}$, this is Legendre's equation and admits as solutions the Legendre functions $\Theta_{mn}(\theta) = P_n^m(\cos\theta)$ with P_n^m Legendre polynomials and $0 \le m \le n$ [NIST, Formula 14.2.2].

Finally, for $\lambda = n(n+1)$, equation (1.15) is Bessel's equation. This is a second order differential equation and has got two linearly independent solutions. Depending on circumstances, different formulations of these solutions are convenient. Typically, in exterior problems one writes them as

$$\begin{aligned} h_n^{(1)}(kr) &= i^{-(n+1)}\frac{e^{ikr}}{kr}\sum_{j=0}^{n}\frac{(n+j)!}{j!(n-j)!}(-2ikr)^{-j}, \\ h_n^{(2)}(kr) &= i^{n+1}\frac{e^{-ikr}}{kr}\sum_{j=0}^{n}\frac{(n+j)!}{j!(n-j)!}(2ikr)^{-j}, \end{aligned}$$

called spherical Hankel functions [NIST, Formulas 10.49.6/7], which in the far field have the following asymptotic behaviour:

$$h_n^{(1)}(kr) \sim i^{-(n+1)}\frac{e^{ikr}}{kr}, \quad h_n^{(2)}(kr) \sim i^{n+1}\frac{e^{-ikr}}{kr}, \tag{1.18}$$

[NIST, Formula 10.52.4]. As the spherical Hankel functions of the second kind represent incoming waves, they are eliminated by the Sommerfeld radiation condition (1.14) for $k \in \mathbb{R}_+$. For general $k \in \mathbb{C}$, we call a function u outgoing if

$$u \sim C_n\frac{e^{ikr}}{kr} \quad \text{as } r \to \infty$$

for some constant C_n depending on the dimension n [Nedelec, 2001].

Collecting results, we can write the solution u as

$$u(r,\theta,\phi) = \sum_{n=0}^{\infty}\sum_{m=-n}^{n} h_n^{(1)}(kr)P_n^m(\cos\theta)(A_{nm}\cos(m\phi) + B_{nm}\sin(m\phi)), \tag{1.19}$$

where the series converges absolutely and uniformly in every compact subset [Colton and Kress, 2013a]. Using the de Moivre identity, (1.19) can be more compactly written as

$$u(r,\theta,\phi) = \sum_{n=0}^{\infty}\sum_{m=-n}^{n} c_{mn}y_{mn}(\theta,\phi)h_n^{(1)}(kr), \tag{1.20}$$

where c_{mn} are complex coefficients and $y_{mn}(\theta,\phi) := P_n^{|m|}(\cos\theta)e^{im\phi}$, with $-n \leq m \leq n$, are the spherical harmonics.

Only minimal changes are necessary if one wants to solve the Helmholtz equation

(1.2) in the interior domain $\mathring{K}$. Spherical coordinates lead to the same equations (1.15), (1.16) and (1.17) as in the case of the exterior problem, but now the domain of the function $\Re = \Re(r)$ is $[0, R)$ instead of (R, ∞). We write now the two linearly independent solutions of Bessel's equation (1.15) as the spherical Bessel functions

$$\begin{aligned} j_n(x) &= (-x)^n \left(\frac{1}{x}\frac{d}{dx}\right)^n \frac{\sin x}{x}, \\ y_n(x) &= -(-x)^n \left(\frac{1}{x}\frac{d}{dx}\right)^n \frac{\cos x}{x}. \end{aligned}$$

As the spherical Bessel functions of the second kind y_n have a singularity at the origin, which belongs now to the domain of the function $\Re$, solutions of the Helmholtz equation inside the sphere B_R take the form

$$u(r, \theta, \phi) = \sum_{n=0}^{\infty} j_n(kr) \sum_{m=-n}^{n} c_{mn} y_{mn}(\theta, \phi). \tag{1.21}$$

1.3.2 Solution of Eigenvalue Problems

Let again K be the sphere B_R, and Γ and Ω as before. We consider now the Exterior Dirichlet (ED) boundary value problem consisting of the Helmholtz equation (1.13), the Sommerfeld radiation condition (1.14) and the homogeneous Dirichlet boundary condition

$$u = 0 \quad \text{on } \Gamma. \tag{1.22}$$

The wave numbers k, with Im $k \geq 0$, such that there exists a non-zero solution u satisfying the ED problem are said to be the ED eigenvalues on the sphere B_R, with the non-zero solution u being the corresponding ED eigenfunctions. Expansion (1.20) can be used to look for such eigenvalues from the boundary condition (1.22), leading to the equality

$$0 = u(r, \theta, \phi)|_{r=R} = \sum_{n=0}^{\infty} h_n^{(1)}(kR) \sum_{m=-n}^{n} c_{nm} y_{nm}(\theta, \phi).$$

Yet, zeros of $h_n^{(1)}(z)$ lay on the lower complex half-plane [NIST, Subsection 10.21(ix)] and violate (1.3). So, there exists no ED eigenvalue for the sphere. Indeed, it is possible to prove that there exists no ED eigenvalue for any compact obstacle K [Taylor, 1996].

An analogue procedure for the Exterior Neumann (EN) boundary value problem (1.13), (1.14) and

$$\frac{\partial u}{\partial n} = 0 \quad \text{on } \Gamma \tag{1.23}$$

leads to the equality

$$0 = \frac{\partial u}{\partial r}(r, \theta, \phi)\big|_{r=R} = \sum_{n=0}^{\infty} k h_n^{(1)'}(kR) \sum_{m=-n}^{n} c_{nm} y_{nm}(\theta, \phi).$$

Again, zeros of $h_n^{(1)'}(z)$ lay on the lower complex half-plane [NIST, Subsection 10.21(ix)], so there exists no EN eigenvalue. As before, such a conclusion can be proved to hold for any compact obstacle K [Taylor, 1996].

When we pass from exterior unbounded domain to interior bounded domain, the situation differs. The Interior Dirichlet (ID) boundary value problem consisting of the Helmholtz equation

$$-\Delta u - k^2 u = 0 \quad \text{in } \mathring{K}, \tag{1.24}$$

and the homogeneous Dirichlet boundary condition (1.22) admits eigenvalues $k_{ID} \in \mathbb{R}$. Using expansion (1.21), the boundary value (1.22) becomes

$$0 = u(R, \theta, \phi) = \sum_{n=0}^{\infty} j_n(k_{ID} R) \sum_{m=-n}^{n} c_{mn} y_{mn}(\theta, \phi)$$

and ID eigenvalues are defined by zeros of the spherical Bessel function of first kind $j_n(z)$. Such roots can be computed numerically by many available libraries (e.g., Python `scipy.special`). Table 1.1 shows the first ten ID eigenvalues for the unit sphere B_1.

Similarly, the Interior Neumann (IN) boundary value problem (1.24)-(1.23) admits eigenvalues $k_{IN} \in \mathbb{R}$. Using again expansion (1.21), the homogeneous Neumann boundary condition (1.22) becomes

$$0 = \frac{\partial u}{\partial n}(R, \theta, \phi) = \sum_{n=0}^{\infty} k_{IN} j_n'(k_{IN} R) \sum_{m=-n}^{n} c_{mn} y_{mn}(\theta, \phi)$$

and IN eigenvalues remain defined by zeros of the derivative $j_n'(z)$ of the spherical Bessel function of first kind (plus $k_{IN} = 0$). Numerical libraries help again in the computation, and Table 1.1 shows also the first ten IN eigenvalues for the unit sphere B_1.

TABLE 1.1: The first ten ID and IN eigenvalues for the unit sphere B_1.

k_{ID}	k_{IN}
3.14159	2.08158
4.49341	3.34209
5.76346	4.49341
6.28319	4.51401
6.98793	5.64670
7.72525	5.94037
8.18256	6.75646
9.09501	7.28993
9.35581	7.72525
9.42478	8.58375

1.4 Integral Equation Methods

In the present Section we introduce the operators arising in the application of boundary integral equation methods to boundary problems involving the Helmholtz equation. This approach is particularly useful in scattering theory as it reduces a problem defined over an unbounded domain to one defined on a bounded domain of lower dimension, that is, the boundary of the scattering obstacle. This fact is crucial from the point of view of numerical analysis.

We already mentioned Green's representation formula (1.7) in Section 1.2. If u is a solution of the Helmholtz equation in Ω (1.13) satisfying the Sommerfeld

radiation condition (1.14), then the exterior Green's representation formula reads

$$u(x) = \mathcal{D}_k\phi(x) - \mathcal{S}_k\sigma(x) \quad \text{for } x \in \Omega, \tag{1.25}$$

where $\mathcal{S}_k$ and $\mathcal{D}_k$ are, respectively, the Helmholtz single- and double-layer potentials

$$\mathcal{S}_k\sigma(x) := \int_\Gamma E_k(x,y)\sigma(y)ds(y) \qquad \text{for } x \in \Omega, \tag{1.26}$$

$$\mathcal{D}_k\phi(x) := \int_\Gamma \frac{\partial E_k(x,y)}{\partial n(y)}\phi(y)ds(y) \qquad \text{for } x \in \Omega, \tag{1.27}$$

and $E_k(x,y)$ is the Helmholtz fundamental solution (1.8) (or (1.9) in $\mathbb{R}^2$) [Colton and Kress, 2013a]. In Green's representation formula (1.25), for the solution of the Helmholtz equation (1.13) in Ω, the densities σ and ϕ are, respectively, the Neumann and Dirichlet data $u|_\Gamma^{\text{ext}}$ and $\partial_n u|_\Gamma^{\text{ext}}$, which are not known simultaneously.

It is possible to obtain boundary integral equations based on Green's representation formula (1.25) by taking the limit as $\Omega \ni x \to x_0 \in \Gamma$ [Kleinman and Roach, 1973]. The idea is to derive from the formula itself a boundary relation in order to find the missing boundary value; once this is found, the representation formula is used to compute the solution u. First of all, we fix the following notation for the usual boundary integral operators

$$\begin{aligned}
\mathcal{S}_k\sigma(x) &\overset{\Omega\ni x\to x_0\in\Gamma}{\longrightarrow} \int_\Gamma E_k(x_0,y)\sigma(y)ds(y) =: \mathcal{V}_k\sigma(x_0),\\
\mathcal{D}_k\phi(x) &\overset{\Omega\ni x\to x_0\in\Gamma}{\longrightarrow} \int_\Gamma \frac{\partial E_k(x_0,y)}{\partial n(y)}\phi(y)ds(y) + \frac{1}{2}\phi(x_0) =: \left(\mathcal{K}_k + \frac{1}{2}\mathcal{I}\right)\phi(x_0),\\
\frac{\partial \mathcal{S}_k\sigma}{\partial n}(x) &\overset{\Omega\ni x\to x_0\in\Gamma}{\longrightarrow} \int_\Gamma \frac{\partial E_k(x_0,y)}{\partial n(x_0)}\sigma(y)ds(y) - \frac{1}{2}\sigma(x_0) =: \left(\mathcal{K}_k' - \frac{1}{2}\mathcal{I}\right)\sigma(x_0),\\
\frac{\partial \mathcal{D}_k\phi}{\partial n}(x) &\overset{\Omega\ni x\to x_0\in\Gamma}{\longrightarrow} \int_\Gamma \frac{\partial^2 E_k(x_0,y)}{\partial n(x_0)\partial n(y)}\phi(y)ds(y) =: -\mathcal{T}_k\phi(x_0),
\end{aligned}$$

[Costabel, 1988]. The operators $\mathcal{V}_k$, $\mathcal{K}_k$, $\mathcal{K}_k'$ and $\mathcal{T}_k$ are respectively known as the Helmholtz single-layer, double-layer, adjoint double-layer and hypersingular boundary integral operators. Taking the boundary limit of Green's representation formula (1.25) and of its normal derivative leads to the following boundary

integral equations:

$$\begin{bmatrix} \mathcal{K}_k + \frac{1}{2}\mathcal{I} & -\mathcal{V}_k \\ -\mathcal{T}_k & -\left(\mathcal{K}_k' - \frac{1}{2}\mathcal{I}\right) \end{bmatrix} \begin{bmatrix} \phi \\ \sigma \end{bmatrix} = \begin{bmatrix} \phi \\ \sigma \end{bmatrix}, \tag{1.28}$$

where the operator matrix appearing in (1.28) is known as the Calderón projector for the exterior domain Ω. ED boundary value problems can then be solved by one of the boundary integral equations

$$\mathcal{V}_k\sigma = f_1, \tag{1.29}$$

$$\left(\mathcal{K}_k' + \frac{1}{2}\mathcal{I}\right)\sigma = f_2, \tag{1.30}$$

with $f_1 := (\mathcal{K}_k - 0.5\mathcal{I})\phi$ and $f_2 := -\mathcal{T}_k\phi$, while EN boundary value problems can be solved by one of the boundary integral equations

$$\left(\mathcal{K}_k - \frac{1}{2}\mathcal{I}\right)\phi = g_1, \tag{1.31}$$

$$\mathcal{T}_k\phi = g_2, \tag{1.32}$$

with $g_1 = \mathcal{V}_k\sigma$ and $g_2 = -(\mathcal{K}_k' + 0.5\mathcal{I})\sigma$.

The same approach can be applied to interior problems, where we have

$$\mathcal{D}_k\phi(x) \overset{\mathring{K}\ni x\to x_0\in\Gamma}{\longrightarrow} \int_\Gamma \frac{\partial E_k(x_0,y)}{\partial n(y)}\phi(y)ds(y) - \frac{1}{2}\phi(x_0) =: \left(\mathcal{K}_k - \frac{1}{2}\mathcal{I}\right)\phi(x_0),$$

$$\frac{\partial \mathcal{S}_k\sigma}{\partial n}(x) \overset{\mathring{K}\ni x\to x_0\in\Gamma}{\longrightarrow} \int_\Gamma \frac{\partial E_k(x_0,y)}{\partial n(x_0)}\sigma(y)ds(y) + \frac{1}{2}\sigma(x_0) =: \left(\mathcal{K}_k' + \frac{1}{2}\mathcal{I}\right)\sigma(x_0).$$

Taking the boundary limit of interior Green's representation formula

$$u(x) = \mathcal{S}_k\sigma(x) - \mathcal{D}_k\phi(x) \quad \text{for } x \in \mathring{K},$$

where now $\phi = u|_\Gamma^{\text{int}}$ and $\sigma = \partial_n u|_\Gamma^{\text{int}}$, and the boundary limit of its normal derivative, we get the following boundary integral equations:

$$\begin{bmatrix} -\left(\mathcal{K}_k - \frac{1}{2}\mathcal{I}\right) & \mathcal{V}_k \\ \mathcal{T}_k & \mathcal{K}_k' + \frac{1}{2}\mathcal{I} \end{bmatrix} \begin{bmatrix} \phi \\ \sigma \end{bmatrix} = \begin{bmatrix} \phi \\ \sigma \end{bmatrix}, \tag{1.33}$$

where the operator matrix appearing in (1.33) is the Calderón projector for the

interior domain K. We then obtain that ID problems can then be solved by one of the boundary integral

$$\mathcal{V}_k\sigma = f_3, \tag{1.34}$$

$$\left(\mathcal{K}'_k - \frac{1}{2}\mathcal{I}\right)\sigma = f_4, \tag{1.35}$$

with $f_3 := (\mathcal{K}_k + 0.5\mathcal{I})\phi$ and $f_4 := -\mathcal{T}_k\phi$, while IN problems can be solved by one of the boundary integral

$$\left(\mathcal{K}_k + \frac{1}{2}\mathcal{I}\right)\phi = g_3, \tag{1.36}$$

$$\mathcal{T}_k\phi = g_4, \tag{1.37}$$

with $g_3 = \mathcal{V}_k\sigma$ and $g_4 = -(\mathcal{K}'_k - 0.5\mathcal{I})\sigma$.

Another strategy to obtain boundary integral equations consists in seeking the solution in the form of an appropriate surface potential [Kupradse, 1934a,b, 1956]. For example, the double-layer potential $u(x) = \mathcal{D}_k f(x)$, for $x \in \Omega$, is a solution of the ED problem if f solves the boundary integral equation

$$\left(\mathcal{K}_k + \frac{1}{2}\mathcal{I}\right) f = \phi \tag{1.38}$$

where ϕ is the known boundary value $u|_\Gamma^{\text{ext}}$. Analogously, $u(x) = \mathcal{D}_k f(x)$, for $x \in \mathring{K}$, is a solution of the ID problem if f solves

$$\left(\mathcal{K}_k - \frac{1}{2}\mathcal{I}\right) f = \phi, \tag{1.39}$$

for $\phi = u|_\Gamma^{\text{int}}$.

Turning to the single-layer potential, $u(x) = \mathcal{S}_k g(x)$, for $x \in \Omega$, is a solution of the EN problem if g is a solution of the boundary integral equation

$$\left(\mathcal{K}'_k - \frac{1}{2}\mathcal{I}\right) g = \sigma \tag{1.40}$$

where σ is the known boundary value $\partial_n u|_\Gamma^{\text{ext}}$. Analogously, $u(x) = \mathcal{S}_k g(x)$, for $x \in \mathring{K}$, is a solution of the IN problem if g solves

$$\left(\mathcal{K}_k' + \frac{1}{2}\mathcal{I}\right) g = \sigma, \tag{1.41}$$

for $\sigma = \partial_n u|_\Gamma^{\text{int}}$.

What we end up with is a network of coupled boundary integral equations, which we summarise in Table 1.2. In the rest of the thesis we will come back to them frequently and we will explore in more details the effect of such couplings.

TABLE 1.2: Boundary integral equations.

	Direct formulation		Indirect formulation	
	BIEs	BVP sol.	BIEs	BVP sol.
ED	$\mathcal{V}_k\sigma = f_1,\ (\mathcal{K}_k' + 0.5\mathcal{I})\sigma = f_2$	$u = \mathcal{D}_k\phi - \mathcal{S}_k\sigma$	$(\mathcal{K}_k + 0.5\mathcal{I})f = \phi$	$u = \mathcal{D}_k f$
EN	$(\mathcal{K}_k - 0.5\mathcal{I})\phi = g_2,\ \mathcal{T}_k\phi = g_2$		$(\mathcal{K}_k' - 0.5\mathcal{I})g = \sigma$	$u = \mathcal{S}_k g$
ID	$\mathcal{V}_k\sigma = f_3,\ (\mathcal{K}_k' - 0.5\mathcal{I})\sigma = f_4$	$u = \mathcal{S}_k\sigma - \mathcal{D}_k\phi$	$(\mathcal{K}_k - 0.5\mathcal{I})f = \phi$	$u = \mathcal{D}_k f$
IN	$(\mathcal{K}_k + 0.5\mathcal{I})\phi = g_3,\ \mathcal{T}_k\phi = g_4$		$(\mathcal{K}_k' + 0.5\mathcal{I})g = \sigma$	$u = \mathcal{S}_k g$

1.5 Resonances

Boundary integral operators are also an effective tool to study resonances. In this Section we define acoustic resonances for the Helmholtz equation (1.13) and we give some characterization using boundary integral operators.

Given the ED boundary value problem consisting of the Helmholtz equation in Ω (1.13), the Sommerfeld radiation condition (1.14) and a Dirichlet boundary condition

$$u = \phi \quad \text{on } \Gamma,$$

it is possible to prove the existence and uniqueness of the solution u for each wave number k with Im $k \geq 0$ [Taylor, 1996]. We can then formally define the solution operator

$$u = \mathcal{B}_k\phi, \tag{1.42}$$

for each $\phi \in L^2(\Gamma)$. Such an operator is uniquely defined and analytic in the open upper half-plane $\{\text{Im } k > 0\}$, strongly continuous in the closed upper half-plane $\{\text{Im } k \geq 0\}$ and can be analytically continued into the whole complex plane except for certain poles lying into the lower half-plane $\{\text{Im } k < 0\}$ [Taylor, 1996]. These poles are known as scattering poles, or resonances, and provide fundamental objects for study in scattering theory.

Remark 1.2. In the two-dimensional case, as the Helmholtz fundamental solution (1.9) has a logarithmic singularity at $k = 0$, we need to exclude a branch cut from zero to infinity in the k-domain.

When k is a resonance, there exists a non-zero $u \in C^\infty(\Omega)$ satisfying the Helmholtz equation on Ω (1.13) and the homogeneous Dirichlet boundary condition (1.22) of the form

$$u = \mathcal{D}_k g_1 + \mathcal{S}_k g_2 \quad \text{on } \Omega,$$

for some $g_j \in L^2(\Gamma)$ [Taylor, 1996]. Equivalently, there exists a solution of the Helmholtz equation on Ω (1.13) which is zero on Γ and outgoing, i.e.,

$$u(x) \sim C\frac{e^{ikr}}{r} \quad \text{as } r \to \infty.$$

However, outgoing solutions with the wave number k having negative imaginary part grow exponentially towards infinity and they do not satisfy the Sommerfeld radiation condition (1.14).

Various relations can be proved to exist between the solution operator $\mathcal{B}_k$ and the boundary integral operators $\mathcal{V}_k$, $\mathcal{K}_k$, $\mathcal{K}'_k$ and $\mathcal{T}_k$ defined in the previous Section. E.g.,

$$\begin{aligned} \mathcal{B}_k &= \mathcal{D}_k \left(\mathcal{K}_k + \frac{1}{2}\mathcal{I}\right)^{-1}, \\ &= \mathcal{S}_k \mathcal{V}_k^{-1} \end{aligned}$$

[Taylor, 1996], and resonances can be detected investigating the generalised spectra of the boundary integral operators $\mathcal{K}_k + 0.5\mathcal{I}$ or $\mathcal{V}_k$.

As the single-layer boundary integral operator $\mathcal{V}_k$ and its adjoint $\mathcal{V}_k^H$ are related by

$$\mathcal{V}_k^H = \mathcal{V}_{-\bar{k}},$$

it is possible to prove that the set of resonances is symmetric about the imaginary axis [Taylor, 1996].

So far we have not established if there actually are resonances. In fact there are infinitely many resonances on the negative imaginary axis, for any nonempty smooth obstacle K as the boundary integral operator $\mathcal{V}_k^{-1}$ has an infinite number of poles on the negative imaginary axis, each of which is a resonance [Taylor, 1996].

Although they represent complex frequencies, resonances may intervene in a wide number of physically relevant 'real' problems. Recently, for example, it has been shown [Betcke and Spence, 2011] that, when resonances are close to the real line (e.g., in the case of trapping domains), coercivity of the modified boundary integral operator $\mathcal{A}_{k,\eta} := \mathcal{K}_k' + 0.5\mathcal{I} - i\eta\mathcal{V}_k$ (with $\eta \in \mathbb{R} \setminus \{0\}$) for a certain real wave-number k strongly depends on the distance to the nearest resonance. In general, resonances are important in the study of numerical stability. When a generic Helmholtz equation $(-\Delta - k^2)u = f$ is well-posed and we are interested in the stability of the solution $u = (-\Delta - k^2)^{-1} f$, we need to study the behavior of the resolvent norm $\|(-\Delta - k^2)^{-1}\|$ which depends on the distance to the nearest resonance. The perfect tool to perform such investigations are pseudospectra, to which we devote the next Chapter.

Chapter 2

Pseudospectra and Non-Normality

Although the solution operator $\mathcal{B}_k$ defined in (1.42) has a bounded inverse for all real wave numbers k, it can nevertheless exhibit large norm-growth on the real axis in the neighbourhood of complex resonances. Pseudospectra are the ideal instrument to describe the influence of these complex values on the norm for real wave numbers.

The present Chapter reviews pseudospectra, an important tool for studying non-normality of linear operators. For a normal operator $\mathcal{A}$, $\|(\mathcal{A}-k)^{-1}\|$ is large only when k is close to an eigenvalue of $\mathcal{A}$. The importance of pseudospectra arises for non-normal operators, for which $\|(\mathcal{A}-k)^{-1}\|$ may be large even when k is far from the spectrum of $\mathcal{A}$ (Section 2.1). As we distinguish standard eigenvalue problems, e.g., $(\mathcal{A}-k)u=0$, from pencil eigenvalue problems, e.g., $(\mathcal{A}_0+k\mathcal{A}_1)u=0$, and from non-linear eigenvalue problems, e.g., $\mathcal{A}_k u=0$ with $(\mathcal{A}_k)_k$ being a k-analytic family of operators, in the same way the notion of standard pseudospectra can be generalized to operator pencils (Section 2.2) and to analytic families (Section 2.3), which arise respectively in the Finite Element (Chapter 3) and Boundary Element (Chapter 4) formulation of acoustic scattering problems.

2.1 Linear Operators and Pseudospectra

In this Section, we introduce the functional setting where we work throughout the whole thesis and we introduce pseudospectra of linear operators. There are many books providing a general introduction to functional analysis (we used mainly the popular book by Reed and Simon [1980]), while for an extensive treatment of pseudospectra of matrices and linear operators and a detailed bibliography on the subject up to 2005, the reader is invited to refer to Trefethen and Embree [2005].

Given a measurable set $G \subset \mathbb{R}^3$, let $\mathcal{H} = L^2(G)$ be the separable Hilbert space of the complex square-integrable functions on G. Pseudospectra can be defined for more general spaces, but in this thesis we work exclusively in the L^2 context (with G being the unbounded domain $\Omega = \mathbb{R}^3 \setminus K$ in FEM and the boundary $\Gamma = \partial K$ in BEM) and we prefer avoiding further generalization. Then, throughout the thesis, the inner product will be

$$(f, g)_{\mathcal{H}} := \int_G \overline{f(x)} g(x) \, dx \quad \forall \, f, g \in \mathcal{H}, \tag{2.1}$$

and the norm will be defined by

$$\|f\|_{\mathcal{H}} := \sqrt{(f, f)_{\mathcal{H}}} = \left(\int_G |f(x)|^2 dx \right)^{\frac{1}{2}} \quad \forall \, f \in \mathcal{H}.$$

We also restrict our attention to operators $\mathcal{A}$ mapping $\mathcal{H}$ into itself, for which the induced operator norm is

$$\|\mathcal{A}\|_{\mathcal{H}} := \sup_{f \in \mathcal{H}} \frac{\|\mathcal{A} f\|_{\mathcal{H}}}{\|f\|_{\mathcal{H}}},$$

and we denote by $B(\mathcal{H})$ the set of bounded operators on $\mathcal{H}$. Given a linear operator $\mathcal{A}$ on $\mathcal{H}$, a bounded inverse is an operators $\mathcal{A}^{-1} \in B(\mathcal{H})$ such that $\mathcal{A}^{-1}\mathcal{A} = \mathcal{A}\mathcal{A}^{-1} = \mathcal{I}$, where $\mathcal{I}$ is the identity operator. If $k \in \mathbb{C}$, the resolvent of $\mathcal{A}$ of k is the operator $(\mathcal{A} - k)^{-1} \in B(\mathcal{H})$, if it exists. The resolvent set $\rho(\mathcal{A})$ is the set of numbers $k \in \mathbb{C}$ for which $(\mathcal{A} - k)^{-1}$ exists as a bounded operator. The resolvent set $\rho(\mathcal{A})$ is open, the resolvent operator $(\mathcal{A} - k)^{-1}$ is

analytic on $\rho(\mathcal{A})$ and the resolvent norm $\|(\mathcal{A}-k)^{-1}\|$ is an unbounded continuous subharmonic function on $\rho(\mathcal{A})$ satisfying the maximum principle for $k \in \rho(A)$ [Hille and Phillips, 1957].

The spectrum of $\mathcal{A}$ is the complement of the resolvent set in the complex plane, i.e. $\sigma(\mathcal{A}) = \mathbb{C} \setminus \rho(\mathcal{A})$. Since $\rho(A)$ is open, $\sigma(A)$ is closed. If $\mathcal{A}u = ku$ for some nonzero $u \in \mathcal{H}$, then k is an eigenvalue of $\mathcal{A}$ and u is the corresponding eigenvector. The spectrum $\sigma(\mathcal{A})$ contains all the eigenvalues of A, but it may be bigger than this. As $\|(\mathcal{A}-k)^{-1}\|_{\mathcal{H}}$ approaches ∞ as k approaches the spectrum, we adopt the notational convention to write $\|(\mathcal{A}-k)^{-1}\|_{\mathcal{H}} = \infty$ if $k \in \sigma(A)$ (even though $(\mathcal{A}-k)^{-1}$ does not exist). In this way the resolvent norm $\|(\mathcal{A}-k)^{-1}\|_{\mathcal{H}}$ is a continuous function from the entire complex plane to $(0, \infty]$.

We are now ready to define the ϵ-pseudospectrum of a linear operator [Trefethen, 1997].

Definition 2.1. Let $\epsilon > 0$ be arbitrary. The ϵ-pseudospectrum $\sigma_\epsilon(\mathcal{A})$ of a linear operator $\mathcal{A}$ is the set of $k \in \mathbb{C}$ defined equivalently by any of the following conditions:

$$\|(\mathcal{A}-k)^{-1}\|_{\mathcal{H}} > \frac{1}{\epsilon}, \tag{2.2}$$

$$\exists\ \mathcal{E} \in B(\mathcal{H}):\ k \in \sigma(\mathcal{A}+\mathcal{E}) \text{ and } \|\mathcal{E}\|_{\mathcal{H}} < \epsilon, \tag{2.3}$$

$$\exists\ u \in \mathcal{H}:\ \|u\|_{\mathcal{H}} = 1 \text{ and } \|(\mathcal{A}-k)u\|_{\mathcal{H}} < \epsilon. \tag{2.4}$$

Such values k are said to be ϵ-pseudoeigenvalues of $\mathcal{A}$ and the u's in (2.4) are the corresponding ϵ-pseudoeigenvectors (or ϵ-pseudoeigenfunctions).

It is possible to prove the following facts about pseudospectra of linear operators [Trefethen and Embree, 2005]. Each $\sigma_\epsilon(\mathcal{A})$ is a non-empty open subset of $\mathbb{C}$, and any bounded connected component of $\sigma_\epsilon(\mathcal{A})$ has a non-empty intersection with $\sigma(\mathcal{A})$. In fact, pseudospectra are strictly nested supersets of the spectrum:

$$\bigcap_{\epsilon>0} \sigma_\epsilon(\mathcal{A}) = \sigma(\mathcal{A}),$$

and conversely, for any $\rho > 0$,

$$\sigma_{\epsilon+\rho}(\mathcal{A}) \supseteq \sigma_\epsilon(\mathcal{A}) + B_\rho,$$

where B_ρ is the open ball $\{|k| < \rho\}$ of radius ρ, as usual.

In applications, considerable interest arises for adjoint operators. If $\mathcal{H}^*$ denotes the adjoint space of the linear functionals $f^* : \mathcal{H} \to \mathbb{C}$, the adjoint of a bounded linear operator $\mathcal{A} \in B(\mathcal{H})$ is the bounded linear operator $\mathcal{A}' \in B(\mathcal{H}^*)$ satisfying

$$(\mathcal{A}' f^*)(g) = f^*(\mathcal{A}g) \quad \forall f^* \in \mathcal{H}^*,\ g \in \mathcal{H}. \tag{2.5}$$

In our context where $\mathcal{A} : \mathcal{H} \to \mathcal{H}$, the application $\mathcal{A} \to \mathcal{A}'$ is an isometry between the space of bounded linear operators $\mathcal{H} \to \mathcal{H}$ into the space of bounded linear operators from $\mathcal{H}^* \to \mathcal{H}^*$ [Reed and Simon, 1980]. As we are considering $\mathcal{H}$ being an Hilbert space, Riesz' representation theorem guarantees the existence of the following bijection

$$\mathcal{C} : \mathcal{H} \longrightarrow \mathcal{H}^*, \quad \mathcal{C}(f) := (f, \cdot)_{\mathcal{H}} \tag{2.6}$$

If we define a new map $\mathcal{A}^*$ as

$$\mathcal{A}^* : \mathcal{H} \longrightarrow \mathcal{H}, \quad \mathcal{A}^* = \mathcal{C}^{-1}\mathcal{A}'\mathcal{C}, \tag{2.7}$$

then $\mathcal{A}^*$ satisfies

$$(g, \mathcal{A}f)_{\mathcal{H}} \overset{(2.6)}{=} (\mathcal{C}g)(\mathcal{A}f) \overset{(2.5)}{=} (\mathcal{A}'\mathcal{C}g)f \overset{(2.7)}{=} (\mathcal{C}\mathcal{A}^*g)f \overset{(2.6)}{=} (\mathcal{A}^*g, f)_{\mathcal{H}}. \tag{2.8}$$

Both the operators $\mathcal{A}'$ and $\mathcal{A}^*$ are usually called adjoint operators of $\mathcal{A}$ despite being different operators. In this thesis their difference will be important in applications, so we are going to call them respectively the Banach and the Hilbert adjoint of $\mathcal{A}$ when confusion may arise. The reason for such names is self-explaining: while the linear operator $\mathcal{A}'$ can be defined for any linear operator $\mathcal{A}$ acting between Banach spaces, the linear operator $\mathcal{A}^*$ is defined only when $\mathcal{H}$ is an Hilbert space.

Besides (2.2)-(2.4), a fourth equivalent condition is available for the definition of the ϵ-pseudospectrum of a linear operator $\mathcal{A}$ when $\mathcal{A}$ is defined on a Hilbert space $\mathcal{H}$ and it is compact: $\sigma_\epsilon(\mathcal{A})$ is the set of $k \in \mathbb{C}$ such that

$$\sigma_{\min}(\mathcal{A} - k) < \epsilon, \tag{2.9}$$

where $\sigma_{\min}(\mathcal{A}-k)$ is the smallest singular value of $\mathcal{A}-k$. In fact, in order to define the notion of singular values and singular vectors, one needs to restrict to the class of compact operators, which have only discrete spectrum [Reed and Simon, 1980]. If we look carefully, this definition, which can be stated only for Hilbert spaces $\mathcal{H}$, remains norm-dependent: in fact, a singular value decomposition

$$\mathcal{A} - k = \mathcal{U}\Sigma\mathcal{V}^* \tag{2.10}$$

requires the linear operators $\mathcal{U}$ and $\mathcal{V}$ to be unitary, i.e., $\mathcal{U}^*\mathcal{U} = \mathcal{V}^*\mathcal{V} = \mathcal{I}$ with the adjoint operators $\mathcal{U}^*$ and $\mathcal{V}^*$ depending on the inner product through the Riesz map $\mathcal{C}$ (cf. (2.7)). In the next Chapter we see the extreme importance of the characterisation (2.9) from the computational point of view.

Many properties connect a linear operator $\mathcal{A}$ with its Hilbert adjoint $\mathcal{A}^*$ apart from (2.8). First of all, the spectrum of $\mathcal{A}^*$ is the complex conjugate of the spectrum of $\mathcal{A}$. Moreover, $\|\mathcal{A}\|_{\mathcal{H}} = \|\mathcal{A}^*\|_{\mathcal{H}}$ and $(\mathcal{A}^{-1})^* = (\mathcal{A}^*)^{-1} =: \mathcal{A}^{-*}$. As far as pseudospectra are concerned, $\sigma_\epsilon(\mathcal{A}^*) = \overline{\sigma_\epsilon(\mathcal{A})}$ [Trefethen and Embree, 2005].

One of the main reasons to use pseudospectra of linear operators is normality. A normal operator on $\mathcal{H}$ is a bounded linear operator $\mathcal{A} \in B(\mathcal{H})$ that commutes with its adjoint $\mathcal{A}^*$, i.e.

$$\mathcal{A}^*\mathcal{A} = \mathcal{A}\mathcal{A}^*.$$

Many different equivalent conditions define normal operators, e.g., an operator $\mathcal{A}$ is normal if its eigenvectors corresponding to different eigenvalues are orthogonal. Normal operators are important because their behaviour is completely determined by their eigenvalues. On the other hand, for non-normal operators eigenvalue analysis may fail to describe the behaviour of the system ('the location of the eigenvalues may be as fragile an indicator of underlying character as the hair colour of a Hollywood actor', Trefethen and Embree [2005]). Pseudospectra

are an important tool to investigate non-normality. Indeed, if $\mathcal{A}$ is normal, the ϵ-pseudospectrum $\sigma_\epsilon(\mathcal{A})$ is the union of the balls of radius ϵ centred at the eigenvalues. For non-normal operators, however, the set $\sigma_\epsilon(\mathcal{A})$ can be much larger [Trefethen, 1997]. A simple plot of pseudospectra of a linear operator $\mathcal{A}$ can then give an insight on the normality property of $\mathcal{A}$.

2.2 Pseudospectra of Operators Pencils

In the present Section we review the generalisation of pseudospectra to the case of operator pencils. Operator pencils and generalised eigenvalue problems arises in many application, and they have been deeply investigated in numerical linear algebra [Golub and Van Loan, 1996]. When the Helmholtz equation is discretised by using PML and FEM, the resulting linear system is a generalised eigenvalue problem where the matrix pencil is linear in the wave number k (cf. Chapter 3).

If we modify the standard eigenvalue equation

$$\mathcal{A}u = ku \quad \text{or} \quad (\mathcal{A} - k)u = 0$$

into the generalised eigenvalue equation

$$\mathcal{A}_0 u = k\mathcal{A}_1 u \quad \text{or} \quad (\mathcal{A}_0 - k\mathcal{A}_1)u = 0, \tag{2.11}$$

where the linear operator $\mathcal{A}_0 - k\mathcal{A}_1$ is known as operator pencil, one may wonder how to generalise the notion of pseudospectra to this new setting.

If the linear operator $\mathcal{A}_1$ is invertible, equation (2.11) is equivalent to

$$\mathcal{A}_1^{-1}\mathcal{A}_0 u = ku \quad \text{or} \quad (\mathcal{A}_1^{-1}\mathcal{A}_0 - k)u = 0, \tag{2.12}$$

and the solution of the generalised eigenvalue problem can be found as the solution of the corresponding standard eigenvalue problem for the modified linear operator $\mathcal{A}_1^{-1}\mathcal{A}_0$. Yet, if one is interested in pseudospectra, which are norm-dependent quantities, (2.11) and (2.12) are not equivalent problems as the application of the linear operator $\mathcal{A}_1^{-1}$ changes the norm.

There is not a unique definition of pseudospectra for operator pencils and different formulations appear in the literature, depending on the particular purpose of the analysis. In the following we summarise the main options and then make our choice.

(i) If the linear operator $\mathcal{A}_1$ is invertible, one can set

$$\sigma_\epsilon(\mathcal{A}_0, \mathcal{A}_1) := \sigma_\epsilon(\mathcal{A}_1^{-1}\mathcal{A}_0),$$

i.e. the ϵ-pseudospectrum can be defined as the ϵ^{-1} level set of the modified resolvent norm $\|(\mathcal{A}_1^{-1}\mathcal{A}_0 - k)^{-1}\|_{\mathcal{H}}$. This definition is easy because it reduces the pencil case to the standard one, but it requires the inversion of the linear operator $\mathcal{A}_1$ and the application of $\mathcal{A}_1^{-1}$ changes the norm.

(ii) Generalizing the definition by perturbations (2.3), one can define $\sigma_\epsilon(\mathcal{A}_0, \mathcal{A}_1)$ by perturbing both $\mathcal{A}_0$ and $\mathcal{A}_1$ by independent amounts: $k \in \sigma_\epsilon(\mathcal{A}_0, \mathcal{A}_1)$ if

$$\exists\, \mathcal{E}_0, \mathcal{E}_1 \in B(\mathcal{H}) :\ (\mathcal{A}_0+\mathcal{E}_0)u = k(\mathcal{A}_1+\mathcal{E}_1)u \text{ and } \|\mathcal{E}_0\|_{\mathcal{H}} < \epsilon\alpha_0, \|\mathcal{E}_1\|_{\mathcal{H}} < \epsilon\alpha_1,$$

where the parameters α_0 and α_1 control the relative perturbations, usually by $\alpha_0^2 + \alpha_1^2 = 1$. This definition has been used for matrix pencils, e.g., in Frayssé et al. [1996] and Tisseur and Higham [2001].

(iii) In the particular case $\mathcal{A}_1$ is a self-adjoint and positive-definite operator, and so $\mathcal{A}_1 = \mathcal{C}_1^*\mathcal{C}_1$ for some invertible $\mathcal{C}_1 \in B(X)$, Riedel [1994] proposes to set

$$\sigma_\epsilon(\mathcal{A}_0, \mathcal{A}_1) := \sigma_\epsilon(\mathcal{C}^{-*}\mathcal{A}_0\mathcal{C}^{-1}),$$

i.e. to define pseudospectra as the ϵ^{-1} level sets of the modified resolvent norm $\|(\mathcal{C}^{-*}\mathcal{A}\mathcal{C}^{-1} - k)^{-1}\|_{\mathcal{H}}$. This corresponds to pseudospectra of $\mathcal{B}^{-1}\mathcal{A}$ with respect to the norm $\|f\|_{\mathcal{A}_1} := \sqrt{(f, \mathcal{A}_1 f)_{\mathcal{H}}}$.

Following instead van Dorsselaer [1997], we adopt the following definition:

Definition 2.2. Let $\epsilon > 0$ be arbitrary. The ϵ-pseudospectrum $\sigma_\epsilon(\mathcal{A}_0, \mathcal{A}_1)$ of an operator pencil $\mathcal{A}_0 - k\mathcal{A}_1$ is the set of $k \in \mathbb{C}$ defined equivalently by any of the

following conditions:

$$\|(\mathcal{A}_0 - k\mathcal{A}_1)^{-1}\|_{\mathcal{H}} > \frac{1}{\epsilon}, \tag{2.13}$$

$$\exists\ \mathcal{E} \in B(\mathcal{H}):\ k \in \sigma(\mathcal{A}_0 + \mathcal{E} - k\mathcal{A}_1) \text{ and } \|\mathcal{E}\|_{\mathcal{H}} < \epsilon, \tag{2.14}$$

$$\exists\ u \in \mathcal{H}:\ \|u\|_{\mathcal{H}} = 1 \text{ and } \|(\mathcal{A}_0 - k\mathcal{A}_1)u\|_{\mathcal{H}} < \epsilon. \tag{2.15}$$

Such values of k are said to be ϵ-pseudoeigenvalues of the operator pencil $\mathcal{A}_0 - k\mathcal{A}_1$ and the u's in (2.15) are the corresponding ϵ-pseudoeigenvectors (or ϵ-pseudoeigenfunctions).

Note that condition (2.14) means that we consider perturbations of $\mathcal{A}_0$ only while $\mathcal{A}_1$ is fixed, differently from (ii) where perturbations of both $\mathcal{A}_0$ and $\mathcal{A}_1$ are allowed. As far as singular values are concerned, the inequality (2.13) is equivalent to

$$\sigma_{\min}(\mathcal{A}_0 - k\mathcal{A}_1) < \epsilon, \tag{2.16}$$

while, for example, formulation (ii) leads to $\sigma_{\min}(\mathcal{A}_0 - k\mathcal{A}_1) < \epsilon(\alpha_0 + |k|\alpha_1)$ [van Dorsselaer, 2003]. In many applications, such as those related to stability questions, one is interested in eigenvalues close to the origin, and so Definition 2.2 can be more functional.

Most of the connections between pseudospectra and normality are lost when passing from the standard to the generalised case. For example, van Dorsselaer [1997] shows that $\sigma_\epsilon(\mathcal{A}_0, \mathcal{A}_1)$ can be much larger than the union of the disks with radius $\epsilon/\|\mathcal{A}_1\|$ around $\sigma(\mathcal{A}_0, \mathcal{A}_1)$ even when both $\mathcal{A}_0$ and $\mathcal{A}_1$ are normal.

2.3 Pseudospectra of Analytic Families

In the present Section a generalization of pseudospectra for analytic families of linear operators is introduced. Such a notion of pseudospectra turns out to be useful when boundary equation methods for the Helmholtz equation are considered. In fact the single-layer, double-layer, adjoint double-layer and hypersingular boundary integral operators $\mathcal{V}_k$, $\mathcal{K}_k$, $\mathcal{K}'_k$ and $\mathcal{T}_k$ defined in Section 1.4 depends on the wave number k through the fundamental solution $E_k(x, y)$ which

is analytic in k. The idea of considering pseudospectra for analytic families of linear operators is not new but very recent, so we start by summarising briefly the literature on the topic that we are aware of.

In the context of delay differential equations, Cullum and Ruehli [2001] consider matrix functions $W(s)$ which are analytic and nonlinear in $s \in \mathbb{C}$ and vectors $z \neq 0$ such that $W(s)z = 0$, and they define the ϵ-psedospectrum of $W(s)$ as the set of $z \in \mathbb{C}$ such that

$$\kappa(W(s)) := \|W(s)\|\|W(s)^{-1}\| \geq \epsilon^{-1},$$

where $\kappa(W(s))$ is the condition number of $W(s)$. The authors propose the use of the pseudospectra to track and estimate the sensitivity of $W(s)$ to changes in s in any specified box in the complex plane, and they suggest an algorithm which uses the equivalence $\|W(s)\|_2\|W(s)^{-1}\|_2 = \sigma_{\max}(W(s))/\sigma_{\min}(W(s))$, where $\sigma_{\max}(W(s))$ and $\sigma_{\min}(W(s))$ are, respectively, the largest and smallest singular values of $W(s)$.

Since then, non-polynomial generalizations of pseudospectra have appeared different times in the context of delay differential equations. Green and Wagenknecht [2006], Michiels and Niculescu [2007], Michiels et al. [2006], Wagenknecht et al. [2008] consider matrices of the form $\Delta(z) := zI - A_0 - A_1e^{-\tau z}$ and give a structured definition of the ϵ-pseudospectrum of $\Delta(z)$ as the set of $z \in \mathbb{C}$ such that

$$\det(\Delta(z) + \tilde{\Delta}(z)) = 0 \tag{2.17}$$

where also the perturbations $\tilde{\Delta}(z)$ have the form $B_0 + B_1e^{-\tau z}$ with $\|B_i\| \leq \epsilon w_i$. Moreover, they prove that the condition (2.17) is equivalent to

$$\|\Delta(z)^{-1}\| \geq (\epsilon g(z))^{-1},$$

with $g(z) := w_0 + w_1|e^{-\tau z}|$.

In a recent paper, Bindel and Hood [2013] define the ϵ-pseudospectrum of a family of analytic matrices $(A_k)_{k\in\mathbb{C}}$ as

$$\bigcup_{E_k\in\mathcal{E}} \sigma(A_k + E_k) \tag{2.18}$$

where $\mathcal{E}$ is the set of analytic E_k such that $\sup_{k\in\mathbb{C}} \|E_k\| < \epsilon$ for the given matrix norm $\|\cdot\|$. The authors use this notion in order to prove localisation results for the spectrum of A_k, and they show that (2.18) is equivalent to

$$\|A_k^{-1}\| > \epsilon^{-1}, \tag{2.19}$$

the condition that we choose to define pseudospectra. In particular, they show

$$\sigma_\epsilon(A_k) = \bigcup_{E\in\mathcal{E}} \sigma(A_k + E_k) = \bigcup_{E_0\in\mathcal{E}_0} \sigma(T + E_0),$$

with $\mathcal{E}_0$ is the set of matrices E_0 such that $\|E_0\| < \epsilon$, extending to non-linear pseudospectra the equivalence which was already known to hold for linear standard pseudospectra [Trefethen and Embree, 2005]. Again, any link between pseudospectra and the normality of $\mathcal{A}_k$ for single k's is lost.

For our purposes, we extend the definition of Bindel and Hood, who give it for matrices only, to analytic families of linear operators, giving the following definitions:

Definition 2.3. Let $\epsilon > 0$ be arbitrary. The ϵ-pseudospectrum $\sigma_\epsilon(\mathcal{A}_k)$ of an analytic family $(\mathcal{A}_k)_{k\in\mathbb{C}}$ of linear operators is the set of $k \in \mathbb{C}$ defined equivalently by any of the following conditions:

$$\|\mathcal{A}_k^{-1}\|_{\mathcal{H}} > \frac{1}{\epsilon}, \tag{2.20}$$

$$\exists\, \mathcal{E} \in B(\mathcal{H}) :\ k \in \sigma(\mathcal{A}_k + \mathcal{E}) \text{ and } \|\mathcal{E}\|_{\mathcal{H}} < \epsilon, \tag{2.21}$$

$$\exists\, u \in \mathcal{H} :\ \|u\|_{\mathcal{H}} = 1 \text{ and } \|\mathcal{A}_k u\|_{\mathcal{H}} < \epsilon. \tag{2.22}$$

Such values of k are said to be ϵ-pseudoeigenvalues of the analytic family $\mathcal{A}_k$ and the u's in (2.22) are the corresponding ϵ-pseudoeigenvectors (or ϵ-pseudoeigenfunctions).

We conclude the Chapter by showing pseudospectra of a boundary integral operator on the sphere. When the obstacle K is the unit sphere, the internal Neumann eigenvalues k_N can be computed numerically (cf. Table 1.1). In this case the Neumann trace can be written as the boundary integral operator $\mathcal{K}_k + 1/2\mathcal{I}$, which is normal for each k [Betcke et al., 2014]. Figure 2.1 shows the resolvent norm of $\mathcal{K}_k + 1/2\mathcal{I}$ on the real segment $2 < k < 8$ and its pseudospectra in the complex domain $\{k \in \mathbb{C} : \ 2 < \text{Re } k <, \ -0.75 < \text{Im } k < 0.75\}$. Both the plots are logarithmic with base 10. The vertical dotted lines indicates the roots of the derivative of the spherical Bessel functions in Table 1.1, while the horizontal dotted line on the pseudospectra shows the x-axis. The plot confirms what we have already stated, namely, pseudospectra are bigger than the balls centered in the generalized eigenvalues and they protrude on the upper part of the complex plane more than in the lower part, even if the $\mathcal{K}_k + 1/2\mathcal{I}$ is normal for each k.

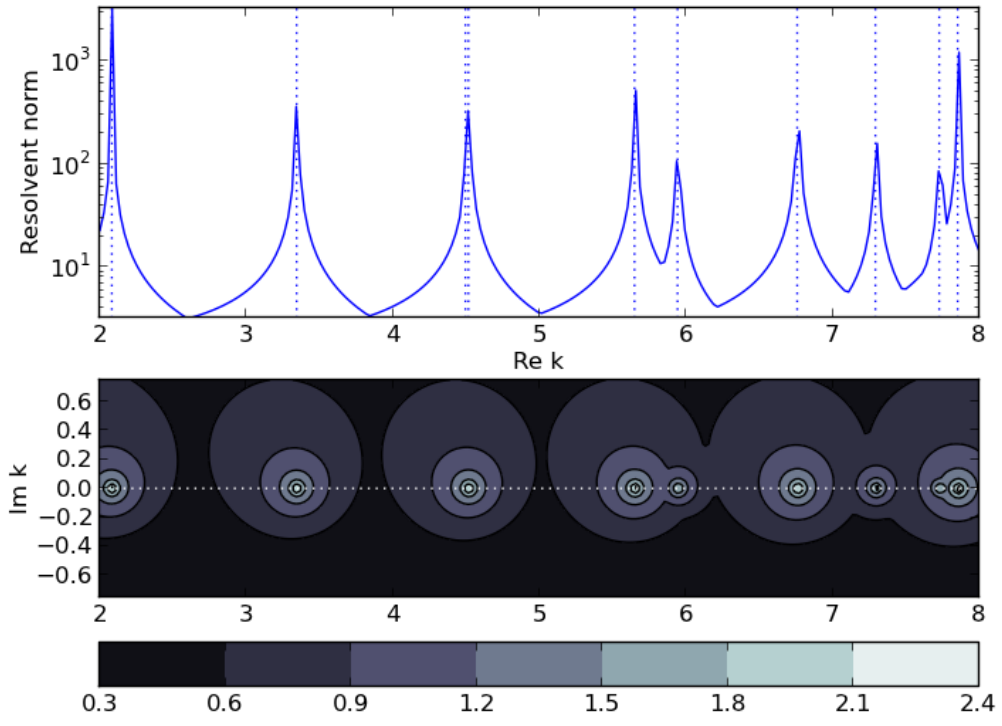

FIGURE 2.1: Pseudospectra of the boundary integral operator $\mathcal{K}_k + 1/2\mathcal{I}$ (Neumann trace) for the three-dimensional unit sphere.

Chapter 3

Finite Element Methods for computing resonances. An overview.

With the present Chapter we start the treatment of the different numerical methods which are used for the computation of resonances and pseudospectra. Many numerical methods are available for the solution of boundary value problems involving the Helmholtz equation. We consider two main classes of such methods: Finite Element Methods and Boundary Element Methods. In the present Chapter we give an overview of the former methods, while the latter will be investigated in more details in Chapter 4.

Any numerical method applied to acoustic scattering problems faces the issue of truncating the unbounded domain without introducing excessive error. An option consists in the introduction of an artificial boundary where a special absorbing condition is used to reduce the reflection of incident waves. Berenger [1994] showed how to perturb the Maxwell system to provide a perfectly matched absorbing layer (PML) for electromagnetic scattering problems. In the PML, the wave is absorbed and decays exponentially into the layer. Thus the PML itself can be truncated to form a narrow absorbing layer with a low reflection. This approach, which is described in Section 3.1, is easy to implement and is very effective.

The PML equation still involves functions and, in order to be directly solved by algorithms, it needs to be first discretised and made finite by some numerical method. Finite Element Methods (FEM) are a popular class of such methods and, roughly speaking, consist in the combination of a 'discrete' weak formulation of the continuous problem and a 'finite' Ritz-Galerkin approximation of its solution (Section 3.2). According to Brenner and Scott [2008], FEM 'should be thought of as a black box into which one puts the differential equation (boundary value problem) and out of which pops an algorithm for approximating the corresponding solutions'.

As we are interested in pseudospectra and resonances, our attention goes to the resolvent norms more than to the solution of particular boundary value problems. Yet the L^2-norm of a linear operator is not simply equal to the 2-norm its matrix discretisation. In Section 3.3 we discuss the approximation of the L^2-norm of a linear operator by the 2-norm of its matrix discretisation.

Even for simple one- and two-dimensional examples, such matrices can be very large and the calculation of pseudospectra becomes computationally expensive. When an eigenvalue decomposition is affordable, much may be gained by projecting matrix discretisations onto the subspace spanned by certain eigenvectors. In Section 3.4 we terminate the discussion of FEM by extending to the case of matrix pencils an eigenspace projection method proposed by Reddy et al. [1993] for standard pseudospectra.

In Section 3.5 we apply PML and FEM to show resonances and pseudospectra for a particular two-dimensional boundary value problem. The scatterer, which contains a rectangular cavity, is an example of 'trapping' obstacle (cf. Section 5.1) and it has already appeared in acoustic scattering scientific literature.

The computation in the present Chapter (as those shown elsewhere in the thesis) were performed using Enthought Python Distribution 7.3 on a cluster of workstations with two 2.4 GHz Intel Xeon six-core processors and 189 GB RAM each.

3.1 The Perfectly Matched Layer

The Perfectly Matched Layer (PML) approach, introduced in the acoustic scattering community by Berenger [1994, 1996], provides a convenient way to deal with problems defined on unbounded sets. The application of PML has become a standard tool to study scattering in open systems because it converts the resonance problem to an eigenvalue problem involving an operator which resembles the original Helmholtz equation transformed by a complex shift in the coordinate system [Collino and Monk, 1998].

As usual, let $K \subset \mathbb{R}^3$ be a compact obstacle with Lipschitz boundary $\Gamma := \partial K$ and connected complement $\Omega := \mathbb{R}^3 \setminus K$. The acoustic scattering problem

$$
\begin{aligned}
(-\Delta - k^2)u &= 0 \quad \text{in } \Omega && (3.1)\\
u &= f \quad \text{on } \Gamma && (3.2)\\
\frac{\partial u}{\partial n} - iku &= o\left(\frac{1}{r}\right) \quad \text{as } r := |x| \longrightarrow +\infty && (3.3)
\end{aligned}
$$

can be treated by a spherical PML [Kim and Pasciak, 2009]. The PML is defined in terms of a function $\tilde{\sigma} \in C^2(\mathbb{R}_+)$ satisfying, for some r_0 and r_1 with $r_1 > r_0 >$ diam $K/2$,

$$
\tilde{\sigma}(r) = \begin{cases} 0 & \text{for } 0 \le r < r_0, \\ \text{increasing} & \text{for } r_0 \le r < r_1, \\ \sigma_0 \text{ constant} & \text{for } r \ge r_1. \end{cases} \tag{3.4}
$$

A typical C^2 function with these properties is given on $[r_0, r_1]$ by the fifth order polynomial

$$
\tilde{\sigma}(r) = \frac{\sigma_0}{\int_{r_0}^{r_1} (t - r_0)^2 (r_1 - t)^2 dt} \int_{r_0}^{r} (t - r_0)^2 (r_1 - t)^2 dt. \tag{3.5}
$$

Figure 3.1 shows the plot of the damping function $\tilde{\sigma} = \tilde{\sigma}(r)$ in (3.5) with $\sigma_0 = 1$, $r_0 = 0.5$ and $r_1 = 1.5$.

The damping function (3.4) corresponds to the exterior scaling function in the theory of quantum resonances, where the Aguilar-Balslev-Combes-Simon theorem identifies the quantum resonances of a self-adjoint operator $\mathcal{A}$ with the

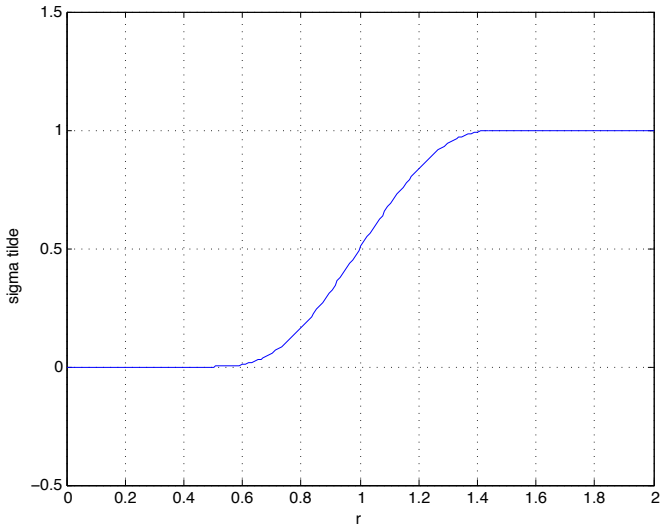

FIGURE 3.1: Plot of the damping function $\tilde{\sigma} = \tilde{\sigma}(r)$ in (3.5) with $\sigma_0 = 1$, $r_0 = 0.5$ and $r_1 = 1.5$.

complex eigenvalues of the operator $\tilde{\mathcal{A}}$ obtained from $\mathcal{A}$ by spectral deformation (cf. Appendix A and Hislop and Sigal [1996]). The whole PML technique is an adaptation of the technique of spectral deformation to the acoustic scattering setting.

The PML approximation can now be defined as a formal complex shift in the coordinate system [Collino and Monk, 1998]: in the PML domain $\Omega_0 := \Omega \setminus B_{r_0}$ we consider the solution $u = u(r, \theta, \phi)$ of the Helmholtz equation (3.1) and we continue it analytically with respect to the variable $r \in \mathbb{R}$ to a complex variable $\tilde{r} \in \mathbb{C}$. The extended solution $\tilde{u}(\tilde{r}, \theta, \phi)$ still satisfies (3.1). Once defined $\tilde{d}(r) := 1 + i\tilde{\sigma}(r)$ with $\tilde{\sigma}$ as in (3.4), we pick the path

$$\tilde{r}(r) := r\tilde{d}, \tag{3.6}$$

and, by the chain rule, we write the elliptic partial differential equation back in the original real variables as

$$(-\tilde{\Delta} - k^2\tilde{d}^2)\tilde{u} = 0 \quad \text{in } \Omega, \tag{3.7}$$

where the modified Laplacian $\tilde{\Delta}$ is given by

$$\tilde{\Delta}u = \frac{1}{dr^2}\frac{\partial}{\partial r}\left(\frac{\tilde{d}^2 r^2}{d}\frac{\partial u}{\partial r}\right) + \frac{1}{r^2\sin\theta}\frac{\partial}{\partial\theta}\left(\sin\theta\frac{\partial u}{\partial\theta}\right) + \frac{1}{r^2\sin^2\theta}\frac{\partial^2 u}{\partial\phi^2}, \tag{3.8}$$

with

$$\sigma(r) := \frac{d(r\tilde{\sigma})}{dr} = \tilde{\sigma}(r) + r\frac{d\tilde{\sigma}}{dr}(r) \quad \text{and} \quad d(r) := \frac{d\tilde{r}}{dr}(r) = 1 + i\sigma(r).$$

When $r < r_0$, we have $d = \tilde{d} = 1$ and (3.8) is the standard Laplacian in spherical coordinates,

$$\Delta = \frac{1}{r^2}\frac{\partial}{\partial r}\left(r^2\frac{\partial}{\partial r}\right) + \frac{1}{r^2\sin\theta}\frac{\partial}{\partial\theta}\left(\sin\theta\frac{\partial}{\partial\theta}\right) + \frac{1}{r^2\sin^2\theta}\frac{\partial^2}{\partial\phi^2}.$$

The PML solution is defined as

$$\tilde{u}(x) = \begin{cases} u(x) & \text{for } r < r_0, \\ \sum_{n=0}^{\infty}\sum_{m=-n}^{n} c_{mn}y_{mn}(\theta,\phi)h_n^{(1)}(k\tilde{r}) & \text{for } r \geq r_0, \end{cases} \tag{3.9}$$

where the expansion in the PML domain corresponds to (1.20) with the real variable r replaced by the complex $\tilde{r}$. Clearly, $\tilde{u}$ coincides with u for $|x| \leq r_0$, while for $|x| \geq r_1$ the asymptotic behavior of the spherical Hankel function (1.18) reads

$$|h_n^{(1)}(k\tilde{r})| \sim \left|\frac{e^{ik\tilde{r}}}{k\tilde{r}}\right| = \left|\frac{e^{ikr}}{kr(1+i\sigma_0)}\right| |e^{-kr\sigma_0}| \quad \text{as } r \longrightarrow +\infty, \tag{3.10}$$

which implies an exponential decay for Im $k \geq 0$.

Kim and Pasciak [2009] prove that the inhomogeneous equation

$$(-\tilde{\Delta} - k^2\tilde{d}^2)\tilde{u} = \tilde{d}^2 f \quad \text{in } \mathbb{R}^3$$

has the following well-posed variational formulation in $H^1(\mathbb{R}^3)$ when k is real and positive:

$$\tilde{\kappa}(\tilde{u},\chi) - k^2\tilde{\mu}(\tilde{u},\chi) = \tilde{\mu}(f,\chi) \quad \forall\chi \in C_0^\infty(\mathbb{R}^3), \tag{3.11}$$

with

$$\begin{aligned}\tilde{\kappa}(\tilde{u},\chi) &:= \left(\frac{\tilde{d}^2}{d}\frac{\partial\tilde{u}}{\partial r},\frac{\partial}{\partial r}\left(\frac{\chi}{\bar{\tilde{d}}}\right)\right)+\left(\frac{1}{r^2}\frac{\partial\tilde{u}}{\partial\theta},\frac{\partial\chi}{\partial\theta}\right)+\left(\frac{1}{r^2\sin^2\theta}\frac{\partial\tilde{u}}{\partial\phi},\frac{\partial\chi}{\partial\phi}\right)\\ \tilde{\mu}(\tilde{u},\chi) &:= \left(\tilde{d}^2\tilde{u},\chi\right),\end{aligned}$$

and $(\cdot,\cdot)$ being the usual L^2 product. In particular, the existence of the solution to the PML problem (3.11) follows by construction. The uniqueness follows from the following result, which is Theorem 2.2 in Kim and Pasciak [2009]:

Theorem 3.1. Let A_{r_0,r_2} be an annulus bounded by two spheres of radius $r_0 < r_2$ and let k be a non-zero complex number not on the negative real axis. Suppose that $u \in H^1(A_{r_0,r_2})$ and satisfies $\tilde{\kappa}(u,v) = k^2\tilde{\mu}(u,v)$ for all $v \in C_0^\infty(A_{r_0,r_2})$; then

$$u(x) = \sum_{n=0}^{\infty}\sum_{m=-n}^{n}\left(a_{n,m}h_n^1(k\tilde{r}) + b_{n,m}h_n^2(k\tilde{r})\right)Y_n^m(\hat{x}), \tag{3.12}$$

and the series converges in $H^1(A_{r_0,r_2})$.

The uniqueness of the solution to the PML problem (3.11) for k real and positive is proved by Kim and Pasciak [2009] by combining the above Theorem with a two-dimensional uniqueness result by Collino and Monk [1998], which states that the unique solution to the PML problem has exactly expansion (3.12). As far as the stability of the PML solution is concerned, this is proved by Kim and Pasciak [2009] by using two inf-sup conditions which follow from the fact that $\tilde{\kappa}(\tilde{u},\chi) - k^2\tilde{\mu}(\tilde{u},\chi)$ is a low-order perturbation of a coercive form on the bounded domain $\Omega_1 := \Omega \cap B_{r_1}$. It is worth highlighting at this point that such inf-sup conditions are not valid for non-circular PML (e.g. elliptic or cartesian PML), and well-posedness in those cases requires different and more complicated arguments.

At this point, once shown the PML weak problem is well-posed, Kim and Pasciak [2009] define the solution operator

$$\mathcal{B}_1 : L^2(\mathbb{R}^3) \longrightarrow H^1(\mathbb{R}^3), \quad \mathcal{B}_1 f = \tilde{u},$$

where $\tilde{u}$ is the solution of (3.11) for $k = 1$. The linear operator $\mathcal{B}_1$ is bounded from $L^2(\mathbb{R}^3)$ into $H^1(\mathbb{R}^3)$ and they restrict it to an operator on $H^1(\mathbb{R}^3)$, in order to define its resolvent and spectrum.

Now, Aguilar-Balslev-Combes-Simon spectral theory connects the resonances with the eigenvalues of the PML solution operator $\tilde{\mathcal{B}}_k$ defined by $\tilde{\mathcal{B}}_k f = u$ for general stretching functions $\tilde{\sigma}$. A proof of the connection independent from this general theory is given by Kim and Pasciak [2009] who prove the following theorem.

Theorem 3.2. Let $d_0 := 1 + i\sigma_0$ with $\mathrm{Im}(d_0 k) > 0$ and $\lambda = 1/(k^2 - 1)$. If there is a non-zero outgoing solution u satisfying (3.1), then $\tilde{u}$ given by (3.9) is an eigenfunction for $\tilde{\mathcal{B}}_1$ with eigenvalue λ. Conversely, if $\tilde{u}$ is an eigenfunction for $\tilde{\mathcal{B}}_1$ with eigenvalue λ, then $\tilde{u}$ is of the form (3.9) for $r \geq r_0$ and $u = u(\tilde{u})$ satisfies (3.1) and is outgoing.

The PML method only gives resonances which satisfy $\mathrm{Im}(d_0 k) > 0$, i.e., those which are in the sector bounded by the positive real axis and the line $\arg(z) = \arg(1/d_0)$. To get the resonances to the left of this line, we need to increase σ_0 (see Figure 3.2).

The Aguilar-Balslev-Combes-Simon theory, which is part of the spectral deformation theory, provides additional information about the spectrum of the PML operator $\tilde{\Delta}/\tilde{d}^2$. In particular, it is possible to prove that the essential spectrum of $\tilde{\Delta}/\tilde{d}^2$ is

$$\sigma_{\mathrm{ess}}\left(\tilde{d}^{-2}\tilde{\Delta}\right) = \{z \in \mathbb{C} : \ \arg(z) = -2\arg(1 + i\sigma_0)\}, \tag{3.13}$$

and the eigenvalues of $\tilde{d}^{-2}\tilde{\Delta}$ corresponding to resonances are isolated and have finite multiplicity.

Once proved the exponential decay (3.10), it is then natural to approximate the unbounded domain Ω with a bounded $\Omega_2 := \Omega \cap B_{r_2}$ for some $r_2 > r_1$ and to impose a zero Dirichlet boundary condition on $S_{r_2} := \{|x| = r_2\}$. Kim and Pasciak [2009] continue their analysis of the PML operator by showing that this truncated problem does not result in spurious eigenvalues in the region of

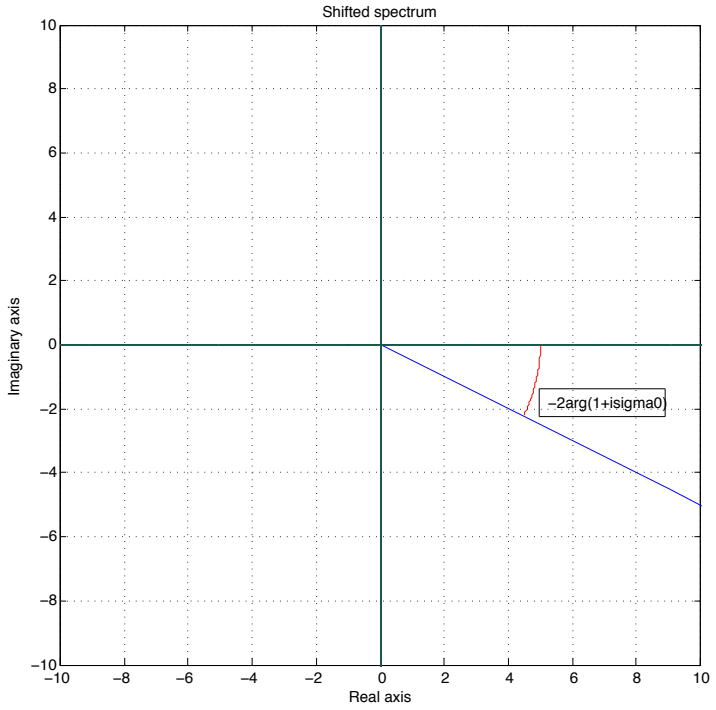

FIGURE 3.2: Shifted essential spectrum of the PML operator $\tilde{\Delta}/\tilde{d}^2$.

interest, where $\mathrm{Im}(d_0 k) > 0$. They define the truncated solution operator

$$\mathcal{B}_1^{(r_2)} : H^1(\mathbb{R}^3) \longrightarrow H_0^1(\Omega_{r_2}), \quad \mathcal{B}_1^{(r_2)} f = u,$$

where $u \in H_0^1(\Omega_{r_2})$ is the unique solution to

$$\tilde{\mu}(u, \phi) - \tilde{\kappa}(u, \phi) = \tilde{\kappa}(f, \phi) \quad \forall \phi \in H_0^1(\Omega_{r_2}),$$

and they investigate how the spectrum of $\mathcal{B}_1^{(r_2)}$ is related to that of $\mathcal{B}_1$. In particular, they show that the resolvent set for $\mathcal{B}_1^{(r_2)}$ approaches that of $\mathcal{B}_1$ as $r_2 \to +\infty$ by proving the following result (Theorem 3.1 in [Kim and Pasciak, 2009]).

Theorem 3.3. Let U be a compact subset of the resolvent set $\rho(\mathcal{B}_1)$ whose image under the map $z \mapsto \sqrt{(1+z)/z} =: k(z)$ satisfies $\mathrm{Im}(d_0 k(z)) > 0$ for all $z \in U$ (with $-\pi < \arg(k(z)) \leq 0$). Then there exists r_2^* depending on U such that

$$U \subset \rho\left(\mathcal{B}_1^{(r_2)}\right) \quad \forall r_2 > r_2^*.$$

Another aspect considered by Kim and Pasciak [2009] is eigenvalue convergence. Let λ be an eigenvalue of $\mathcal{B}_1$ corresponding to a resonance. Such λ is isolated and it has a circular neighbourhood of radius $\eta > 0$ with all points excluding λ in $\rho(\mathcal{B}_1)$. We denote by Γ the boundary of such neighbourhood. For $u \in H^1(\mathbb{R}^3)$, the spectral projector is defined as

$$P_\Gamma(u) := \frac{1}{2\pi i} \int_\Gamma R_z(\mathcal{B}_1)u \; dz.$$

Its range $V := \text{range}(P_\Gamma)$ is the generalised eigenspace associated with the eigenvalue λ. By the previous Theorem, Γ is contained also in $\rho\left(\mathcal{B}_1^{(r_2)}\right)$ for $r_2 >> 1$, so it is possible to define also

$$P_\Gamma^{(r_2)}(u) := \frac{1}{2\pi i} \int_\Gamma R_z(\mathcal{B}_1^{(r_2)})u \; dz.$$

Its range $V^{(r_2)} := \text{range}(P_\Gamma^{(r_2)})$ is the subspace of $H_0^1(\Omega_{r_2})$ spanned by the generalised eigenfunctions associated with the eigenvalues of $\mathcal{B}_1^{(r_2)}$ inside Γ. Kim and Pasciak [2009] prove the following

Theorem 3.4. For any η sufficiently small, there exists $r_2^* > 0$ such that

$$\dim V = \dim V^{(r_2)} \quad r_2 > r_2^*.$$

This is equivalent to saying that the eigenvalues of the truncated problem converge to those of the full problem, and such convergence respects the eigenvalue multiplicity. At this point it is clear that the PML weak equation (3.11) is a mathematical formulation that we can consistently adopt to compute the resonances of the Helmholtz operator by using a numerical method.

In order to show how PML works in practice, we describe a 2D case of scattering by the unit circle and plot the PML solution. We choose the following geometry: a circle of radius $R = 1$ centered in the origin and surrounded by a second circle of radius $r_2 = 5$ centered in the origin. We get two nested connected region: the central one is the obstacle K, the outer one is the computational domain Ω_0. Let $k = 40$, $r_0 = 4$ and $r_1 = 4.5$. Let $u^{(i)}$ be the constant number $0.00736689 + i0.12593642$, that is the value of the Hankel function $h_0^{(1)}(z)$ at

$z = Rk = 40$. Figure 3.3 shows the (real part of the) scattered field due to this constant boundary value, which is given by the Hankel function $h_0^{(1)}(kr)$. The visible damping near the computational boundary is due to the implementation of a radial PML.

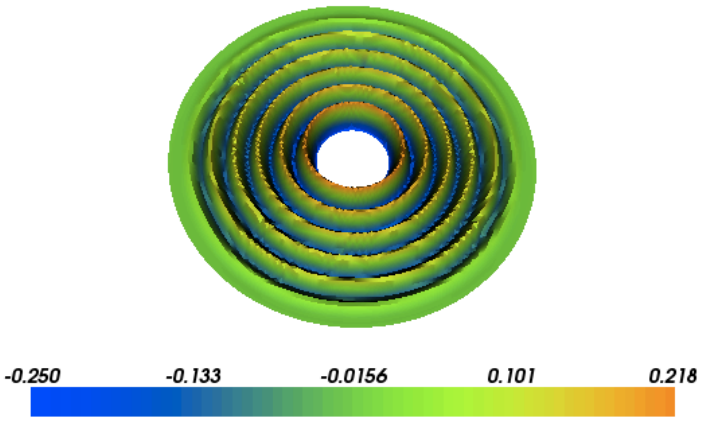

FIGURE 3.3: PML solution around the 2D unit sphere for a constant boundary value (FEM parameters: mesh size $h = 0.1$, interpolation order $p = 3$).

3.2 FEM discretisation of the PML

Continuous problems in infinite-dimensional spaces (e.g., the PML equation (3.11) on the $L^2(\mathbb{R}^3)$ space) can not be directly solved by algorithms, but they need first to be discretised and made finite. FEM are a popular class of such methods and, roughly speaking, they consist in the combination of a 'discrete' weak formulation of the continuous problem and a 'finite' Ritz-Galerkin approximation of its solution. In the present Section we introduce some tools from the mathematical theory of FEM which are applied to boundary value problems involving the PML Helmholtz equation (3.7).

As we are interested in the numerical computation of resonances and pseudospectra, we consider (3.11) with $f = 0$ and the bilinear forms $\tilde{\kappa}$ and $\tilde{\mu}$ restricted to Ω_2. We end with the variational problem

$$\tilde{\kappa}(\tilde{u}, \chi) = k^2 \tilde{\mu}(\tilde{u}, \chi) \quad \forall \chi \in L^2(\Omega_2), \tag{3.14}$$

which we want to solve by FEM.

In general, a variational problem is posed as follows. Let $\mathcal{V}$ be a subspace of the Hilbert space $\mathcal{H}$, and $a(\cdot,\cdot)$ be a bilinear form on $\mathcal{H}$. Given a linear functional $F \in \mathcal{V}'$, find $u \in \mathcal{V}$ such that

$$a(u,v) = F(v) \quad \forall v \in \mathcal{V}. \tag{3.15}$$

Every variational problem implicitly defines an operator which maps every linear functional $F \in \mathcal{H}'$ to the solution $u \in \mathcal{H}$, as the Riesz map (2.6).

Usually, the subspace $\mathcal{V}$, where the solution is looked for, is infinite-dimensional, and equation (3.15) is a linear system with an infinite number of equations. This issue is overcome by the second step of FEM, namely the Galerkin method. The Galerkin method for approximating the solution of a variational problem defined on an infinite-dimensional space $\mathcal{V}$ consists in the redefinition of the problem in a finite-dimensional subspace $\mathcal{P}$ of $\mathcal{V}$. The Galerkin approximation problem is the following: Given a finite-dimensional subspace $\mathcal{P} \subset \mathcal{V}$ and $F \in \mathcal{V}'$, find $p \in \mathcal{P}$ such that

$$a(p,v) = F(v) \quad \forall v \in \mathcal{P}. \tag{3.16}$$

Remark 3.5. When the bilinear form is coercive and symmetric, the discrete solution is also characterized by the property

$$J(p) = \inf_{q \in \mathcal{P}} J(q),$$

where $J(v) := \frac{1}{2}a(v,v) - F(v)$. This alternate definition of the discrete solution is known as the Ritz method [Ciarlet, 2002].

To approximate the solution of the finite variational problem (3.16) we use Lagrange elements and we piece them together to create subspaces of Sobolev spaces [Brenner and Scott, 2008]. Let us proceed with a few definitions. We begin by defining the local interpolant.

Definition 3.6. Given a finite element $(K, \mathcal{P}, \mathcal{N})$, let $(\phi_i)_{i=1}^n \subseteq \mathcal{P}$ be the function basis dual to the nodal basis $\mathcal{N}$. If v is a function for which all $N_i \in \mathcal{N}$,

$i = 1, \ldots, n$, are defined, then we define the local interpolant by

$$\mathcal{I}_K(v) := \sum_{i=1}^{n} N_i(v)\phi_i. \tag{3.17}$$

Brenner and Scott [2008] show that:

i. $\mathcal{I}_K$ is linear;

ii. $N_i(\mathcal{I}_K(f)) = N_i(f)$ for all $1 \leq i \leq n$, i.e., $\mathcal{I}_K(f)$ is the unique shape function having the same nodal values as f;

iii. $\mathcal{I}_K(f) = f$ for $f \in \mathcal{P}$.

We now put the elements together and define the global interpolant.

Definition 3.7. Suppose Ω is a domain with a subdivision $\mathcal{T}$ and each $K_j \in \mathcal{T}$ is equipped with shape functions $\mathcal{P}_j$ and nodal variables $\mathcal{N}_j$ such that $(K_j, \mathcal{P}_j, \mathcal{N}_j)$ forms a finite element. Let m be the order of the highest partial derivatives involved in the nodal variables. For $f \in C^m(\overline{\Omega})$, the global interpolant is defined by

$$\mathcal{I}_{\mathcal{T}} f|_{K_j} = \mathcal{I}_{K_j} f \quad \forall K_i \in \mathcal{T}.$$

Interpolants are important because they are the approximated solution we look for by FEM. According to (3.17), the FEM solution

$$u = \sum_{j=1}^{n} u_i \phi_j$$

to the weak PML problem (3.14) defines the linear system of the form

$$\tilde{K}\underline{u} = k^2 \tilde{M}\underline{u}, \tag{3.18}$$

where $\underline{u}$ is the vector of the coefficients of $\tilde{u}$, while $\tilde{K}$ and $\tilde{M}$ are respectively the PML stiffness and mass matrices, defined by

$$K_{i,j} = \tilde{\kappa}(\phi_i, \phi_j), \quad M_{i,j} = \tilde{\mu}(\phi_i, \phi_j).$$

We get these matrices using the software FEniCS [Logg et al., 2012]. The FEniCS Project is a collection of free software with an extensive list of features for automated, efficient solution of differential equations by FEM. To learn more about the project and the software, the reader is referred to the book by Logg et al. [2012] and to the website `http://fenicsproject.org/`.

3.3 Weighted Norms

When we pass from a continuous problem, e.g. the PML equation (3.7), to a discrete one, e.g. the generalised eigenvalue equation (3.18), the L^2-norm of the solution function u is not simply approximated by the 2-norm of its coefficient vector $\underline{u}$. In the present Section we discuss the correct weighted 2-norm we need to compute to have a numerical approximation of the continuous L^2-norm of functions and linear operators.

Let $\Phi = (\phi_i)_{i=1}^n$ be a basis of $\mathcal{P}$ and consider the mapping $\mathcal{J}_\Phi : \mathbb{R}^n \to \mathcal{P}$ defined by

$$\mathcal{J}_\Phi \underline{u} = \sum_{i=1}^{n} u_i \phi_i = u.$$

This map represents the correspondence between vectors of coefficients and function in FEM. The linear operator $\mathcal{J}_\Phi$ is clearly invertible, and $\mathcal{J}_\Phi^{-1}$ maps functions in $\mathcal{P}$ into their vectors of coefficients.

Similarly, one can view vectors as linear functionals by a mapping $\mathcal{J}'_\Phi : \mathbb{R}^n \to \mathcal{P}'$, where

$$(\mathcal{J}'_\Phi \underline{f})(u) = \underline{f} \cdot (\mathcal{J}_\Phi^{-1} u),$$

i.e. a vector is considered as a linear functional on $\mathcal{V}$ by computing its dot product with the vector of coefficients of the input function.

Kirby [2010] proves a general case of the following result, which we prefer to state in term of the particular Hilbert space $L^2(\Omega_2)$ from our model problem.

Proposition 3.8. Let $\mathcal{P} \subset L^2(\Omega_2)$ be a finite-dimensional subspace and $\Phi = (\phi_i)_{i=1}^n$ a basis of $\mathcal{P}$. For every $u \in \mathcal{P}$ and $f \in \mathcal{P}'$ (with $\underline{u} = \mathcal{J}_\Phi^{-1} u$, $\underline{f} = \mathcal{J}_\Phi'^{-1} f \in$

$\mathbb{R}^n$ being their discretisations), we have

$$\|u\|_{L^2} = \|\mathcal{J}_\Phi \underline{u}\|_{L^2} = \|C\underline{u}\|_2, \tag{3.19}$$

$$\|f\|_{L^2} = \|\mathcal{J}'_\Phi \underline{f}\|_{(L^2} = \|C^{-t}\underline{f}\|_2, \tag{3.20}$$

where C is the Cholesky decomposition matrix of the standard mass matrix M associated to Φ, $M_{i,j} := (\phi_i, \phi_j)_{L^2}$.

From (3.19) and (3.20) we compute the L^2 norm of continuous linear operators $\mathcal{A} : L^2(\Omega_2) \to (L^2(\Omega_2))'$, for which we get

$$\|\mathcal{A}\|_{L^2} = \sup_{v \in L^2} \frac{\|\mathcal{A}v\|_{L^2}}{\|v\|_{L^2}} = \sup_{\underline{v} \in \mathbb{R}^n} \frac{\|C^{-t}A\underline{v}\|_2}{\|C\underline{v}\|_2}$$

by using (3.19) and (3.20), and then

$$\|\mathcal{A}\|_{L^2} = \sup_{\underline{w} \in \mathbb{R}^n} \frac{\|C^{-t}AC^{-1}\underline{w}\|_2}{\|\underline{w}\|_2} = \|C^{-t}AC^{-1}\|_2.$$

For their inverses $A^{-1} : (L^2(\Omega_2))' \to L^2(\Omega_2)$, we get

$$\begin{aligned} \|\mathcal{A}^{-1}\|_{L^2} &= \sup_{v \in L^2} \frac{\|\mathcal{A}^{-1}v\|_{L^2}}{\|v\|_{L^2}} = \sup_{\underline{v} \in \mathbb{R}^n} \frac{\|CA^{-1}\underline{v}\|_2}{\|C^{-t}\underline{v}\|_2} \\ &= \sup_{\underline{w} \in \mathbb{R}^n} \frac{\|CA^{-1}C^t\underline{w}\|_2}{\|\underline{w}\|_2} = \|CA^{-1}C^t\|_2. \end{aligned}$$

We remark that by $\|\cdot\|_{L^2}$ we mean different norms depending on $\cdot$ being a function or an operator (in the second case, the induced L^2 norm is considered).

Let us improperly use the same notation for the operator $(-\tilde{\Delta} - k^2\tilde{d}^2)^{-1} : L^2(\Omega) \to L^2(\Omega)$ and for the operator $(L^2(\Omega))' \to L^2(\Omega)$ defined by its weak formulation (3.14). We get

$$\begin{aligned} \|(-\tilde{\Delta} - k^2\tilde{d}^2)^{-1}\|_{L^2} &= \|(C^{-t}(\tilde{K} - k^2\tilde{M})C^{-1})^{-1}\|_2 \\ &= \|(\hat{K} - k^2\hat{M})^{-1}\|_2 = \sigma_{\min}(\hat{K} - k^2\hat{M}) \end{aligned}$$

with

$$\hat{K} = C^{-t}\tilde{K}C^{-1}, \quad \hat{M} = C^{-t}\tilde{M}C^{-1}. \tag{3.21}$$

So, in order to compute the correct approximation of the L^2-norm $\|(-\tilde{\Delta} - z^2\tilde{d}^2)^{-1}\|_{L^2}$, we replace the matrices of the linear system (3.18) with those in (3.21).

3.4 Subspace Projection Methods

In the present Section we describe a subspace projection method to approximate a big pencil $(\hat{K}, \hat{M})$ of dimension n with a pencil $(\check{K}, \check{M})$ of dimension $m \ll n$.

Even for simple examples, matrices in system (3.18) or in (3.21) can be very large, and the calculation of pseudospectra becomes computationally expensive, much more than that of a single eigenvalue decomposition. When the latter is affordable, much may be gained by simply calculating an eigenvalue decomposition of the pencil $(\hat{K}, \hat{M})$, then projecting it onto the subspace spanned by certain eigenvectors.

As far as we know, the idea of projecting on eigenspaces in order to speed up pseudospectra computation appears for the first time in the paper by Reddy et al. [1993], where the authors compute pseudospectra of the Orr-Sommerfeld operator that generates a standard eigenvalue problem. As the extension to the generalized case is quite straightforward, we report their method just adapting it to the L^2 setting (they work in H^1).

Let $(\phi_j)_{j=1}^m$ be a set of m eigenfunctions of a linear operator $\mathcal{S}$, with associated eigenvalues $(\lambda_j)_{j=1}^m$, and let W denote the finite-dimensional space spanned by these eigenfunctions. If $\phi \in W$, then $\psi = \mathcal{S}\phi$ also satisfies $\psi \in W$. The operator $\mathcal{S}$ can be projected onto the space W. This projected operator, which is denoted by $\mathcal{S}_W$, satisfies $\mathcal{S}\phi = \mathcal{S}_W\phi$ for all $\phi \in W$.

The operator $\mathcal{S}_W$ can be represented by a matrix S_W of dimension m. The matrix representation depends on the basis chosen for W. If the basis is the set of eigenfunctions (ϕ_j), then $S_W = D_W$, where D_W is the diagonal matrix of the eigenvalues (λ_j). Reddy et al. [1993] define a matrix representation of $\mathcal{S}_W$ based on an orthonormal basis for W.

Let v_j be a vector of coefficients associated with ϕ_j and let V_W be corresponding eigenvector matrix. If $\|\phi_j\|_{L^2} = 1$, then $\|Cv_j\|_2 = 1$, with C being the Choleski decomposition matrix of the mass matrix M. By applying the QR decomposition to the matrix product CV_W [Golub and Van Loan, 1996], we can compute an orthonormal basis (ψ_j) for W . We have

$$CV_W = (CQ_W)U_W.$$

The columns of Q_W satisfy $\|Cq_j\|_2 = 1$ and $q_j^t C^t C q_k = q_j^t M q_k = \delta_{jk}$. Let ψ_j be the function associated to q_j. These functions satisfy $\|\psi_j\|_{L^2} = 1$ and $(\psi_j, \psi_k)_{L^2} = \delta_{jk}$ and hence form an orthonormal basis for W. The matrix U_W is a square matrix of dimension m, which relates the expansion coefficients in the bases (ϕ_j) and (ψ_j). If $p \in W$ and

$$p = \sum_{i=1}^{m} a_i \phi_i = \sum_{i=1}^{m} b_i \psi_i, \tag{3.22}$$

then $b = U_W a$, where a and b are the m-vectors of the expansion coefficients in (3.22). It is now straightforward to check that

$$\|p\|_{L^2}^2 = \sum_{i,j=1}^{m} b_i (\psi_i, \psi_j)_{L^2} \bar{b}_j = \sum_{l=1}^{m} b_l \bar{b}_l = \|b\|_2^2. \tag{3.23}$$

Since D_W is the matrix representation of $\mathcal{S}_W$ in the eigenfunction basis and U_W relates that basis to the orthonormal basis, it follows that the matrix representation of $\mathcal{S}_W$ in the orthonormal basis is

$$S_W = U_W D_W U_W^{-1}. \tag{3.24}$$

It follows from (3.23) that

$$\sup_{f \neq 0} \frac{\|\mathcal{S}_W f\|_{L^2}}{\|f\|_{L^2}} = \sup_{\underline{f} \neq \underline{0}} \frac{\|D_W \underline{f}\|_M}{\|\underline{f}\|_M} = \sup_{\underline{f} \neq \underline{0}} \frac{\|U_W D_W U_W^{-1} \underline{f}\|_2}{\|\underline{f}\|_2} = \sup_{\underline{f} \neq \underline{0}} \frac{\|S_W \underline{f}\|_2}{\|\underline{f}\|_2},$$

that is

$$\|\mathcal{S}_W\|_{L^2} = \|S_W\|_2.$$

In addition, from (3.24) we have

$$\|(\mathcal{S}_W - k\mathcal{I})^{-1}\|_{L^2} = \|(kI - S_W)^{-1}\|_2 = \|U_W(kI - D_W)^{-1}U_W^{-1}\|_2,$$

with $k \in \mathbb{C}$ and $\mathcal{I}$ and I being respectively the identity operator and matrix. Since D_W is diagonal, it follows that

$$\|(\mathcal{S}_W - k\mathcal{I})^{-1}\|_{L^2} \leq \|U_W\|_2\|(kI - D_W)^{-1}\|_2\|U_W^{-1}\|_2 = \frac{\kappa(U_W)}{\operatorname{dist}(k, \sigma(\mathcal{S}_W))},$$

where $\kappa(U_W) := \|U_W\|_2\|U_W^{-1}\|_2$ is the condition number of U_W.

Before discussing the application of subspace projection methods to the case of matrix pencils, we want to show one of the numerical examples given by Reddy et al. [1993], so that one can assess the effect of the size of the projection subspace on the computed pseudospectra. Reddy et al. [1993] - and their numerical examples are rediscussed by Trefethen and Embree [2005] - consider a discretization of size $n = 1,000$ of the Orr-Sommerfeld operator, and they are interested in the rightmost part of the corresponding pseudospectra as they are interested in analysing its stability properties. Figure 3.4 [Trefethen and Embree, 2005, Figure 40.1] shows its pseudospectra resulting from projection onto eigenspaces of dimension $m = 20, 40, 60$ compared to the unprojected one. In particular, the pseudospectra computed by projecting on a 60-dimensional eigenspace is a perfect approximation of the true pseudospectra in the region of interest, and reducing the dimension of the problem from $n = 1,000$ to $m = 60$ accelerates the compution by a factor of 50 (from four hours to five minutes, according to Trefethen and Embree [2005]). For more numerical examples of subspace projection for the Orr-Sommerfeld operator and other operators, the reader is invited again to refer to Reddy et al. [1993] and to Trefethen and Embree [2005].

In the context of matrix pencils, we just have to make small arrangements. Let $(k_j)_{j=1}^n$ and $(\phi_j)_{j=1}^n$ be now m generalised eigenvalue-eigenvector couples of the equation

$$-\tilde{\Delta}\phi = k^2\tilde{d}^2\phi.$$

We consider the eigenspace W spanned by (ϕ_j) and we consider the generalized eigenvalue problem on W. The operator will be now represented by a matrix

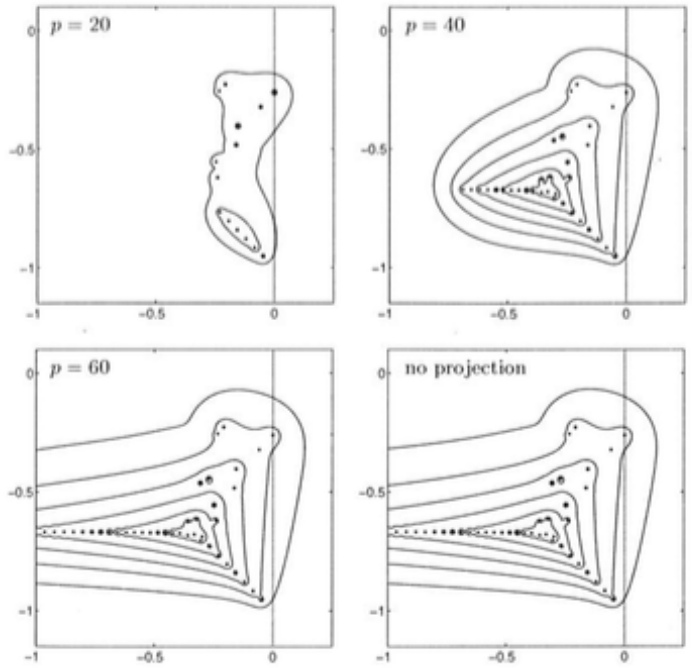

FIGURE 3.4: Pseudospectra of a discretization of the Orr-Sommerfeld operator with $n = 1,000$ by projection onto eigenspaces of dimensions $m = 20, 40, 60$ (p in the Figure) associated with the rightmost eigenvalues. The level sets correspond to $\epsilon = 10^{-2}, 10^{-3}, \ldots, 10^{-7}$. [Trefethen and Embree [2005], Figure 40.1]

pencil (K_W, M_W) of dimension m. Again, we can compute an orthonormal basis $(\psi_j)_j$ for W by applying the QR decomposition to the eigenvectors matrix V_W. Analogously we get the following result for the L^2-norm of the reduced operator

$$\begin{aligned} \|((-\tilde{\Delta} - k^2\tilde{d}^2)|_W)^{-1}\|_{L^2} &= \|(K_W - k^2 M_W)^{-1}\|_2 = \|U_W(K - k^2M)^{-1}U_W^{-1}\|_2 \\ &\leq \|U_W\|_2\|(K - k^2M)^{-1}\|_2\|U_W^{-1}\|_2 = \frac{\kappa(U_W)}{\operatorname{dist}(k, \sigma(K, M))}. \end{aligned}$$

Now we have got an explicit representation of the reduced operator but it has not yet been proved that the reduced operator is a valid approximation of the full operator. Even if this hypothesis can look trivial, we think it is not trivial at all to approximate pseudospectra of an operator with its projection on some eigenspace. Some light on this point has been made by Kressner and Vandereycken [2014], who consider again the case of pseudospectra of a matrix, not of a matrix pencil, and do a partial rather than a full projection.

First of all, they show that, for every $(u_j)_{j=1}^m$ and $(v_j)_{j=1}^m$ orthonormal bases of subspaces $\mathcal{U}$ and $\mathcal{V}$ in $\mathbb{C}^{n\times n}$ with $\mathcal{U} \subset \mathcal{V}$, we have $\sigma_\epsilon(AU, U) \subset \sigma_\epsilon(AV, V) \subset \sigma_\epsilon(A)$ where U and V are the corresponding eigenvectors matrix. The extension of this result from matrix to pencil pseudospectra is trivial.

Proposition 3.9. Let U and V be orthonormal bases of subspaces $\mathcal{U}$ and $\mathcal{V}$ in $\mathbb{C}^{n\times n}$ with $\mathcal{U} \subset \mathcal{V}$. Then

$$\sigma_\epsilon(AU, BU) \subset \sigma_\epsilon(AV, BV) \subset \sigma_\epsilon(A, B).$$

Proof. This is really a rewriting of the proof of Lemma 3.1 in Kressner and Vandereycken [2014]. Let $ks \in \sigma_\epsilon(AU, BU)$. By definition of pencil pseudospectra,

$$\begin{aligned} \epsilon &> \|AU - kBU\| = \min_{x\in\mathbb{C}^m} \frac{\|(AU - kBU)x\|}{\|x\|} = \min_{u\in\mathcal{U}} \frac{\|(A - kB)u\|}{\|u\|} \\ &\geq \min_{v\in\mathcal{V}} \frac{\|(A - kB)v\|}{\|v\|} = \|AV - kBV\|, \end{aligned}$$

which implies $k \in \sigma_\epsilon(AV, BV)$ and thus shows the first inclusion. The second inclusion follows from the first by noting that $\sigma_\epsilon(A, B) = \sigma_\epsilon(AI, BI)$. □

Even if we have considered only projection on eigenspaces, projections methods can be applied to much more general subspaces. Toh and Trefethen [1996] approximate the pseudospectra of a matrix A by those of the Hessenberg matrices constructed by an Arnoldi iteration, that is equivalent to consider a projection on Krylov subspaces. Moreover, they make the interesting suggestion that for very large problems a combination of the Arnoldi iteration and eigenvalue projections might be advantageous, with a speedup over a naive calculation of pseudospectra on the order of many thousands. This can be the starting point of our further researches.

Algorithm 1 shows the strategy we adopt to compute pseudospectra of operators discretised by FEM. First of all, we compute m eigenvectors of the matrix pencil (A, B) and we make them orthonormal (lines 1-2). Then we project the original pencil (A, B) into the reduced pencil $(\tilde{A}, \tilde{B})$ (lines 5-6). Finally, we loop over each point in a complex grid performing a singular value decomposition (line 12).

When the process is finished, we can plot the contour of the computed values, which are the desired pseudospectra.

Data: A, B, M, m, target, x_0, x_1, y_0, y_1

```
1  Y = m eigenvectors y_i of (A, B) with eigenvalues close to target;
2  Q, R = qr(Y);
3  C = chol(M);
4  P = C^{-1}Q;
5  Ã = P'AP;
6  B̃ = P'BP;
7  x = x_0, ..., x_1;
8  y = y_0, ..., y_1;
9  for l = 1 → size(x) do
10     for j = 1 → size(y) do
11         k = x(l) + i · y(j);
12         S[l, j] = 1/ min(svd(Ã − k^2 B̃));
13     end
14 end
```

Result: Contour plot of the resolvent norm S over (x, y) (i.e. pseudospectra).

Algorithm 1: Pseudocode for the computation of pseudospectra of FEM matrix pencils by eigenspace projection method.

3.5 A Two-Dimensional Rectangular Cavity

In order to show an application of the techniques summarised in the current Chapter, in the present Section we consider acoustic scattering by the a two-dimensional rectangular cavity and we look at its resonances and pseudospectra. In Subsection 3.5.1 we describe the setting of a Dirichlet boundary value problem and the application of PML and FEM, while in Subsection 3.5.2 we show and analyse its pseudospectra in the neighbourhood of scattering poles.

The rectangular cavity in Figure 3.5 has already appeared in the acoustic scattering scientific literature. Chandler-Wilde et al. [2009] provided a two-dimensional Lipschitz domain Ω with boundary Γ for which the resolvent norm $\|A_{k,\eta}^{-1}\|$ of

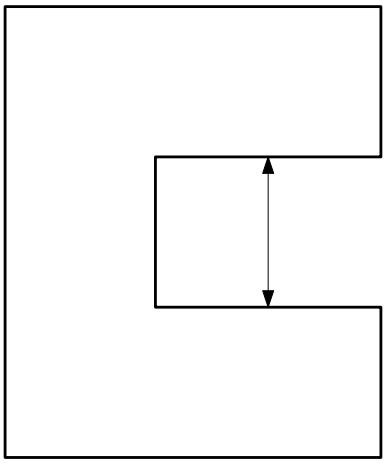

FIGURE 3.5: Two-dimensional rectangular cavity with a trapped ray.

the compined boundary integral operator $\mathcal{A}_{k,\eta} = \mathcal{K}_k + 0.5\mathcal{I} + i\eta\mathcal{V}_k$ grows as $k^{7/5}$ as $k \to +\infty$; such a domain contains a square whose two parallel sides form part of Γ. Later, Betcke and Spence [2011] considered exactly the two-dimensional trapping domain in Figure 5.1 to demonstrate that coercivity for a certain wavenumber k seems to be strongly dependent on the distance to the nearest resonance. The same two-dimensional rectangular cavity was used again by Betcke et al. [2011] to support evidence for some theoretical results on condition number estimates.

3.5.1 The setting

In the present Subsection we consider a two-dimensional acoustic scattering problem involving a two-dimensional rectangular cavity, we describe the application of a spherical PML and the replacement of the physical unbounded domain with a numerical bounded domain, and finally we describe the FEM implementation and the resulting generalised eigenvalue problem.

Let $K \subset \mathbb{R}^2$ be the compact caved rectangle in Figure 5.1, $\Gamma := \partial K$ be its piecewise linear boundary, and $\Omega := \mathbb{R}^2 \setminus K$ be its connected unbounded complement. The obstacle K is a rectangle of dimension $\pi/2 \times 3\pi/5$ with a rectangular cavity of dimension $3\pi/10 \times \pi/5$. We consider the following boundary value problem

involving the Helmholtz equation:

$$\begin{aligned}(-\Delta - k^2)u &= 0 \quad \text{in } \Omega,\\ u &= 0 \quad \text{on } \Gamma,\\ \frac{\partial u}{\partial r} - iku &= O(r^{-1/2}) \quad \text{as } r \to +\infty.\end{aligned}$$

We construct a curvilinear PML as described in Subsection 3.1. The PML starts at some $r_0 > 0$ such that B_{r_0} contains K, and we define $\Omega_0 := \Omega \cap B_{r_0}$. Figures 3.6 shows the setting with $r_0 = 2$. Then we define the damping function $\tilde{\sigma} = \tilde{\sigma}(r)$ as in (3.5), and set $\tilde{d}(r) := 1 + i\tilde{\sigma}(r)$. We continue the solution $u = u(r, \theta)$, $r, \theta \in \mathbb{R}$, analytically into the complex plane by replacing the real radius r with the complex variable $\tilde{r}(r) = \tilde{d}(r)r$. Let $d(r) := \tilde{r}'(r)$. For $r > r_0$ the PML solution $\tilde{u}$ satisfies

$$-\frac{1}{r}\left(\frac{\partial}{\partial r}\left(\frac{\tilde{d}(r)r}{d(r)}\frac{\partial \tilde{u}}{\partial r}\right) + \frac{d(r)}{\tilde{d}(r)r}\frac{\partial^2 \tilde{u}}{\partial \theta^2}\right) - k^2 d(r)\tilde{d}(r)\tilde{u} = 0 \quad \text{in } \Omega. \tag{3.25}$$

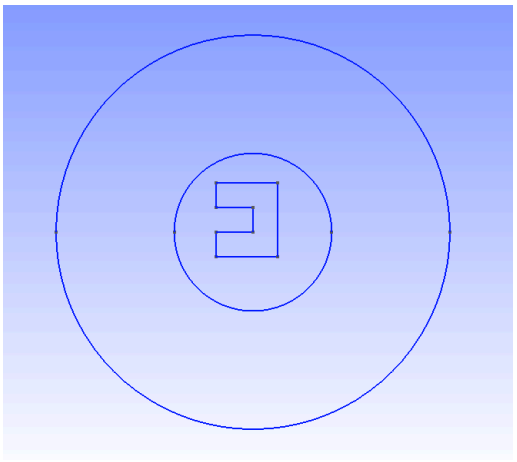

FIGURE 3.6: The rectangular cavity inside circles B_{r_0} and B_{r_2} (the circular annulus is the PML).

In order to solve the two-dimensional problem numerically, it is convenient to define the symmetric matrix function

$$A = A(r, \theta) = \begin{pmatrix} \frac{\tilde{d}(r)}{d(r)}\cos^2\theta + \frac{d(r)}{\tilde{d}(r)}\sin^2\theta & \left(\frac{\tilde{d}(r)}{d(r)} - \frac{d(r)}{\tilde{d}(r)}\right)\cos\theta\sin\theta \\ \left(\frac{\tilde{d}(r)}{d(r)} - \frac{d(r)}{\tilde{d}(r)}\right)\cos\theta\sin\theta & \frac{\tilde{d}(r)}{d(r)}\sin^2\theta + \frac{d(r)}{\tilde{d}(r)}\cos^2\theta \end{pmatrix},$$

and to rewrite the 2d PML Helmholtz equation (3.25) in its divergence form:

$$-\nabla \cdot (A\nabla \tilde{u}) - k^2 d\tilde{d}\tilde{u} = 0 \quad \text{in } \Omega.$$

Finally, we cut the domain: for some $r_2 > r_1$ we replace Ω by the computational domain $\Omega_2 := B_{r_2} \cap \Omega$ and we set $S_{r_2} := \partial B_{r_2}$ (in Figure 3.6 we show $r_2 = 5$). Finally, the computable problem is

$$\begin{aligned} -\nabla \cdot (A\nabla \tilde{u}) - k^2 d\tilde{d}\tilde{u} &= 0 \quad \text{in } \Omega_2 \\ \tilde{u} &= 0 \quad \text{on } \Gamma \cup S_{r_2}. \end{aligned}$$

By using the software FEniCS, we get the generalised eigenvalue equation

$$\tilde{K}\underline{u} = k^2 \tilde{M}\underline{u}, \tag{3.26}$$

where $\tilde{K}$ and $\tilde{M}$ are respectively the complex stiffness and mass PML matrices for the problem and $\underline{u}$ is the vector of coefficients. We can now compute pseudospectra of the PML Helmholtz operator $\mathcal{A}_k := -\tilde{\Delta} - k^2 d\tilde{d}$ by applying Algorithm 1 proposed in Section 3.4 to the matrix pencil $(\tilde{K}, \tilde{M})$.

3.5.2 Spectrum and pseudospectra analysis

In the present Subsection we show plots of the spectrum and of pseudospectra for the matrix pencil appearing in the generalised eigenvalue problem (3.26), which is a FEM discretisation of the PML Helmholtz operator $\mathcal{A}_k := -\tilde{\Delta} - k^2 d\tilde{d}$.

Figure 3.7 shows a portion of the spectrum of the matrix pencil $(\tilde{K}, \tilde{M})$ from (3.26). In the spectrum three distinct parts are observed: the shifted discretisation of the essential spectrum, the isolated resonances and a cloud of spurious eigenvalues due to numerical pollution. The essential spectrum of the Laplacian $\sigma_{\text{ess}}(-\Delta)$ is the closed positive real half line $[0, +\infty)$ [Hislop and Sigal, 1996]. The application of a PML shifts such line in the lower complex half plane and reveals two scattering poles close to the real axis, one near $k = 6$ and one near $k = 10$.

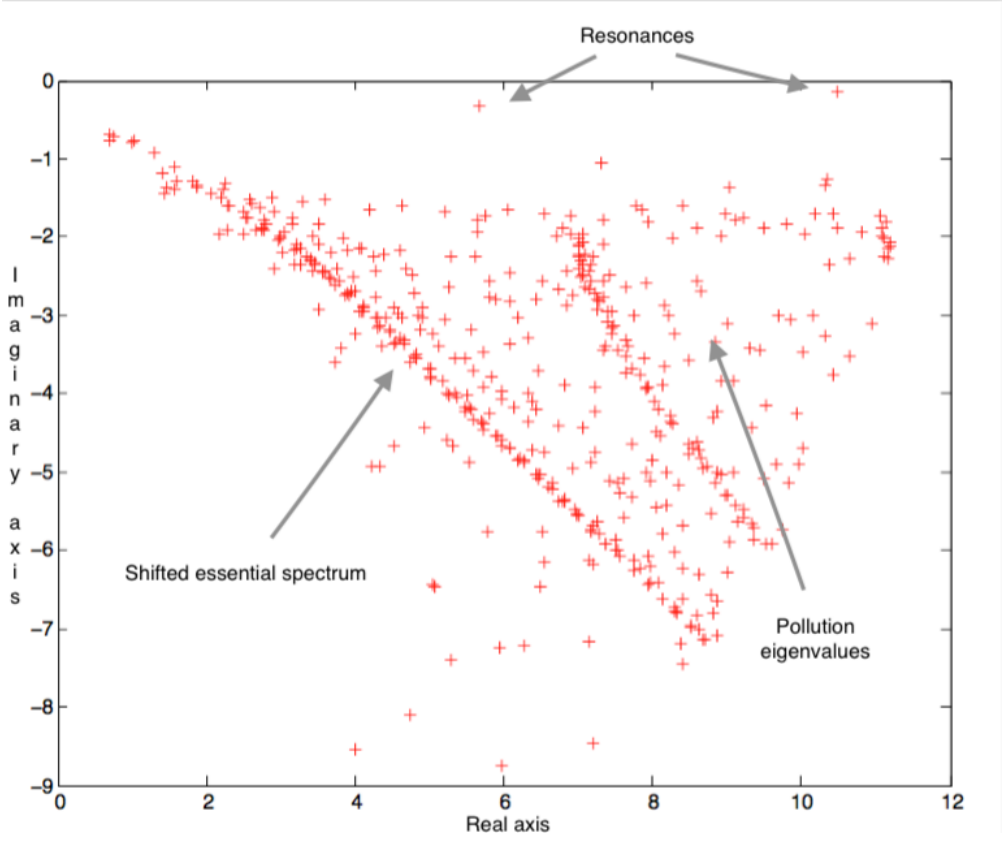

FIGURE 3.7: Portion of the spectrum of the discretised PML operator for the rectangular cavity.

Between the discretised essential spectrum and the resonances, a large number of spurious eigenvalues appear, due to the discretisation procedure. Changing the PML and the FEM parameters, this cloud of eigenvalues moves around between the discretised essential spectrum and the real axis, revealing its non-physical nature. The behaviour of the spurious eigenvalues depends on the distance of the PML from the obstacle [Kim and Pasciak, 2009].

In the following we show pseudospectra $\sigma_\epsilon(\tilde{K}, \tilde{M})$ for different values of the distance $\ell = r_0 - \pi/2$ between the obstacle and the PML. The damping coefficient $\sigma_0 = 1.0$ and the total length of the PML $\delta = r_2 - r_0 = 3.0$ are kept fixed. In particular, we consider the following set of values:

$$\ell \in \left\{ \frac{1}{2}\pi,\ \pi,\ \frac{3}{2}\pi \right\}.$$

The distance ℓ influences both spurious eigenvalues and pseudospectra.

Figure 3.8 shows the norm growth and pseudospectra close to the resonance $k = 5.7 - i0.3$ for $\ell = \pi/2$. The norm growth on the real axis is strongly damped at the boundary of the interval because of the eigenspace projection method (cf. Section 3.4), which has been used for the present computation. Even if the resonance belongs to the complex plane, in its neighbourhood the resolvent norm on the real line is very large, and pseudospectra are confirmed to be the ideal tool to show and quantify such an influence. This first pseudospectra plot highlights another powerful function of pseudospectra: such sets are far from being unions of circles centered in the eigenvalues, and they reveal the non-normality of the PML Helmholtz operator.

Figures 3.10 and 3.12 respectively show pseudospectra for the same modified Helmholtz operator for $\ell = \pi$ and for $\ell = 3\pi/2$. As ℓ increases, the numerical pollution increases and eventually resonances become not appreciable. This confirms a remark already observed by Kim and Pasciak [2009]. Very similar observations can be stated from the analysis of Figures 3.9, 3.11 and 3.13, which show pseudospectra close to the resonance $k = 10.5 - i0.1$. In particular, this pole is closer than the previous to the real axis, and the damping of the resolvent norm on the real axis is even more evident. Moreover, the analysis of $k = 10.5 - i0.1$ reveals another resonance at $k = 11.5 - i0.5$ which was not shown in Figure 3.7.

Figures 3.14, 3.16, 3.18, 3.15, 3.17 and 3.19 suggest further remarks about the non-normality of the PML Helmholtz operator. These are snapshots of the pseudospectra on smaller neighbourhood of the resonant values $k = 5.7 - i0.3$ and $10.5 - i0.1$. As the distance ℓ between the PML and the obstacle increases, pseudospectra around resonances get farther from being circles, suggesting once more the fundamental role of the parameter ℓ in the spectral properties of the modified operator. The application of different PML has deep consequences on the spectral properties of the resulting equation, and depending on the particular problem one may prefer for example the layer to be either closer or farer from the scattering obstacle.

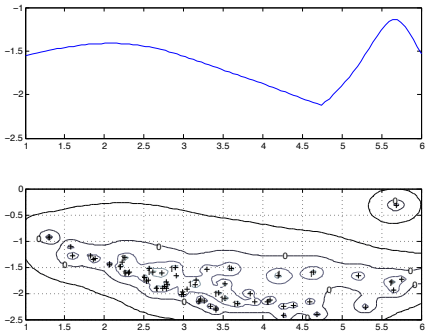

FIGURE 3.8: Norm growth on real line and pseudospectra of the PML operator for the rectangular cavity close to the resonance $k = 5.7 - i0.3$ with $\ell = \pi/2$ (logarithmic scale).

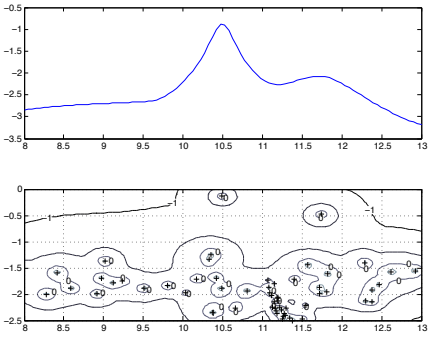

FIGURE 3.9: Norm growth on real line and pseudospectra of the PML operator for the rectangular cavity close to the resonance $k = 10.5 - i0.1$ with $\ell = \pi/2$ (logarithmic scale).

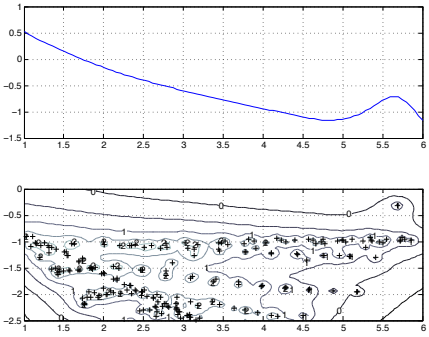

FIGURE 3.10: As in Figure 3.8 with $\ell = \pi$.

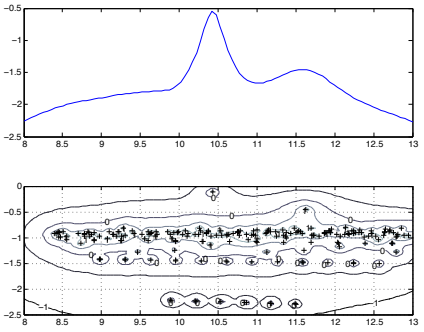

FIGURE 3.11: As in Figure 3.9 with $\ell = \pi$.

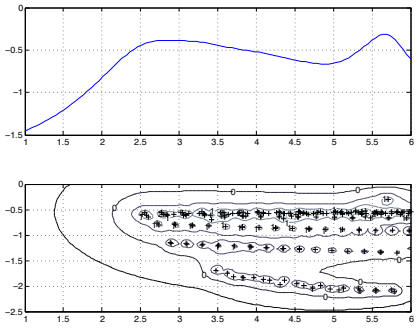

FIGURE 3.12: As in Figure 3.8 with $\ell = 3\pi/2$.

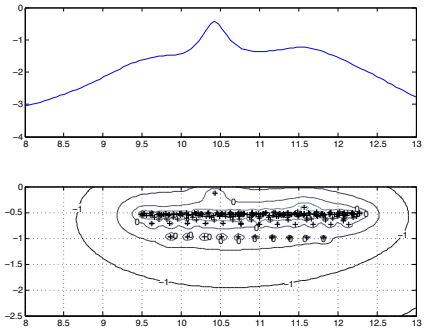

FIGURE 3.13: As in Figure 3.9 with $\ell = 3\pi/2$.

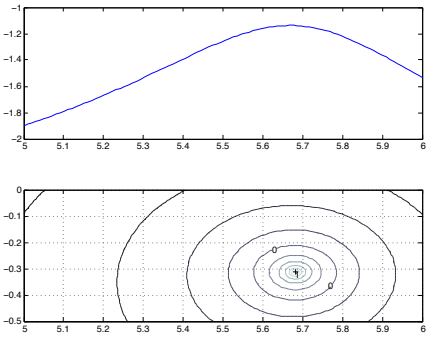

FIGURE 3.14: Detail of norm growth on real line and pseudospectra of the PML operator for the rectangular cavity close to the resonance $k = 5.7 - i0.3$ with $\ell = \pi/2$ (logarithmic scale).

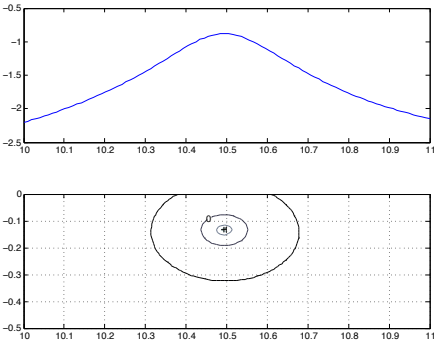

FIGURE 3.15: Detail of norm growth on real line and pseudospectra of the PML operator for the rectangular cavity close to the resonance $k = 10.5 - i0.1$ with $\ell = \pi/2$ (logarithmic scale).

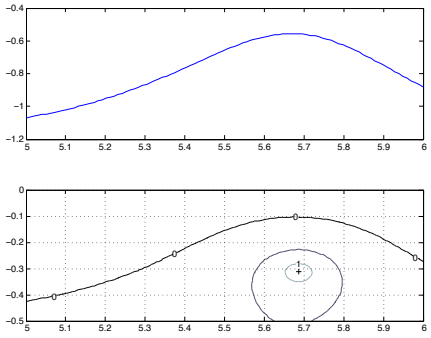

FIGURE 3.16: As in Figure 3.14 with $\ell = \pi$.

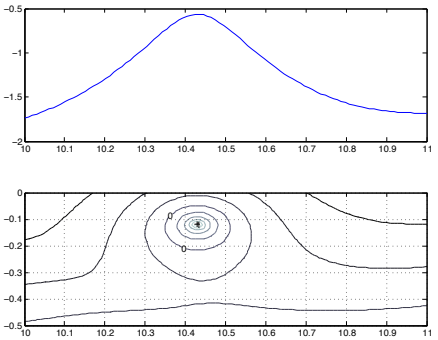

FIGURE 3.17: As in Figure 3.15 with $\ell = \pi$.

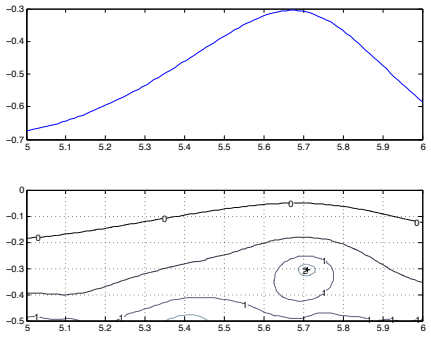

FIGURE 3.18: As in Figure 3.14 with $\ell = 3\pi/2$.

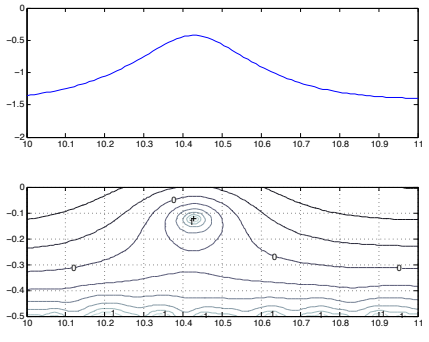

FIGURE 3.19: As in Figure 3.15 with $\ell = 3\pi/2$.

Chapter 4

Boundary Element Methods for computing resonances

An alternative strategy to the application of PML and FEM is represented by the Boundary Element Method (BEM). We call BEM any numerical method for solving linear partial differential equations which have been formulated in boundary integral form, i.e. as boundary integral equations. The present Chapter is devoted to the Galerkin BEM. The main advantage of using BEM to solve boundary value problems on unbounded domains is that this approach reduces a problem defined over an unbounded domain to one defined on a bounded domain of lower dimension, i.e., the boundary of the scattering obstacle. This fact, as we already mentioned, is crucial from the numerical point of view. The BEM does not provide only benefits: boundary integral methods require the numerical integration of singular functions and the possible regularisation of those equations which may not be uniquely solvable due to interior eigenvalues.

The structure of the Chapter is the following. In Section 4.1 we return to the subject of boundary integral equations, already anticipated in Section 1.4, and in particular we treat in more detail the functional setting and some existence and uniqueness results. In Section 4.2 we present theoretical results that we will use in the treatment of acoustic scattering problems, focusing on the differences between BEM and FEM.

The rest of the Chapter is devoted to the algorithms we developed for the numerical computation of resonances and pseudospectra of the Helmholtz boundary integral operators. In Section 4.3 we propose a straightforward direct method which resembles that used for matrices of FEM discretisations. In Section 4.4 we review the Fast Multipole Method (FMM) while in Section (4.5) the theory of $\mathcal{H}$-matrices and Adaptive Cross Approximation (ACA) is summarised. In Section 4.6 we construct an iterative strategy which uses the FMM and the $\mathcal{H}$-matrices. In Section 4.7 we investigate different linear solvers for the iterative method described, while in Section 4.8 we shift our attention to the values of the different tolerances which need to be set in the same method in order to optimise its time performance.

More information about the BEM can be found in Sauter and Schwab [2011]. As elsewhere in the thesis, the computation were performed using Enthought Python Distribution 7.3 on a cluster of workstations with two 2.4 GHz Intel Xeon six-core processors and 189 GB RAM each.

4.1 More about Boundary Integral Equations

In Section 1.4 we have introduced the minimum information about boundary integral equations in order to treat resonances in a self-contained way. In the present Section we intend to extend those notions and to provide a more detailed treatment of boundary integral equations and operators. In particular, we want to give the precise functional setting in which such equations are investigated and solved, and state some existence and uniqueness results.

In Chapter 1 we have introduced the Helmholtz single- and double-layer potentials $\mathcal{S}_k$ and $\mathcal{D}_k$, and we have defined the boundary integral operators $\mathcal{V}_k$, $\mathcal{K}_k$, $\mathcal{K}'_k$ and $\mathcal{T}_k$ as

$$\mathcal{V}_k\sigma := \gamma_0(\mathcal{S}_k\sigma), \qquad \mathcal{K}_k\phi := \gamma_0(\mathcal{D}_k\phi),$$
$$\mathcal{K}'_k\sigma := \gamma_1(\mathcal{S}_k\sigma), \qquad \mathcal{T}_k\phi := -\gamma_1(\mathcal{D}_k\phi),$$

where γ_0 and γ_1 are the exterior Dirichlet and Neumann trace operators. Standard results about trace operators for Lipschitz domain state that for $-1/2 < s < 1/2$ the exterior Dirichlet trace operator

$$\gamma_0 : H^{1+s}_{\mathrm{loc}}(\Omega) \longrightarrow H^{1/2+s}(\Gamma)$$

is continuous [Sauter and Schwab, 2011, Theorem 2.6.8], where the Sobolev space $H^s_{\mathrm{loc}}(\Omega)$ is defined as the set of the continuous linear functionals $u \in C^\infty_{\mathrm{comp}}(\Omega)'$ such that $\phi u \in H^s(\Omega)$ for all $\phi \in C^\infty_{\mathrm{comp}}(\Omega)$, and $C^\infty_{\mathrm{comp}}(\Omega) := C^\infty_0(\mathbb{R}^3)|_\Omega$. Likewise, it is possible to prove that the exterior Neumann trace operator

$$\gamma_1 : H^{1+s}_{\mathrm{L}}(\Omega) \longrightarrow H^{-1/2+s}(\Gamma)$$

is continuous [Sauter and Schwab, 2011, Theorem 2.7.7], with $H^1_{\mathrm{L}}(\Omega) := \{u \in H^1_{\mathrm{loc}}(\Omega) : \ (-\Delta - k^2)u \in L^2_{\mathrm{comp}}(\Omega)\}$. Once defined the Newton potential

$$\mathcal{N}_k f(x) := \int_{\mathbb{R}^3} E_k(x,y) f(y) dy, \quad \forall x \in \mathbb{R}^3,$$

which is continuous as

$$\mathcal{N}_k : H^s_{\mathrm{comp}}(\mathbb{R}^3) \longrightarrow H^{2+s}_{\mathrm{loc}}(\mathbb{R}^3) \quad \forall s \in \mathbb{R},$$

it is possible to redefine the Helmholtz single- and double-layer potentials $\mathcal{S}_k$ and $\mathcal{D}_k$ in terms of the Newton operator and the trace operators as

$$\mathcal{S}_k := \mathcal{N}_k \gamma_0', \quad \mathcal{D}_k := \mathcal{N}_k \gamma_1',$$

where γ_0' and γ_1' are the dual operators of γ_0 and γ_1 respectively [Sauter and Schwab, 2011].

It is now possible to give a full characterisation of the mapping properties of the integral operators defined so far. In fact, for $-1/2 < s < 1/2$ the following

operators are continuous:

$$\begin{aligned} \mathcal{S}_k &: H^{-1/2+s}(\Gamma) \longrightarrow H^{1+s}_{\text{loc}}(\Omega), & \mathcal{D}_k &: H^{1/2+s}(\Gamma) \longrightarrow H^{1+s}_{L}(\Omega), \\ \mathcal{V}_k &: H^{-1/2+s}(\Gamma) \longrightarrow H^{1/2+s}(\Gamma), & \mathcal{K}_k &: H^{1/2+s}(\Gamma) \longrightarrow H^{1/2+s}(\Gamma), \\ \mathcal{K}'_k &: H^{-1/2+s}(\Gamma) \longrightarrow H^{-1/2+s}(\Gamma), & \mathcal{T}_k &: H^{1/2+s}(\Gamma) \longrightarrow H^{-1/2+s}(\Gamma), \end{aligned}$$

[Sauter and Schwab, 2011, Theorem 3.1.16]. With such mapping properties it is now clear in which space one looks for the solution of the boundary integral equations shown in Table 1.2.

We have already discussed that the exterior Dirichlet (ED) and the exterior Neumann (EN) Helmholtz problems with the radiation condition have a unique solution for every $k \in \mathbb{R}$. Yet, we have also already shown that some of the integral equations that appear during the boundary reduction of the interior and exterior problems are identical. As a result, although the exterior problems have a unique solution, the corresponding integral operators are not invertible in the natural Sobolev space on Γ for every wavenumber. As this fact is fundamental for the computation of resonances and pseudospectra by BEM, we conclude the Section with some results about this topic.

For example, the interior Dirichlet (ID) problem with boundary value $f \in H^{1/2}(\Gamma)$ is solved by the integral equation $\mathcal{V}_k\sigma = f$ (cf. (1.34)). It is possible to prove that the single-layer boundary integral operator $\mathcal{V}_k$ is invertible on $H^{-1/2}(\Gamma)$ if and only if k is not an eigenvalue of ID, and that the null space of $\mathcal{V}_k$ is given by

$$\left\langle \gamma_1^- v : \ (-\Delta - k^2)v = 0 \text{ in } K, \ \gamma_0^- v = 0 \text{ on } \Gamma \right\rangle$$

where γ_0^- and γ_1^- are respectively the interior Dirichlet and Neumann trace operators [Sauter and Schwab, 2011, Theorem 3.9.1]. As a result, although ED has a unique solution for all $k \geq 0$, the first kind integral equation (1.34) for ED does not have a solution for all $f \in H^{1/2}(\Gamma)$ if k is an eigenvalue of ID.

A similar result appears for equations of the second kind. We have seen that EN can be solved by solving the boundary integral equation $(\mathcal{K}'_k - 0.5\mathcal{I})g = \sigma$ for

a given $\sigma \in H^{-1/2}(\Gamma)$ (cf. (1.40)). It then turns out that for every eigenvalue k of ID, the boundary integral operator $\mathcal{K}_k' - 0.5\mathcal{I}$ is not injective [Sauter and Schwab, 2011, Theorem 3.9.3], and so EN cannot be solved for all $\sigma \in H^{-1/2}(\Gamma)$ by the integral equation (1.40) if k is an eigenvalue of ID.

Again, if k is an eigenvalue of the internal Neumann (IN) problem and $w \in H^1(K)$, $w \neq 0$, an associated eigenfunction, then $(\mathcal{K}_k + 0.5\mathcal{I})(\gamma_1^- w) = 0$ and $\mathcal{T}_k(\gamma_0^- w) = 0$, and so the boundary integral operators in the equations $(\mathcal{K}_k + 0.5\mathcal{I})f = \phi$ and $\mathcal{T}_k\phi = g$ respectively for ED and EN are not invertible for these values of k.

These observations highlight one of the biggest issues of standard integral equation methods and BEM: the solution of a given problem can be uniquely determined for all k; yet, the corresponding boundary integral equations cannot be solved for the resonant frequencies of the interior problems for arbitrary boundary data. This problem has been overcome by the introduction of modified boundary integral equations [Sauter and Schwab, 2011, Subsection 3.9.4].

4.2 Galerkin BEM

As FEM, Galerkin BEM is based on the restriction of a boundary integral equation to a finite-dimensional subspace. The construction of the finite-dimensional boundary element subspace $\mathcal{P}$ of an Hilbert space $\mathcal{H}$ is now based on a decomposition of the boundary Γ of the domain Ω.

Let $K \subset \mathbb{R}^3$ be a compact obstacle and let its Lipschitz boundary Γ be piecewise smooth in such a way that $\Gamma = \bigcup_{j=1}^J \overline{\Gamma}_j$, where each piece Γ_j admits a local parametrisation $\Gamma_j = g_j(G)$ for some $G \subset \mathbb{R}^2$ and

$$0 < c_j \leq |\det g_j(s)| \leq C_j < \infty, \quad s \in G,\ j = 1, \ldots, J.$$

We then consider a sequence $(\Gamma_N)_{N\in\mathbb{N}}$ of meshes

$$\Gamma_N = \bigcup_{l=1}^{N} \overline{\tau}_l \tag{4.1}$$

where each τ_l is said to be a boundary element. Each boundary element τ_l is supposed to belong to a unique boundary piece Γ_j. A decomposition of Γ_j into τ_l implies a decomposition of the parameter domain G into finite elements $q_{j,l}$ with $\tau_l = g_j(q_{j,l})$. In the present thesis the boundary elements τ_l are always supposed to be triangles.

Given a mesh Γ_N, let us consider the trial space $\mathcal{P}$ of piecewise linear and globally continuous basis functions p_i. Given the boundary decomposition (4.1), a function $u \in \mathcal{P}$ is determined by the values at the mesh nodes $(x_i)_{i=1}^n$. Hence, a basis of the finite-dimensional space $\mathcal{P}$ is given by

$$p_i(x) = \begin{cases} 1 & \text{for } x = x_i, \\ 0 & \text{for } x = x_j \neq x_i, \\ \text{linear} & \text{elsewhere.} \end{cases}$$

In each boundary element τ_l, a piecewise linear function $u \in \mathcal{P}$ is then uniquely determined by the nodal values $u(x_k)$ for x_k vertices of the triangle element, i.e., by using the parametrisation $\tau_l = g_j(q_{j,l})$ we can write

$$u(x) = u(g_j(s)) =: \tilde{u}_{j,l}(s) \quad \text{for } s \in q_{j,l} \subset G.$$

A boundary element $\tau_l \subset \Gamma$ can then be identified with a finite element $q_{j,l}$ in the parameter domain G, and most of the local error estimates which can be proved for FEM can be extended to BEM [Sauter and Schwab, 2011, Steinbach, 2008]. BEM turns out to be nothing but FEM applied to the domain boundary.

Let us consider the application of a BEM to the solution of an exterior Dirichlet (ED) boundary value problem. Given a boundary density ϕ, an indirect formulation for the ED problem lead to the solution $u = \mathcal{D}_k f$ where

$$\left(\mathcal{K}_k + \frac{1}{2}\mathcal{I}\right) f = \phi \tag{4.2}$$

(cf. Table 1.2). As we have seen in the previous Section, the operator $\mathcal{K}_k : H^{1/2}(\Gamma) \longrightarrow H^{1/2}(\Gamma)$ is bounded, and so it is natural to set $f, \phi \in H^{1/2}(\Gamma)$. The corresponding variational formulation is then given as follows: find $\tilde{f} \in H^{1/2}(\Gamma)$

such that

$$\left(g, \left(\mathcal{K}_k + \frac{1}{2}\mathcal{I}\right)\tilde{f}\right)_{L^2(\Gamma)} = (g, \phi)_{L^2(\Gamma)}, \quad \forall g \in H^{-1/2}(\Gamma). \tag{4.3}$$

In the context of Galerkin methods dual spaces play an important role: while the functions on both sides of the boundary integral equation are elements of $H^{1/2}(\Gamma)$, in order for (4.3) to be well defined we need $g \in H^{-1/2}(\Gamma)$ [Sauter and Schwab, 2011, Sub-subsection 3.4.1.2].

By restricting both $H^{1/2}(\Gamma)$ and $H^{1/2}(\Gamma)$ to $\mathcal{P}$, where every function u is uniquely determined with respect to the basis $(p_i)_{i=1}^n$ by some coefficient vector $\underline{u} = (u_i)_{i=1}^n$, i.e.,

$$u = \sum_{i=1}^{n} u_i p_i, \tag{4.4}$$

and by inserting the ansatz (4.4) into (4.3), we obtain

$$\sum_{i=1}^{n} \left(p_j, \left(\mathcal{K}_k + \frac{1}{2}\mathcal{I}\right) p_i\right)_{L^2(\Gamma)} f_i = (p_j, \phi)_{L^2(\Gamma)}, \quad \forall 1 \leq j \leq n.$$

If we give the following definitions:

$$(K_k)_{i,j} = (p_j, \mathcal{K}_k p_i), \quad (M)_{i,j} = (p_j, p_i), \quad \phi_i = (p_i, \phi), \quad 1 \leq i, j \leq n, \tag{4.5}$$

the previous linear system can be written more compactly as

$$\left(K_k + \frac{1}{2}M\right)\underline{f} = \underline{\phi}.$$

The Galerkin solution $\tilde{f}$ results from the vector $\underline{f}$ through (4.4). In order to evaluate the Galerkin solution efficiently, one applies quadrature methods to determine the entries of the system matrix and solves the resulting linear system.

A lot of attention is paid at the question of the stability of the numerical solution $\underline{f}$. If the matrix $K_k + 0.5M$ is invertible, then one is allowed to write

$$\underline{f} = \left(K_k + \frac{1}{2}M\right)^{-1}\underline{\phi}$$

and the solutions vector $\underline{f}$ can be computed by an iterative method. In order to

monitor the propagation of roundoff errors, we are interested in the behaviour of the L^2-norm of such a solution:

$$\begin{aligned} \|\underline{f}\|_{L^2(\Gamma)} &= \left\| \left(K_k + \frac{1}{2} M \right)^{-1} \underline{\phi} \right\|_{L^2(\Gamma)} \\ &\leq \left\| \left(K_k + \frac{1}{2} M \right)^{-1} \right\|_{L^2(\Gamma)} \|\underline{\phi}\|_{L^2(\Gamma)}, \end{aligned}$$

where the resolvent norm $\|(K_k+0.5M)^{-1}\|_{L^2}$ is the well-known quantity we have seen before in the definition of pseudospectra. In this context pseudospectra play then a double role. First, it is well-know how they can provide an insight into the behaviour of iterative methods in the solution of linear system [Higham, 1996, Trefethen and Embree, 2005], and this happens not only in the acoustic scattering field, but in the iterative solution of any linear system $Ax = b$. Secondly, in the specific context we are treating in the thesis, pseudospectra can be used to measure the influence of the wave number k on the stability of the problem, and in particular they can measure the influence of nearest-neighbour resonance on the particular wave number k for which we are solving the linear system.

At this point of our work, we already know what we can expect from the pseudospectra computation of the Helmholtz boundary integral operators. Pseudospectra are the level-sets of the resolvent norm of an operator, and they are meromorphic functions with poles in the singularities of the operator (cf. Chapter 2). Furthermore, as we have shown in Table 1.2, boundary integral equations in interior and exterior problems are coupled and each operator appears twice, both in a formulation for an interior problems and in a formulation for an exterior one. As a result, when pseudospectra are computed, we can expect to see both the eigenvalues of the interior problems and the resonances of the exterior ones. For example, if we compute pseudospectra of the boundary integral operator $\mathcal{K}_k + 0.5\mathcal{I}$, which appears both in the indirect formulation of exterior Dirichlet problems and in the direct formulation of interior Neumann problems, we expect to the see both the interior Neumann eigenvalues and the exterior Dirichlet resonances. This duality will appear in each of the many figures shown in the next Chapter.

In order to compute the pseudospectra of $\mathcal{K}_k+0.5\mathcal{I}$, we need to estimate resolvent norms of the form

$$\left\| \left(\mathcal{K}_k + \frac{1}{2}\mathcal{I} \right)^{-1} \right\|_{L^2(\Gamma)}$$

for a large number of points $k \in \mathbb{C}$. Let us remark that, if one is interested in the Dirichlet resonances and wants to consider the boundary single-layer operator $\mathcal{V}_k$, then the $L^2(\Gamma)$ setting that we consider in this thesis is not appropriate as the range of $\mathcal{V}_k^{-1}$ belongs to $H^{-1/2}(\Gamma)$. More research about the $L^2(\Gamma)$ norm of the single-layer boundary operator $\mathcal{V}_k$ was conducted recently by Spence [2015]. An analysis similar to that shown in the present Section can be conducted for exterior Neumann (EN) boundary value problem by considering a direct formulation with the hypersingular boundary integral operator $\mathcal{T}_k : H^{1/2}(\Gamma) \to H^{-1/2}(\Gamma)$.

Before doing any pseudospectra-specific computation, the primary task in adopting the BEM is the approximation of the coefficients of the system matrix given by integrals of the form

$$\int_\Gamma p_i(x) \int_\Gamma k_k(x,y) p_j(y)\ dS(y)\ dS(x),$$

for some kernel function k_k depending on the boundary integral operator $\mathcal{A}_k$ and the fundamental solution E_k defined in (1.8). The application of a quadrature rule to such integrals leads to sums of the form

$$\sum_{p=1}^{N} p_i(x_p) \sum_{q=1}^{N} k_k(x_p, y_q) p_j(y_q),$$

where $(x_p)_{p=1}^N$ and $(y_q)_{q=1}^N$ are nodes on the boundary Γ. Direct evaluation of such sums, which requires $\mathcal{O}(N^2)$ operations, rapidly becomes inefficient in the economy of a global numerical method. After considering in the next Section a simple algorithm for computation of pseudospectra computation, in the following Sections we are going to consider a popular fast summation method, the Fast Multipole Method (FMM), which reduces the cost of numerical quadrature to $\mathcal{O}(n \log n)$.

4.3 Computation by a direct method

The simplest way of computing pseudospectra of a boundary integral operator $\mathcal{A}_k$ consists in initialising a fine grid in the complex plane and proceeding for each point as follows. First of all, the operators is discretised by a BEM. Moreover, if we are interested in the L^2-norm, an appropriate transformation has to be applied before computing the 2-norm of the matrix, as for FEM (cf. Section 3.3). Finally, the 2-norm is computed by performing a singular value decomposition, as for a matrix A $\|A^{-1}\|_2 = \sigma_{\max}(A^{-1}) = (\sigma_{\min}(A))^{-1}$ where $\sigma_{\max}(A)$ and $\sigma_{\min}(A)$ are respectively the largest and the smallest singular value of A. In the following we describe with more details this approach, whose pseudocode is shown in Algorithm 2.

Data: x_0, x_1, y_0, y_1
$M =$ discretisation of $\mathcal{I}$
$C =$ Cholesky(M) $(M = C^T C)$
$x = x_0, \ldots, x_1$
$y = y_0, \ldots, y_1$
for $i = 1 \rightarrow$ size(y) **do**
  for $j = 1 \rightarrow$ size(x) **do**
    $k = x(i) + iy(j)$
    $A =$ discretisation of $\mathcal{A}_k$
    $\overline{A} = C^{-T} A C^{-1}$
    $S[i, j] = 1/\min(\text{svd}(\overline{A}))$
  end
end
Result: Contour plot of the resolvent norm S over X, Y (i.e., pseudospectra).
Algorithm 2: Pseudocode for the computation of pseudospectra of a boundary integral operator by a direct method for dense matrices.

We perform the discretisation of the boundary integral operators using `BEM++`, an open-source C++/Python library for BEM. `BEM++` provides the Galerkin discretisation of single-, double-, adjoint double-layer potential and hypersingular operator for Laplace, Helmholtz, modified Helmholtz and Maxwell problems in three-dimensions. `BEM++` handles triangular surface meshes and imports them in Gmsh format. Piecewise constant and continuous piecewise linear basis functions are provided, as well as the dense-matrix representation of the boundary integral operators. Moreover, `BEM++` can assemble $\mathcal{H}$-matrix representation of

boundary integral operators via Adaptive Cross Approximation (ACA) providing $\mathcal{H}$-matrix-based preconditioners, and FMM representations. Further information about `BEM++` can be found in Śmigaj et al. [2015] and at the website `www.bempp.org`.

As for FEM, the L^2-norm of a linear operator is not simply the 2-norm of its Galerkin BEM discretisation matrix. If $\mathcal{A}_k$ is a boundary integral operator and A_k is its Galerkin discretisation, again with the same notation for strong and weak operators, we get

$$\left\|\mathcal{A}_k^{-1}\right\|_{L^2(\Gamma)} = \left\|CA_k^{-1}C^T\right\|_2 = \sigma_{\max}\left[CA_k^{-1}C^T\right] = \frac{1}{\sigma_{\min}\left[C^{-T}A_kC^{-1}\right]}. \tag{4.6}$$

In Algorithm 2 we compute the Cholesky decomposition of the mass matrix M, invert and transpose its factor just once before entering the double loop, and then for each grid point we compute the Galerkin discretisation A and the weighted matrix $\overline{A}$ (lines 8-9).

The problem of computing the $L^2(\Gamma)$-norm of the boundary integral operator $\mathcal{A}_k$ is now reduced to computing the minimum singular value of a dense matrix A. At this point, a direct singular value solver (e.g., LAPACK singular value routine wrapped by `numpy.linalg.svd` in Python) can be used (line 10). After iterating the computation for each point of the grid and collecting the values of the norm, we can plot the pseudospectra as the level set of the array.

We tested Algorithm 2 on discretisation matrices of different size of the exterior Neumann trace operator $\mathcal{K}_k + 0.5\mathcal{I}$ on the unit sphere. Table 4.1 reports the corresponding times (in seconds) per grid point. For the plot of Figure 2.1 (matrix of size $2,500 \times 2,500$) Algorithm 2 takes approximately 17 seconds per point. In order to reach a good plotting accuracy, $10,000$ points may be necessary, and the required total time highlights the necessity to develop high performance algorithms for pseudospectra computation of boundary integral operators.

A natural alternative to a dense eigensolver method consists in the adoption of iterative methods. In an iterative method, the solution to a certain problem is approximated iteration-by-iteration, typically using a certain (large) number of matrix-vector products. Yet, such products for dense matrices of dimensions n

cost $\mathcal{O}(n^2)$ operations each. Before exploring iterative techniques for the computation of pseudospectra, we want then to adopt a 'cheap' alternative to dense matrix-vector products.

4.4 The Fast Multipole Method

The Fast Multipole Method (FMM) is a numerical technique that was developed to speed up the calculation of long-ranged forces in n-body problems. The idea at the base of FMM consists in expanding the kernel of a boundary integral using a multipole expansion, which allows to group sources that lie close together and treat them as if they are a single source [Rokhlin, 1985]. The FMM, introduced by Greengard and Rokhlin [1987], is considered one of the top ten algorithms of the 20th century, because it reduces the complexity of matrix-vector products for dense matrices which can arise in many physical problems. In the present Section we review the Fast Multipole Method by describing its application on a surface $\Gamma \subset \mathbb{R}^3$ [Rokhlin, 1993].

Let u be a solution of the Helmholtz equation (1.2) outside an open ball $B_R(x_0)$ of radius R and centre x_0 with the Sommerfeld radiation condition (1.11). Then we have already discussed that there exists a sequence of spherical harmonics $y = (y_m)_{m\geq 0}$, such that

$$u(x) = \sum_{m=0}^{\infty} y_m(\theta,\phi) h_m^{(1)}(kr) \quad \forall x \in \mathbb{R}^3 \setminus \overline{B_R(x_0)} \tag{4.7}$$

where (θ, ϕ, r) are the spherical coordinates of $x - x_0$ and y_m is a spherical harmonic of degree m (cf. Equation (1.20)).

Let Y be the set of all sequences $y = (y_m)_{m\geq 0}$ such that y_m is a spherical harmonic of degree m. We can define the following operator:

$$F : Y \to L^2(S^2), \quad F(y)(\theta,\phi) = \sum_{m=0}^{\infty} y_m(\theta,\phi) e^{-i(m+1)\pi/2}. \tag{4.8}$$

If u is defined by (4.7), then

$$\lim_{t\to+\infty} u(x_0 + tE(\theta,\phi))\ te^{-ikt} = F(y)(\theta,\phi), \tag{4.9}$$

where S^2 is the unit sphere and $E : S^2 \to \mathbb{R}^3$ is its natural embedding in $\mathbb{R}^3$. Because of relation (4.9), $F(y)$ is referred to as the far-field representation of u.

We are interested in the behaviour of expansion (4.7) under translations of x. In particular, let us suppose $u : \mathbb{R}^3 \setminus \overline{D}_1 \to \mathbb{C}$ is an potential analytic outside a ball D_1 and satisfying the Sommerfeld radiation condition, for which the following expansion holds:

$$u(x) = \sum_{m=0}^{\infty} y_m(\theta_1,\phi_1) h_m^{(1)}(kr_1) \quad \forall x \in \mathbb{R}^3 \setminus D_1, \tag{4.10}$$

where (r_1, θ_1, ϕ_1) are the spherical coordinates with respect to the centre c_1 of D_1. Let D_2 be another ball such that $D_2 \cap D_1 = \emptyset$, and let us suppose the function u admits also the following expansion:

$$u(x) = \sum_{m=0}^{\infty} \tilde{y}_m(\theta_2,\phi_2) j_m(kr_2) \quad \forall x \in D_2, \tag{4.11}$$

where j_m is the spherical Bessel function of order m and (r_2, θ_2, ϕ_2) are the spherical coordinates with respect to the centre c_2 of D_2. We can then define the translation operator

$$W_{c_1,c_2} : Y \to Y, \quad W_{c_1,c_2}(y) := \tilde{y}, \tag{4.12}$$

where y and $\tilde{y}$ are the sequences of spherical harmonics defined in (4.10) and (4.11) respectively. Such an operator maps each sequence of spherical harmonics in the exterior expansion with respect to the point $c_1 \in D_1$ into the corresponding sequence of spherical harmonics in the interior expansion with respect to the point $c_2 \in D_2$.

Rokhlin [1993] described the diagonal form of the translation operator W_{c_1,c_2} in the following Theorem, which is one of the main theoretical tools behind FMM. Given $(\theta_0, \phi_0) \in S^2$, $n \in \mathbb{N}$ and $z \in \mathbb{C}$, we define first the operator

$M^{z,n}_{\theta_0,\phi_0} : L^2(S^2) \to L^2(S^2)$ by

$$M^{z,n}_{\theta_0,\phi_0}(f)(\theta,\phi) = \sum_{m=0}^{n} i^m(2m+1)P_m((E(\theta_0,\phi_0),E(\theta,\phi)))f(\theta,\phi)h_m(z), \quad (4.13)$$

where P_m is the Legendre polynomial of order m. The following Theorem proves that such an operator is the diagonal form of the translation operator W_{c_1,c_2}.

Theorem 4.1. Let $(r_{12},\theta_{12},\phi_{12})$ be the spherical coordinates of $c_2 - c_1$, and let $y^n = (y^n_m)_{m\in\mathbb{N}}$ be a sequence of spherical harmonics defined by

$$\tilde{y}^n = F^{-1} \circ M^{kr_{12},n}_{\theta_{12},\phi_{12}} \circ F(y), \quad (4.14)$$

where $F(y)$ is the far-field representation (4.8) of u. If, for any $n \geq 1$, we denote by $u_n : D_2 \to \mathbb{C}$ the potential

$$u_n(x) = \sum_{m=0}^{\infty} \tilde{y}^n_m(\theta_2,\phi_2)j_m(kr_2), \quad (4.15)$$

then for any $x \in D_2$

$$\lim_{n\to\infty} u_n(x) = u(x), \quad (4.16)$$

where u is defined in (4.11).

The previous Theorem contains the fundamental motivation of FMM. Formula (4.14) provides the diagonal form of the operator W_{c_1,c_2} shifting the origin of an expansion in the functions $h^{(1)}_m$ into that of an expansion in the functions j_m; limit (4.16) allows to approximate u on the subset D_2 of its domain $\mathbb{R}^3 \setminus \overline{D}_1$ with the 'truncated' diagonal expansion (4.15). Moreover, in addition to this exterior-to-interior case, Rokhlin [1993] proved similar results for translations for interior-to-interior and for exterior-to-exterior expansions. From this latter results, Rokhlin [1993] derived the following Lemma about the translation properties of the far-field representation of the fundamental solution E_k and its normal derivative.

Lemma 4.2. Let x_1 be an arbitrary point in $\mathbb{R}^3$, $x_1 \neq x_0$. If u in (4.7) is $E_k(x,x_1)$ (i.e., a monopole in x_1), then

$$F(y)(\theta,\phi) = e^{ik(x_0-x_1,E(\theta,\phi))} \quad \forall(\theta,\phi) \in S^2. \quad (4.17)$$

If u in (4.7) is a $\partial_n E_k(x, x_1)$ (i.e., a dipole in x_1 with direction n) potential, then

$$F(y)(\theta,\phi) = e^{ik(x_0-x_1,E(\theta,\phi))} ik \cos(P(x_0-x_1),(\theta,\phi)) \quad \forall(\theta,\phi)\in S^2, \tag{4.18}$$

where $P : \mathbb{R}^3 \to S^2$ is the projection on the unit sphere.

The Lemma allows us to calculate asymptotic representations $F(y)$ of the form (4.8) for monopoles and dipoles without having to evaluate the coefficients of their expansions (4.7) for each different point. This fast formula justifies the multiple expansion at the core of FMM.

As we approach the numerical evaluation of the translation operators, we need to define a suitable notation. Given u from (4.10), we denote by F^n_{u,c_1} the function $F(y)$ tabulated at the n^2 nodes $(\theta_j,\phi_k)^n_{j,k=1}$ on the unit sphere S^2 so that

$$F^n_{u,c_1}(j,k) := F(y)(\theta_j,\phi_k). \tag{4.19}$$

Similarly, for a potential u analytic inside D_2 defined by (4.11) we denote by G^n_{u,c_2} the table of n^2 complex numbers defined by the formula

$$G^n_{u,c_2}(j,k) := F(\tilde{y})(\theta_j,\phi_k). \tag{4.20}$$

Such F^n_{u,c_1} and G^n_{u,c_2} are finite-dimensional approximations of the asymptotic representations of the corresponding potentials u.

Let $D^n \subset S^2$ be the discretisation of the unit sphere. Given a function $G : D^n \to \mathbb{C}$, consider the potential $\overline{G} : \mathbb{R}^3 \to \mathbb{C}$ defined by the formula

$$\overline{G}(x) = \sum_{j,k=1}^{n} w^n_{j,k} G(j,k) e^{ik(x_0-x,E(s^n_{j,k}))}. \tag{4.21}$$

This is a quadrature formula approximating the integral

$$u(x) = \int_{S^2} F(\tilde{y})(s) e^{ik(x_0-x,E(s))}\, ds, \quad x \in D.$$

We then define the map

$$S^{m,n}_{\theta_{12},\phi_{12}} : \mathbb{C}^{n\times n} \to \mathbb{C}^{n\times n}, \quad S^{m,n}_{\theta_{12},\phi_{12}} = M^{kr_{12},m}_{\theta_{12},\phi_{12}}\Big|_{D^n}.$$

As $S^{m,n}_{\theta_{12},\phi_{12}}$ is the restriction of the diagonal form $M^{kr_{12},m}_{\theta_{12},\phi_{12}}$ to the nodes $(\theta_j,\phi_k) \in D^n$, we consider the operator $S^{m,n}_{\theta_{12},\phi_{12}}$ as the discrete approximation of the translation operator $W^{mn}_{\theta_{12},\phi_{12}}$.

Following again Rokhlin [1993], we describe now the procedure to evaluate the potential created by a monopole $E_k(x,x_i)$ (i.e., the case of the boundary integral operator $\mathcal{V}_k$). The case of the potential created by a dipole, of the normal derivative of a monopole potential and of the normal derivative of a dipole potential (i.e., of the boundary integral operators $\mathcal{K}_k$, $\mathcal{K}'_k$ and $\mathcal{V}_k$ respectively) can be treated analogously.

Let us consider the situation depicted in Figure 4.1. The surface $\Gamma \subset \mathbb{R}^3$ is discretised into n uniform nodes $(x_i)_{i=1}^n$, and $(a_i)_{i=1}^n$ are the boundary values at the points $(x_i)_{i=1}^n$ of a certain boundary function a. We are interested in the approximations of sums of the form

$$G_a(x_i) = \sum_{j=1,\ j\neq i}^{n} a_j E_k(x_j,x_i), \quad 1 \le i \le n. \tag{4.22}$$

This n^2 process - evaluating n fields at n points - can be approximated by using Lemma 4.2 and significantly speeded up.

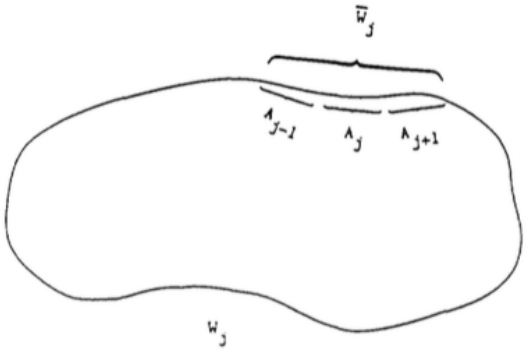

FIGURE 4.1: A surface Γ (from Rokhlin [1993]).

We subdivide the surface Γ into $m \geq 4$ non-intersecting patches P_i, each patch containing approximately n/m nodes x_i. For each i, let r_i be the radius of the smallest circle containing P_i, and $r := \max_i r_i$. For $m \gg 1$, we have

$$r \sim \frac{L}{\sqrt{m}},$$

where L is the diameter of the surface Γ. Let c_i be the centre of the i^{th} patch, A_i be the set of the values a_i such that $x_i \in P_i$, and B_i be the disk of radius r with the centre at c_i. We denote by W_j the union of all A_i such that

$$\|c_j - c_i\| > 3r,$$

and by $\overline{W_j}$ the union of all A_i such that $\|c_j - c_i\| \leq 3r$ (cf. Figure 4.1). As $A_j \subset B_j$ for any j, the triangle inequality implies that

$$\min_{x_i \in A_i, x_j \in A_j} \|x_i - x_j\| \geq r$$

for any i, j such that $A_i \subset W_j$.

Let ϕ_j be the patch potential generated by the values a_i for every i such that $x_i \in A_j$. If $x_i \in A_i$, then

$$G_a(x_i) = \sum_{x_j \in W_i} \phi_j(x_i) + \sum_{x_j \in \overline{W}_i} a_j E_k(x_j, x_i). \tag{4.23}$$

The potential (4.22) is approximated in five steps.

Step 1. For $1 \leq j \leq m$, obtain discretized far-field representations

$$F^n_{\phi_j, c_j}$$

of the patch potential ϕ_j by using Lemma 4.2.

Step 2. For $1 \leq i, j \leq m$ such that $A_i \subset W_j$, calculate the representation

$$G^n_{i,j} = S^{M,n}_{\theta_{ij}, \phi_{ij}}(F^n_{\phi_j, c_j})$$

of the diagonal patch-to-patch potential $\psi_{i,j} = \overline{G^n_{i,j}}$ and view it as an approximation of the far-field representation of the patch potential ϕ_i on B_j.

Step 3. For $1 \leq j \leq m$, view the diagonal patch potential $\psi_j = \sum_i \psi_{i,j}$ as an approximation to the total patch potential $\sum_{A_i \subset W_j} \phi_i$ and calculate its finite-dimensional approximation

$$G^n_{\psi_j, c_j} = \sum_{A_i \subset W_j} G^n_{i,j}.$$

Step 4. For $1 \leq j \leq m$, for all i such that $x_i \in P_j$, approximate the diagonal patch potential $\psi_j(x_i)$ by calculating

$$\overline{G^n_{\psi_j, c_j}}(x_i).$$

Step 5. For $1 \leq j \leq m$, for all i such that $x_i \in P_j$, approximate $G_a(x_i)$ by evaluating the sum

$$\overline{G^n_{\psi_j, c_j}}(x_i) + \sum_{x_l \in \overline{W}_j} a_l E_k(x_l, x_i).$$

For a proper choice of the different parameters, the previous algorithm decreases the computational cost of a matrix-vector product from $\mathcal{O}(n^2)$ to $\mathcal{O}(n^{3/2})$ [Rokhlin, 1993]. Yet, a recursive use of the same algorithm, subdividing each of the sets A_i into subsets $(B_{i,j})_{j=1}^p$, leads to an asymptotic time estimate of $n^{4/3}$. By continuing the process further, until only a small number of nodes are left on a surface patch on the finest level, one can obtain an order $n \log(n)$ algorithm for evaluating a dense matrix-vector product.

The described method, which is often referred to as the high-frequency FMM, breaks down in the case that many of the points reside in a region a wavelength or smaller in size, i.e. in case of low frequencies. then the diagonal translation operators used increase in norm and become ill-conditioned, producing numerical errors [Gumerov and Duraiswami, 2005]. Different subversions of FMM have been proposed in order to target different frequency range and to maintain the $\mathcal{O}(n \log n)$ performance. Yet, the discussion of such modifications is out of the

scope of our thesis, and we invite to refer to Cheng et al. [2006] for further readings on the topic.

At the end of previous Section, we have motivated the investigation of FMM with the need of a cheap alternative to dense matrix-vector products. FMM provides such alternative, and it is an helpful tool when one wants to adopt iterative techniques for the computation of eigenvalues of discretizations of boundary integral operators.

4.5 Hierarchical Matrices and Adaptive Cross Approximation

A technique alternative to FMM for the fast computation of BEM discretization matrices is obtained by using hierarchical matrices ($\mathcal{H}$-matrices). The basic idea of $\mathcal{H}$-matrices consists in replacing subblocks of the original dense matrix with low-rank approximations. The general framework of $\mathcal{H}$-matrices goes back to Hackbush [1999], who introduced $\mathcal{H}$-matrices and their arithmetic, and showed that matrix-vector products can be performed with almost linear complexity for certain matrices, and early research is reported also by Tyrtyshnikov [1998] and Bebendorf et al. [2000]. An extensive introduction to $\mathcal{H}$-matrices is given by Bebendorf [2008] and by Rjasanow and Steinbach [2007]. While many algorithms have been proposed to compute such low-rank approximations, in this thesis we consider Adaptive Cross Approximation (ACA). ACA is proposed by Bebendorf [2000] and Bebendorf and Rjasanow [2003] and aims at finding the low-rank approximation within the $\mathcal{H}$-matrix while only using some of the entries of a dense BEM discretisation matrix.

The comparison between the FMM and $\mathcal{H}$-matrices using ACA for an Helmholtz BEM is another topic which has been throughly investigated. Brunner et al. [2010] compared again the FMM with $\mathcal{H}$-matrices in a half-space Helmholtz BEM problem for both the low- and the high-frequency regime, and showed that the set-up time of $\mathcal{H}$-matrices is longer compared to FMM while the computation time for a single matrix-vector product is significantly faster for $\mathcal{H}$-matrices. Hence, the choice of the most efficient method depends on the case of application.

Another advantage of $\mathcal{H}$-matrices over FMM is that the approximation of the global matrix can be used for preconditioning: a hierarchical LU decomposition-based preconditioner is discussed by [Bebendorf, 2005].

We have already pointed out that the standard matrix-vector product for a dense matrix $A \in \mathbb{C}^{n\times n}$ is in general a $\mathcal{O}(n^2)$ operation. Such an operation is cheaper for rank-k matrices $A \in \mathbb{C}_k^{n\times n}$, which can be written in the outer-product form

$$A = \sum_{i=1}^{k} u_i v_i^H = UV^H, \tag{4.24}$$

with $U, V \in \mathbb{C}^{n\times k}$. The storage requirement in (4.24) is $2kn$ instead of the standard n^2 entries, so the outer-product form (4.24) is advantageous if

$$k < \frac{n}{2}. \tag{4.25}$$

Matrices satisfying (4.25) are said to be low-rank. For such matrices, the matrix-vector product $y = Ax$ can be performed more efficiently by using the outer-product form (4.24) in two steps,

$$z = V^H x, \quad y = Uz,$$

requiring $2kn < n^2$ floating point operations.

Low-rank matrices A^k approximating a full-rank A can be found by using the ACA algorithm [Bebendorf, 2008]. Such algorithm works recursively as follows. Let

$$A^0 = 0 \quad \text{and} \quad R^0 = A$$

be respectively the initial approximation and residual matrices, with $0 \in \mathbb{C}^{n\times n}$ being the zero matrix. For $k \geq 0$, given indexes i_k and j_k, $1 \leq i_k, j_k \leq n$, we define

$$u_k = R^k_{1:n,j_k} \quad \text{and} \quad v_k^H = \frac{1}{R^k_{i_k,j_k}} R^k_{i_k,1:n}$$

and respectively the k^{th} residual and approximation matrices as

$$A^{k+1} = A^k + u_k v_k^H \quad \text{and} \quad R^{k+1} = R^k - u_k v_k^H. \tag{4.26}$$

From (4.26) clearly follows that, for every $k \geq 0$, $A = A^k + R^k$ and $A^k = \sum_{l=1}^{k} u_l v_l^H$ is a rank-k matrix.

As matrices arising from BEM discretizations typically show a singularity along the geometric diagonal $x = y$, the ACA is only applied to matrix partitions, where the column and row corresponds to BEM basis functions with supports far away from each other, while diagonal partitions are stored in the classical dense representation. A visualization of the partitioning of a resulting $\mathcal{H}$-matrix is shown in Figure 4.2, taken from Brunner et al. [2010]. As one can see, when the basis functions represented by a row and by a column are far, large blocks can be approximated with a very low rank.

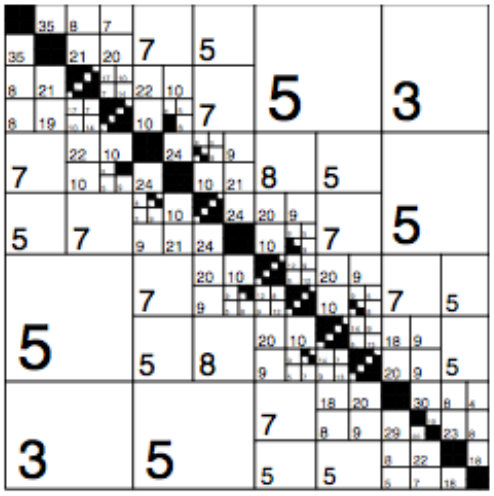

FIGURE 4.2: Example of a $\mathcal{H}$-matrix representation. Black partitions are stored in traditional dense representation. For all other partitions the outer-product form is applied, where the number corresponds to the rank k (from Brunner et al. [2010]).

In order to find separated variables x and y, cluster trees T_I and T_J are respectively built for the index sets I and J of rows and columns by a recursive bisection process. The division stops when a prescribed number of indexes in a cluster is reached. Then, a block cluster tree $T_{I\times J}$ has to be set up from the two cluster trees T_I and T_J . As for the FMM, for a given pair of clusters C_I^ℓ and C_J^ℓ on the level ℓ, the admissibility condition

$$2\min\{r_I^\ell, r_J^\ell\} \leq \eta |z_I^\ell - z_J^\ell| \tag{4.27}$$

is defined, where r_I^ℓ and r_J^ℓ are the radii and z_I^ℓ and z_J^ℓ are the centres respectively of the clusters C_I^ℓ and C_J^ℓ, and η is said to be the admissibility constant. If condition (4.27) is satisfied, then the cluster pair is said to be admissible and the corresponding block is approximated in outer-product form, otherwise either the algorithm is called recursively or the corresponding block is represented exactly in the traditional dense manner.

For $\mathcal{H}$-matrices a hierarchical lower-upper ($\mathcal{H}-LU$) factorization is available [Bebendorf, 2005]. In particular, it is possible to generate an LU decomposition with any prescribed accuracy δ, i.e., a respectively lower- and upper-triangular hierarchical matrices L and U such that

$$\|I_n - A(LU)^{-1}\| < \delta.$$

In order to define the $\mathcal{H}-LU$ decomposition, we exploit the hierarchical block structure of a hierarchical matrix:

$$A_{I,J} = \begin{bmatrix} A_{I_1J_1} & A_{I_1J_2} \\ A_{I_2J_1} & A_{I_2J_2} \end{bmatrix} = \begin{bmatrix} L_{I_1J_1} & \\ L_{I_2J_1} & L_{I_2J_2} \end{bmatrix} \begin{bmatrix} U_{I_1J_1} & U_{I_1J_2} \\ & U_{I_2J_2} \end{bmatrix},$$

where I_1, I_2 and J_1, J_2 are respectively the bisections of I and J. Hence, the LU decomposition of a block A_{IJ} is reduced to the following four problems on the bisections:

1. Compute $L_{I_1J_1}$ and $U_{I_1J_1}$ from the LU decomposition $L_{I_1J_1}U_{I_1J_1} = A_{I_1J_1}$;
2. Compute $U_{I_1J_2}$ from $L_{I_1J_1}U_{I_1J_2} = A_{I_1J_2}$.
3. Compute $L_{I_2J_1}$ from $L_{I_2J_1}U_{I_1J_1} = A_{I_2J_1}$.
4. Compute $L_{I_2J_2}$ and $U_{I_2J_2}$ from the LU decomposition $L_{I_2J_2}U_{I_2J_2} = A_{I_2J_2} - L_{I_2J_1}U_{I_1J_2}$.

If a block has no further bisections, the usual LU decomposition if employed. Further details and results about the $\mathcal{H}-LU$ procedure can be found in Bebendorf [2005].

As we have already mentioned, the ACA have some advantages over the FMM. Besides the fact that no series expansion of the fundamental solution is required and that matrix-vector products are usually faster, an approximation of the whole BEM matrix is stored in an explicit way and this allows to set up preconditioners. Yet, the main drawback of the ACA with respect to FMM consists in its longer setting up time. This is the reason why we have chosen to adopt both the FMM and the ACA in the iterative algorithm for pseudospectra computation described in the next Section.

4.6 Computation by an iterative method

Some features of the direct computation proposed in Algorithm 2 suggest possible improvements. First of all, as the size of the discretisations becomes larger, time can be saved if we can avoid dense matrices assembling and if we rather work with iterative methods and matrix-vector products only. Moreover, as we are interested only in one extreme singular value (the largest or the smallest one), or equivalently in one extreme eigenvalue (as the singular values of a matrix A are the square-rooted eigenvalues of $A^H A$), much can be gained if instead of the whole spectrum we compute just one value by an iterative method. Finally, as only a couple of decimal figures of the norm are necessary to plot pseudospectra, further time can be saved if we choose a value of tolerance higher than that reached by direct solvers in finite arithmetic. Again, in the following we describe each step in more details following Algorithm 3.

First of all, we highlight the mathematical formula underlying this second algorithm. Indicating the largest singular value and eigenvalue of a matrix A respectively by $\sigma_{\max}(A)$ and $\lambda_{\max}(A)$, and the inverse of A^H by A^{-H}, we can rewrite (4.6) as

$$\left\|(\mathcal{A}_k)^{-1}\right\|_{L^2(\Gamma)} = \sigma_{\max}\left[CA_k^{-1}C^T\right] = \left(\lambda_{\max}\left[A_k^{-H}MA_k^{-1}M\right]\right)^{\frac{1}{2}},$$

and we can compute the $L^2(\Gamma)$-norm by the largest eigenvalue of a combination of the matrix A_k and the mass matrix M.

Data: x_0, x_1, y_0, y_1, factor
M = ACA discretisation of $\mathcal{I}$
$PR = []$; $TH = []$
v_0 = random (starting) vector
$x = x_0, \ldots, x_1$; $y = y_0, \ldots, y_1$
$k_1 = x(1) + iy(1)$
A = ACA discretisation of $\mathcal{A}_{k_1}$
P = ACA preconditioner for A
$PR \leftarrow P$
def L2NORM(A, P, v_0):
    def MatVec(x):
        $b_1 = Mx$
        $b_2 = PA \backslash Pb1$
        $b_3 = Mb_2$
        $y = P^H A^H \backslash P^H b_3$
    return y
    $\lambda, v,$ iter = iterative eigensolver on MatVec starting with v_0
    $\sigma = \sqrt{\lambda}$
return $\sigma, v,$ iter
for $j = 1 \rightarrow$ size(y) **do**
    for $i = 1 \rightarrow$ size(x) **do**
        $k_n = x(i) + iy(j)$
        A = FMM discretisation of $\mathcal{A}_{k_n}$
        $P \leftarrow$ nearest point preconditioner from PR
        $S[i, j], v_0,$ iter = L2NORM(A, P, v_0)
        if P is new **then**
            $TH \leftarrow$ factor $\times$ iter
        end
        threshold $\leftarrow$ nearest point threshold from TH
        if iter $>$ threshold **then**
            $k_{n+1} = x(i+1) + iy(j)$
            A = ACA discretisation of $\mathcal{A}_{k_{n+1}}$
            P = ACA preconditioner for A
            $PR \leftarrow P$
        end
    end
end

Result: Contour plot of the resolvent norm S over X, Y (i.e., pseudospectra).
Algorithm 3: Pseudocode for the computation of pseudospectra of a boundary integral operator by an iterative method for FMM representations and ACA preconditioners.

We choose to compute resolvent norms by this formulation with iterative methods for two reasons. First of all, the convergence for largest values is faster, and so the computation of $\sigma_{\max}(A)$ and $\lambda_{\max}(A)$ is usually preferred to that of $\sigma_{\min}(A)$ and $\lambda_{\min}(A)$. Moreover, in order to avoid the explicit inversions of A at each grid point, we perform products $A^{-1}y = x$ and $A^{-H}y = x$ by solving linear

systems $Ax = y$ and $A^H x = y$ with appropriate preconditioners; as the Python library `scipy.sparse` provides the option of using preconditioners for the iterative eigenvalues computation but not for singular value one, we just look for $\lambda_{\max}$ instead of $\sigma_{\max}$ and then take the square-root of the result. Indeed, we use what is known as a 'inner-outer iteration' strategy: roughly speaking, the algorithm consists in iterating a function which, given A, its preconditioners P and an initial vector v_0, defines an appropriate matrix-vector product, where the product by inverses is performed by an iterative linear solver (performing the 'inner' iteration), and then computes the largest eigenvalue by an iterative eigensolver (performing the 'outer' iteration). We will explore inner-outer iteration methods in more depth in Section 4.7.

Two advanced scientific computing techniques are used: Adaptive Cross Approximation (ACA, cf. Section 4.5) and Fast Multipole Method (FMM, cf. Section 4.4). ACA constructs hierarchical matrix approximations based on few of the original matrix entries [Bebendorf, 2008] and preconditioners as approximate LU inverses can then be easily assembled. FMM speeds up the calculation of long-ranged potentials expanding the Green's function by a multipole expansion and, as no explicit matrix assembling is needed, a further speed up is provided in the computation (cf. Section 4.4 for more details).

Algorithm 3 starts building a fine grid for the complex domain and computing the preconditioner P for A by the ACA with a given tolerance `ACATol` using `BEM++` for the very first point (lines 5-8). Let us remark that, as the complex conjugate of the fundamental solution $E_k(x, y)$ defined in (1.8) is $E_{-\overline{k}}(x, y)$, the adjoint operators of $\mathcal{V}_k$, $\mathcal{K}_k$, $\mathcal{K}'_k$ and $\mathcal{T}_k$ with respect to the complex $L^2(\Gamma)$ inner product (2.1) are respectively is $\mathcal{V}_{-\overline{k}}$, $\mathcal{K}'_{-\overline{k}}$, $\mathcal{K}_{-\overline{k}}$ and $\mathcal{T}_{-\overline{k}}$, we initialise two different FMM representations and assemble two different ACA preconditioners, which are not exactly one the conjugate transpose of the other. Nonetheless, we use the notation A, A^H and P, P^H.

When the preconditioners have been computed, A and A^H are initialised by FMM (line 22). Once both the preconditioners and the FMM representations have been created, they can be passed to the function `L2NORM` (line 24) together with a starting vector for the iterative eigensolver (this can be a random vector

for the first complex grid point). The approximated norm, the leading eigenvector and the number of interior iterations will be returned, and we pass to the next point. After the first step, one passes to `L2NORM` the last computed eigenvector as starting vector for the iterative eigensolver (as Lui [1997] proposed for singular vectors in the computation of linear pseudospectra) and the preconditioners computed at the nearest available node (line 23).

In fact, there is no need of computing new preconditioners at each step, as their effectiveness is large on a wide area around the point where they have been created. In order to speed up the computation, we save the computed preconditioners in a list $PR = [\dots]$ (lines 8 and 33) and we assemble new ones only if the number of iterations passes a given threshold (lines 29-34). This saves us from computing new preconditioners at every step which would not improve significantly the performance of the linear solver. Moreover, such a threshold value for the number of iteration is not fixed, but depends on interior iterations performed at the preconditioners node by some threshold factor (lines 25-28). The threshold values are saved in an appropriate list $TH = [\dots]$ (lines 2 and 26). By adopting such an 'adaptive' threshold, we take into account the intrinsic ill-posedness of the wave-numbers close to resonances and we make our method more flexible and efficient.

Figure 4.3 shows in the left column the nodes at which the preconditioners are actually computed (red dots) over the contour plot of pseudospectra for different values of the threshold factor ($2, 3, 5$ times the number of matrix-vector products in the preconditioner nodes, respectively) for the exterior Dirichlet trace operator $\mathcal{K}_k + 0.5\mathcal{I}$ on the unit sphere of Figure 2.1. A variable threshold takes into consideration the increasing ill-posedness of operator discretisations for large values of k and avoids the very inhomogeneous preconditioner grids that would arise with fixed iteration thresholds. The right column of Figure 4.3 shows what the preconditioner grids would look like with fixed thresholds ($8, 16, 32$ matrix-vector products respectively), where most of the preconditioners are assembled close to the eigenvalues, where the operator is worse conditioned.

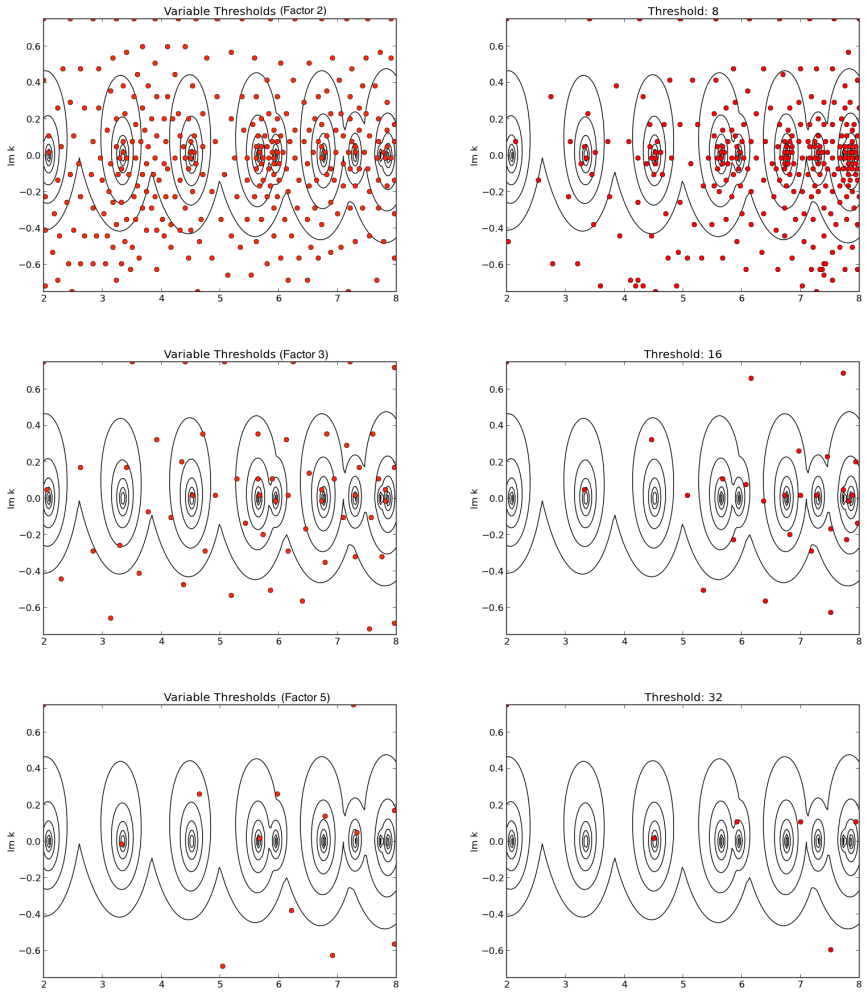

FIGURE 4.3: Preconditioners nodes over the contour plot of pseudospectra for different values of the threshold factor ($2, 3, 5\times$ matrix-vector products respectively) on the left column, while on the right column for fixed threshold ($8, 16, 32$ matrix-vector products respectively).

The function `L2NORM` takes as input the BEM discretisation matrix A, its preconditioner P and the approximated eigenvector v_0, and it returns the singular value σ (which is the approximated L^2-norm of the corresponding boundary integral operator), the eigenvector v and the number of required iterations. `L2NORM`, which is the core of Algorithm 3, performs the inner-outer iteration strategy. In order to avoid explicit inversions, the matrix-vector product function for $A^{-H}MA^{-1}M$ is implemented in lines 10-15 by the solution of two linear systems, for A and A^H respectively (lines 12 and 14). An iterative 'inner' linear solver (e.g., Generalized Minimal Residual implemented by `scipy.sparse.linalg.gmres` in Python) is used with preconditioners P and P^H

to approximate the solution of the linear systems only up to a certain tolerance `gmresTol`. The function `L2NORM` then uses an iterative 'outer' eigenvalue solver (e.g., Implicitly Restarted Arnoldi Method, IRAM, implemented in Python by `scipy.sparse.linalg.eigs`) with the given starting vector v_0 to approximate the largest eigenpair up to a given tolerance `eigsTol` (line 16). The function returns the largest singular value, the leading eigenvector and the number of 'inner' iterations needed by the linear solver to reach the chosen accuracy.

We report in Table 4.1 the time performance of the iterative algorithm and we compare it with the dense algorithm previously presented. The tolerances chosen for the computations presented in this Thesis are $\texttt{AcaTol}, \texttt{LuTol} = 10^{-3}$, $\texttt{EigsTol} = 10^{-2}$ and $\texttt{GmresTol} = 10^{-5}$, while the threshold factor is 2 (that is, in each point the threshold is twice the number of matrix-vector products performed at the point where the used preconditioners have been assembled). Figure 4.4 shows that, while the time required by Algorithm 2 grows approximately as the cube of the matrix size, the complexity of Algorithm 3 looks log-linear.

TABLE 4.1: Performances of Algorithms 2 (Direct) and 3 (Iterative).

Matrix size	Direct	Iterative
2,500	16.9s	5.6s
3,260	34.0s	7.5s
4,500	84.7s	10.9s
6,280	228.3s	16.4s
9,800	793.3s	29.4s
17,100	3,803.9s	90.4s

Before passing to the next Section, we mention an alternative formulation of the norm computation problem. Given a matrix A of shape $n \times n$, the singular value problem $Av = \sigma u$ is equivalent to the $2n \times 2n$ eigenvalue problem

$$\begin{bmatrix} & A \\ A^H & \end{bmatrix} \begin{bmatrix} u \\ v \end{bmatrix} = \lambda \begin{bmatrix} u \\ v \end{bmatrix},$$

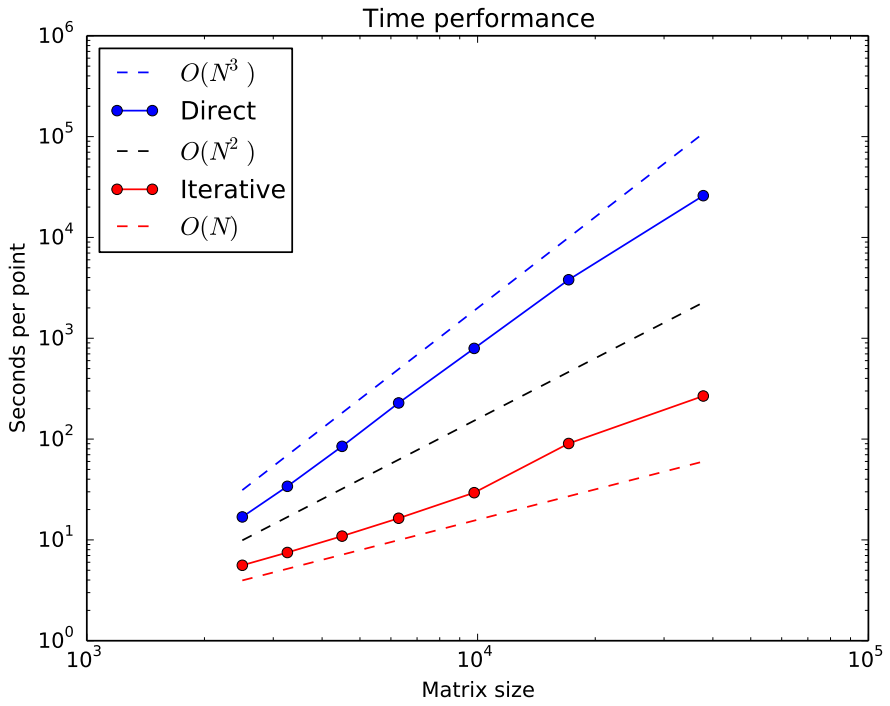

FIGURE 4.4: Logarithmic plot of the time performance of Algorithm 2 (direct method) and Algorithm 3 (iterative method).

with $\sigma = |\lambda|$. Then the largest singular value of $CA^{-1}C^T$ can be computed as the largest eigenvalue of the matrix product

$$\begin{bmatrix} & A^H \\ A & \end{bmatrix}^{-1} \begin{bmatrix} M & \\ & M \end{bmatrix}. \tag{4.28}$$

Using (4.28) we can compute pseudospectra by solving a unique $2n \times 2n$ linear system at each outer iteration instead of two $n \times n$ systems, halving the total inner iterations of the linear solver. Yet, numerical tests show that this formulation is not competitive with Algorithm 3, as the number of the eigensolver iterations more than double: Figure 4.5 shows a semilogarithmic plot of such iterations with respect to the wavenumber $k \in [2, 8]$ for the unit sphere whose pseudospectra are reported in Figure 2.1 ('A' is the iterative Algorithm 3 while 'B' is the alternative formulation). The number of green peaks are greater than the number of blue peaks and the total number of linear solver ('inner') iterations is bigger for (4.28) despite halving the iterations at each eigensolver ('outer') iteration.

This phenomenon can be explained looking at the eigenvalues effectively computed by IRAM, which are different in the two-$(n \times n)$-system and in the one-$(2n \times 2n)$-system formulations (in particular, the first are the squares of the seconds). Figure 4.6 shows the six largest magnitude eigenvalues computed by IRAM with the two-$(n \times n)$-system formulation (blue dots) and with the one-$(2n \times 2n)$-system formulations (red dots) for different wavenumbers ($k = 3.0, 4.0, 6.0, 7.0$). It is known that fast convergence of Arnoldi iterations occurs when the eigenvalues are clustered away from the origin [Trefethen and Bau, 1997], and this explains the difference in the IRAM iterations between the two approaches.

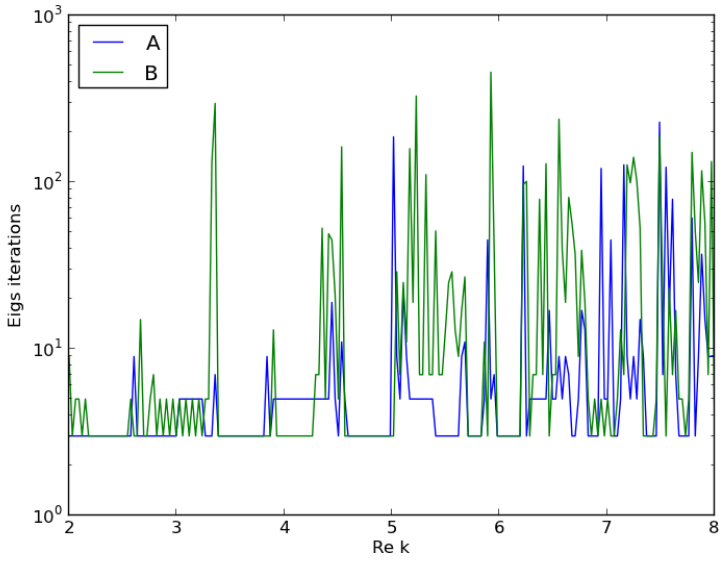

FIGURE 4.5: Semilogarithmic plot of the number of eigensolver iterations with respect to the wavenumber k for the sphere whose pseudospectra are reported in Figure 2.1 ('A' is the iterative Algorithm 3 while 'B' is the alternative formulation 4.28).

4.7 The Inner-Outer Iteration Method

In general, an inner-outer iteration method is any iterative method which, at each iteration, calls another iterative method, in such a way that each 'outer' iteration leads to a certain number of 'inner' iterations. Inner-outer iteration methods, also called nested iteration methods or simply nested methods, arise

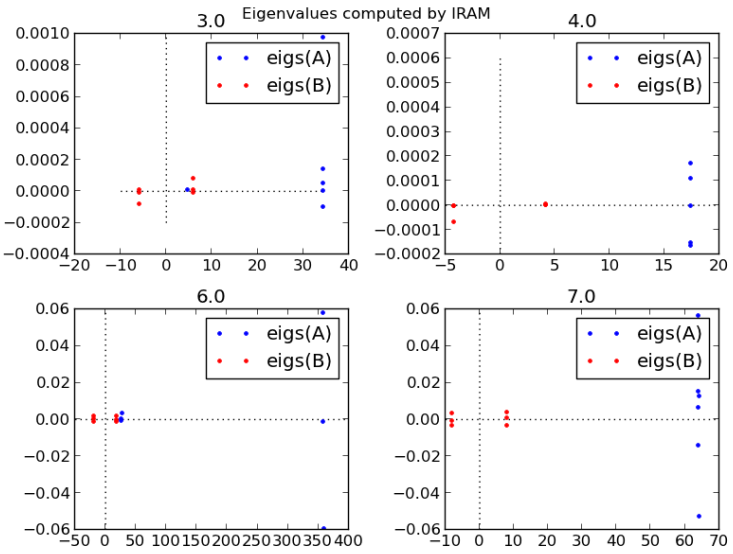

FIGURE 4.6: Semilogarithmic plot of the number of eigensolver iterations with respect to the wavenumber k for the sphere whose pseudospectra are reported in Figure 2.1 ('A' is the iterative Algorithm 3 while 'B' is the alternative formulation)).

naturally in a wide range of different numerical problems [Simoncini and Szyld, 2007].

In the case of pseudospectra computation, one wants to compute the resolvent norm of a linear operator by the smallest eigenvalue of an inverse matrix, so it comes natural to consider iterative eigensolvers which, at each iteration, call a linear solver which replaces the computation of the inverse of the matrix. This is what we have implemented in Algorithm 3. Such an idea is all but new [Freitag, 2007].

In the previous Section we adopted a nested method with GMRES as 'inner' method and IRAM as 'outer' method. Such a choice is arbitrary. In the present Section we investigate different 'inner' linear solvers and their convergence and time performance, while the 'outer' IRAM remains fixed. Further investigation may consider also different 'outer' eigenvalue solvers. In particular, we consider:

1. Generalized Minimal Residual (GMRES);
2. Conjugate Gradient Squared (CGS);
3. Biconjugate Gradient Stabilized (BICGSTAB);

4. Loose Generalised Minimal Residual (LGMRES).

We have measured the time performance of the different 'inner' linear solvers in the computation of pseudospectra of the boundary integral operator $\mathcal{K}_k + 0.5\mathcal{I}$ on the unit sphere by a discretisation of shape $2,500 \times 2,500$ on a complex grid of 10,000 points (with preconditioner threshold factor equal to 2). The results, in seconds per point, are shown in Figure 4.7. The most efficient method is LGMRES with 5.4399 seconds per point on average, outperforming GMRES (5.5898 sec/point) of 2%. Both BICGSTAB (6.1663 sec/point) and CGS (6.2364 sec/point) result to be both slower than GMRES, respectively of a 10% and a 12%.

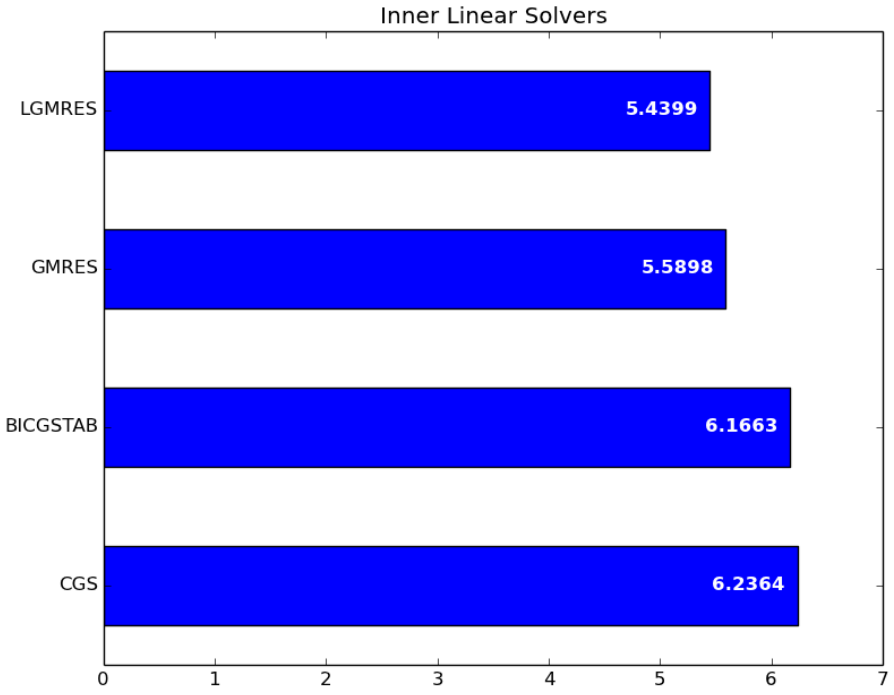

FIGURE 4.7: Average time performance of different 'inner' linear solvers in the computation of pseudospectra of the boundary integral operator $\mathcal{K}_k + 0.5\mathcal{I}$ on the unit sphere by a discretisation of shape $2,500 \times 2,500$ on a complex grid of 10,000 points (threshold factor = 2) [in seconds per point].

Such results can be explained looking at the residual convergence for a few wave numbers k. Figure 4.8 shows residuals over matrix-vector products for the different iterative linear solvers with preconditioners in the case of four different wave numbers: $k_1 = 2.081$, $k_2 = 3.0$, $k_3 = 7.0$ and $k_4 = 7.725$. The choice of such

wave numbers is not casual: while k_1 and k_4 correspond to interior Neumann eigenvalues for the unit sphere, k_2 and k_3 are relatively far from the poles of the resolvent norm. We have opted for the less usual choice of plotting residuals over products than over iterations because different linear solvers define different iterations while the matrix-vector products always represent the most expensive step in each method. A confirmation of this can be seen by a comparison of Figures 4.7 and 4.8: the slightly better performance of GMRES and LGMRES over CGS and BICGSTAB is reflected in the mildly faster convergence of residuals. In Figure 4.8 the difference between the numbers of dots corresponding to each linear solver is due to the different numbers of matrix-vector products performed in a single iteration of each method. In order to make such differences clearer, we finish the Section with a brief overview of the linear solvers which we have tested. Further information can be found in any numerical linear algebra textbook [Golub and Van Loan, 1996, Trefethen and Bau, 1997].

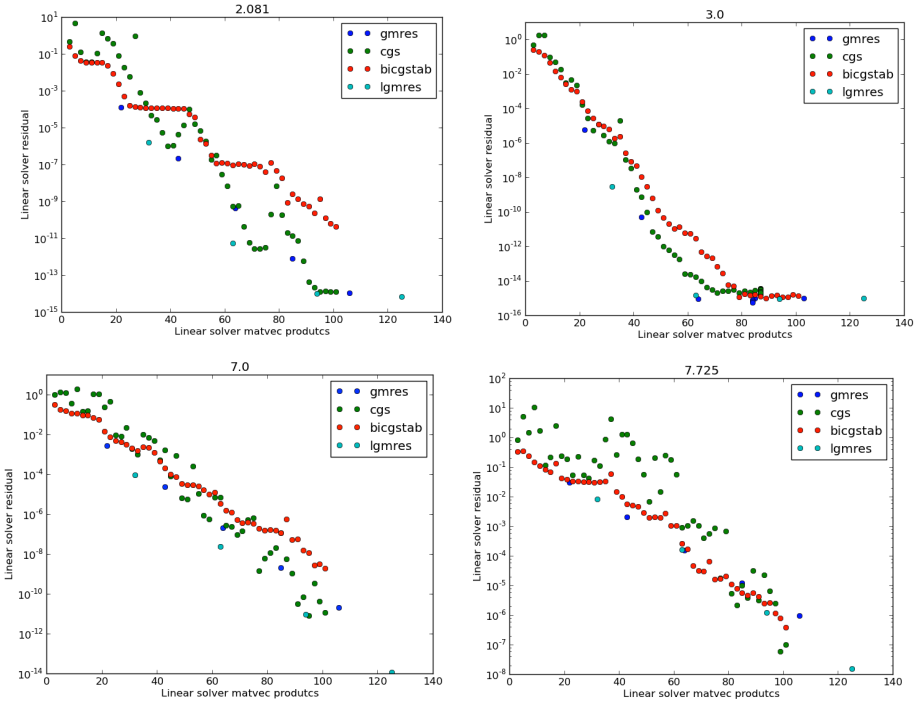

FIGURE 4.8: Residuals over matrix-vector products for the different iterative linear solvers with preconditioners in the case of four different wave numbers ($k_1 = 2.081$, $k_2 = 3.0$, $k_3 = 7.0$, $k_4 = 7.725$).

4.7.1 GMRES

In the GMRES method, proposed by Saad and Schultz [1986], at step i the solution is found from the Krylov subspace

$$\mathcal{K}_i(A, b) := \left\langle b, Ab, A^2b, \dots A^{i-1}b \right\rangle$$

as the vector $x_i \in \mathcal{K}_i(A, b)$ that minimises the Euclidean norm of the residual $r_i := Ax_i - b$. If A has size $n \times n$, then GMRES finds the exact solution in at most n steps; however, the process is usually carried out for a smaller number $m \ll n$ of steps. The approximate solution x_m found after m steps may be used as a new starting estimate for the solution. The resulting method is called GMRES(m) or Restarted GMRES, and it is what is implemented in the Python function `scipy.sparse.linalg.gmres`, which has been used in our computation (with the default value $m = 20$).

The basic idea of GMRES is similar to the Gram-Schmidt procedure to orthonormalize a set of linearly independent vectors; applying the process to a Krylov subspace is called an Arnoldi process. The Arnoldi process, introduced by Arnoldi [1951], is used to reduce a dense matrix to Hessenberg form. First of all, a matrix K_i with columns the orthonormalised vectors $b, Ab, A^2b, \dots, A^{i-1}b$, and an upper Hessenberg matrix $H_{i+1,i}$ are built so that

$$AK_i = K_{i+1}H_{i+1,i},$$

where K_i and $H_{i+1,i}$ have respectively dimension $n \times i$ and $i + 1 \times i$. At step i, the solution x_i is searched in $\mathcal{K}_i$ as $x_i = Ky_i$ with y_i minimising $\|b - AK_iy\|$, which is equivalent to $\|\|b\|e_1 - H_{i+1,i}y_i\|$.

Useful information about the convergence of GMRES arises if we look at the corresponding polynomial approximation problem solved by GMRES [Trefethen and Bau, 1997]: If P_i is the set of polynomials p of degree $\leq i$ with $p(0) = 1$, then find $p_i \in P_i$ such that

$$\|r_i\| = \|p_i(A)b\| = \min .$$

The convergence rate of GMRES is determined by the inequality

$$\frac{\|r_i\|}{\|b\|} \leq \inf_{p_i \in P_i} \|p_i(A)\|.$$

If A is diagonalisable, with $A = V\Lambda V^{-1}$ for some nonsingular V and diagonal Λ, then we have

$$\|p(A)\| \leq \|V\|\|p(\Lambda)\|\|V^{-1}\| = \kappa(V) \sup_{z \in \Lambda} |p(z)|$$

and

$$\frac{\|r_i\|}{\|b\|} \leq \inf_{p_i \in P_i} \|p_i(A)\| \leq \kappa(V) \inf_{p_i \in P_i} \sup_{z \in \Lambda} |p_i(z)|.$$

So, if A is not too far from normal, i.e. $\kappa(V)$ is not too large, and if properly normalised degree i polynomials can be found whose size on the spectrum $\Lambda(A)$ decreases quickly with i, then GMRES converges quickly.

4.7.2 CGS

The Conjugate Gradient Square (CGS) method was originated by Sonneveld [1989] as a modification of the BiConjugate Gradient (BICG) method. BICG is based, as GMRES, on the Krylov subspace $\mathcal{K}_i(A, b)$. Yet, while the principle of GMRES is to find $x_i \in \mathcal{K}_i(A, b)$ such that $r_i \perp \left\langle Ab, A^2b, \ldots, A^ib \right\rangle =: A\mathcal{K}_i(A, b)$ and the norm $\|r_n\|_2$ is minimised, the principle of BICG algorithm is instead to choose $x_i \in \mathcal{K}_i(A, b)$ such that

$$r_i \perp \left\langle s_i, A^H s_i, \ldots, (A^H)^{i-1} s_i \right\rangle =: \mathcal{K}_i(A^H, s_i)$$

for some $s_i \in \mathbb{C}^n$. BICG does not minimise $\|r_n\|_2$, and it is not optimal from the point of view of minimising the number of iterations. Its advantage is that it can be implemented with three-term (x_k, x_{k-1} and q_{k-1}) recurrences rather than the $(n+1)$-term recurrences of GMRES. Moreover, at each step, GMRES requires one matrix-vector multiplication involving A, whereas BICG requires multiplications involving both A and A^H. For problems where matrix-vector multiplications dominate the work, GMRES may consequently be twice as fast

as BICG or faster. There is no guarantee that the method does not break down or become unstable, but in practice is rare.

The Conjugate Gradient Squared (CGS) algorithm is based on the observation that combining two steps of BICG, one can avoid multiplication by A^H and get a 'transpose-free' method that sometimes converges twice as quickly as BICG [Trefethen and Bau, 1997]. In BICG, the residual vector r_i can be written as

$$r_i = P_i(A)r_0$$

where r_0 is the initial residual and P_i is an i-th degree matrix polynomial in A. The same polynomial satisfies

$$s_i = P_i(A^H)s_0$$

so that

$$(s_i, r_i) = (P_i(A^H)s_0, P_i(A)r_0) = (s_0, P_i^2(A)r_0).$$

This suggests that if $P_i(A)$ reduces r_0 to a smaller vector r_i, then it might be advantageous to apply this 'contraction' operator twice, and compute $P_i^2(A)r_0$.

4.7.3 BICGStab

The BiConjugate Gradient Stabilized (BICGStab) method was developed by Van der Vorst [1992] to have a faster and smoother convergence than both BICG and CGS. We have already mentioned that the BICG iteration parameters can be recovered by requiring that, e.g., r_i is perpendicular to $\tilde{P}_j(A^H)s_0$, or, equivalently, that $(\tilde{P}_j(A)P_i(A)r_0, s_0) = 0$, for another suitable set of polynomials $\tilde{P}_j$ of degree j. In BICG one takes $\tilde{P}_j = P_j$, namely, $r_j = P_j(A^H)s_0$. Of course, we can construct other iteration methods, by which x_i are generated so that $r_i = \tilde{P}_i(A)P_i(A)r_0$ with other i-th degree polynomials. E.g., one can take for $\tilde{P}_j$ a polynomial of the form

$$Q_i(x) = (1 - \omega_1 x)(1 - \omega_2 x) \dots (1 - \omega_i x),$$

for suitable constants ω_j. This expression leads to a recurrence relation for the Q_i. An obvious possibility to select ω_j in the j-th iteration step is to minimise r_j,with respect to ω_j, for residuals that can be written as $r_j = Q_j(A)P_j(A)r_0$. As usual, we have used the implementation of BICGSTAB provided by the Python function `scipy.sparse.linalg.bicgstab`.

4.7.4 LGMRES

The Loose GMRES (LGMRES) algorithm was designed by Baker et al. [2005] to avoid slow convergence in GMRES(m) due to alternating residual vectors. In GMRES(m) approximation spaces generated at successive restarts are not orthogonal, so slow convergence or even stalling can occur. In the case of slow convergence, it has been observed that the residual vectors point in nearly the same direction at the end of every other restart cycle, i.e., the 'skip' angle between r_{i+1} and r_{i-1} is small,

$$r_{i+1} \approx \alpha r_{i-1},$$

while 'sequential' angles between consecutive restart cycles remain of reasonable size. In order to prevent this alternating behaviour, LGMRES(m,k) augments the standard Krylov approximation space with k previous approximations to the error $z_{i+1} := x_{i+1} - x_i$. Therefore, at the end of restart cycle $i+1$, LGMRES(m,k) finds an approximate solution as

$$x_{i+1} = x_i + p_{i+1}^{m-1}(A)r_i + \sum_{j=i-k+1}^{i} \alpha_{ij} z_j,$$

where polynomial p_{i+1}^{m-1} and α_{ij} are chosen such that $\|r_{i+1}\|_2$ is minimised. If $k = 0$, then LGMRES(m,k) reduces to GMRES(m).

The implementation of LGMRES(m,k) requires minimal changes to that of the standard GMRES(m). The approximation space becomes

$$\mathcal{M} := \mathcal{K}_m(A, r_i) \cup \left\langle \{z_j\}_{j=i-k+1}^{i} \right\rangle.$$

Typically the number k of vectors appended is much smaller than the restart parameter m. We have used the implementation `scipy.sparse.linalg.lgmres`, where the default values of $k = 3$ and $m = 30$.

4.8 Tolerances in the Inner-Outer Iteration Method

Multiple iterative methods are present in Algorithm 3, and a key step to optimise its time performance consists in choosing appropriate values of the different tolerances. In this Section we describe which is the best choice of such values for the computation of pseudospectra.

At this point of our thesis, we have understood that the computation of pseudospectra is a computationally expensive procedure but it has the advantage that it does not require an accurate estimation of the resolvent norm for all the complex nodes. Values as large as 1e-2, 1e-3, 1e-4 are then reasonable choice for the tolerance of the eigensolver. Yet, supposing that for each point on some complex grid, we want to compute an extreme eigenvalue with 'outer' tolerance of 1e-2, what is the best choice for the linear solver tolerance in order to optimise the performance of our algorithm? This is the first question we want to answer with the present Section.

		GMRES tolerance				
		1e-3	1e-4	1e-5	1e-6	1e-7
IRAM tolerance	1e-2	6.175	6.565	7.185	7.765	8.423
	1e-3	13.98	16.52	18.58	23.23	27.705
	1e-4	94.608	127.72	154.41	184.07	238.45

TABLE 4.2: Time performance (in seconds/point) of Algorithm 3 for pseudospectra computation of $\mathcal{K}_k + 0.5\mathcal{I}$ on the unit sphere over a complex grid of 400 points for different tolerances values for the eigensolver (IRAM) and the linear solver (GMRES).

Table 4.2 shows the time performance (in seconds/point) of Algorithm 3 for pseudospectra computation of $\mathcal{K}_k + 0.5\mathcal{I}$ on the unit sphere over a complex grid of 400 points for different tolerances values for the eigensolver (IRAM) and the linear solver (GMRES). The result is quite clear: a GMRES tolerance value as

large as 1e-3 is sufficient to optimise the code even when the tolerance value required to IRAM is smaller (e.g. 1e-4). Performing more 'inner' iterations in order to get more accurate solutions and to decrease the number of 'outer' iterations is not convenient.

Yet, showing that large values of tolerance guarantee good time performance in such inner-outer iteration method is not enough if we do not take into account accuracy as well. Indeed, the 'outer' eigensolver sees the operator only through the solution of the 'inner' linear solvers, and so different values of linear solver tolerances can potentially describe different linear matrices, and then lead to different resolvent norms. Table 4.3 shows the values of the resolvent norm of $\mathcal{K}_k + 0.5\mathcal{I}$ on the unit sphere in the case of four different wave numbers ($k_1 = 2.081$, $k_2 = 3.0$, $k_3 = 7.0$, $k_4 = 7.725$) for the same tolerances as in Figure 4.2. The accuracy is shown to be more than acceptable from the point of view of pseudospectra computation. In order to complete the comparison, Figure 4.4 shows the values of the resolvent norm for the same operators computed by the dense algorithm (Algorithm 2).

Let us suppose now that we want to compute pseudospectra by an eigensolver tolerance value of 1e-2 and that we choose linear solver tolerance values as large as 1e-2 or 1e-3. What is now the best choice for the preconditioner tolerance (ACA and LU tolerance of Algorithm 3) in order to optimise again the performance of our algorithm? This is the second question we want to answer here.

Table 4.5 shows the time performance (in seconds/point) of Algorithm 3 for pseudospectra computation of $\mathcal{K}_k + 0.5\mathcal{I}$ on the unit sphere over a complex grid of 10,000 points for different tolerances values for the linear solver (GMRES) and the preconditioners (ACA/LU). The result is again limpid: ACA and LU tolerances value as large as 1e+0 is sufficient to optimise the code. Computing accurate preconditioners in order to decrease the number of 'inner' iterations is not the best strategy.

$k_1 = 2.081$		GMRES tolerance				
		1e-3	1e-4	1e-5	1e-6	1e-7
IRAM tolerance	1e-2	854.81	854.11	854.63	855.15	854.13
	1e-3	855.15	855.17	855.17	855.15	855.14
	1e-4	855.17	855.17	855.17	855.17	855.17

$k_2 = 3.0$		GMRES tolerance				
		1e-3	1e-4	1e-5	1e-6	1e-7
IRAM tolerance	1e-2	5.8614	5.8618	5.8616	5.8616	5.8616
	1e-3	5.8616	5.8616	5.8616	5.8620	5.8620
	1e-4	5.8622	5.8621	5.8622	5.8621	5.8622

$k_3 = 7.0$		GMRES tolerance				
		1e-3	1e-4	1e-5	1e-6	1e-7
IRAM tolerance	1e-2	7.9664	7.9670	7.9646	7.9648	7.9674
	1e-3	7.9761	7.9750	7.9761	7.9758	7.9753
	1e-4	7.9766	7.9766	7.9766	7.9766	7.9766

$k_2 = 7.725$		GMRES tolerance				
		1e-3	1e-4	1e-5	1e-6	1e-7
IRAM tolerance	1e-2	167.98	167.98	167.98	167.98	167.98
	1e-3	167.98	167.98	167.98	167.98	167.98
	1e-4	167.98	167.98	167.98	167.98	167.98

TABLE 4.3: Resolvent norm values for $\mathcal{K}_k + 0.5\mathcal{I}$ on the unit sphere in the case of four different wave numbers ($k_1 = 2.081$, $k_2 = 3.0$, $k_3 = 7.0$, $k_4 = 7.725$) for different tolerances values for the eigensolver (IRAM) and the linear solver (GMRES).

k	Res. norm
$k_1 = 2.081$	855.27
$k_2 = 3.0$	5.8622
$k_3 = 7.0$	7.9766
$k_4 = 7.725$	167.97

TABLE 4.4: Resolvent norm values for $\mathcal{K}_k + 0.5\mathcal{I}$ as in Table 4.3 computed through the direct algoritm (Algorithm 2).

		ACA/LU tolerance				
		1e+0	1e-1	1e-2	1e-3	1e-4
GMRES tolerance	1e-2	4.6008	4.7724	4.8069	4.8289	4.8612
	1e-3	4.6157	4.8140	4.8358	4.8506	4.8893

TABLE 4.5: Time performance (in seconds/point) of Algorithm 3 for pseudospectra computation of $\mathcal{K}_k + 0.5\mathcal{I}$ on the unit sphere over a complex grid of 10,000 points for different tolerances values for the linear solver (GMRES) and the preconditioners (ACA/LU).

Although we have considered the same values for the ACA and the LU tolerances, such a choice is not guaranteed to be the best option and further investigation should be done to highlight what the best values are also for these two different tolerances. Morever, we want to underline that the computation in the present Section shows that, at least in the specific case of pseudospectra computation of $\mathcal{K}_k + 0.5\mathcal{I}$ on the unit sphere, a time-efficient choice of the tolerance values for Algorithm 3 is the following:

$$\begin{aligned} \texttt{eigsTol} &= 1\mathrm{e}-2; \\ \texttt{gmresTol} &= 1\mathrm{e}-2; \\ \texttt{AcaTol}, \texttt{LuTol} &= 1\mathrm{e}-0. \end{aligned}$$

There is nothing of general in such a tolerances value choice, but it has shown to be an extremely good starting point for more physically relevant computation as those in Chapter 5. In the very few cases where there is no convergence for some complex point, or the Algorithm 3 has revealed sensibly slower than usual, a tolerance decrease for the linear solver or/and for the preconditioners has solved the issue in most of the cases.

Chapter 5

Three-Dimensional Trapping Domains

One of the most important open questions in acoustic scattering theory concerns the link between the geometry of a generic obstacle K and the scattering poles of the corresponding solution operator $(\mathcal{B}_k)_{k\in\mathbb{C}}$ defined by (1.42). Only for trivial cases the question can be answered analytically. In particular, large interest arises for the class of trapping domains, which can 'trap' acoustic waves and exhibit scattering poles exponentially close to the real axis.

We begin the present Chapter by introducing the notion of trapping domain and by reviewing the so-called Lax-Phillips conjecture (cf. Section 5.1). The rest of the Chapter is a catalogue of different trapping scatterers whose resonances and pseudospectra are investigated by using BEM. In particular, a parallelepipedal and an ellipsoidal cavities, which have already appeared in the acoustic scattering community, are considered in Sections 5.2 and 5.3 respectively. Then new obstacles inspired from very different areas are considered: a Pantheon from civil engineering (Section 5.4), a dumbbell from mechanical engineering (Section 5.5) and a guitar from music (Section 5.6).

5.1 Trapping obstacles

A fundamental question in scattering theory concerns the connection between the geometry of an obstacle K and the analytic properties of the corresponding family of solution operators $(\mathcal{B}_k)_{k\in\mathbb{C}}$ defined by (1.42), in particular the existence and location of scattering poles. The connecting link between the shape of obstacles and the corresponding resonances has been looked for in geometrical optics. In the present Section we review this link, in particular the so-called Lax-Phillips conjecture.

Let us start by defining precisely what we mean by trapping obstacle. As usual, K is a compact obstacle while $\Omega := \mathbb{R}^n \setminus K$ is its unbounded connected complement.

Definition 5.1. Let B_ρ be the ball of radius ρ centered in the origin, and consider all rays starting in $B_\rho \cap \Omega$ and continued according the laws of reflection whenever they impinge on K, until they finally leave the ball B_ρ. One calls K trapping if there are arbitrarily long paths or closed paths of this kind; otherwise, K is non-trapping.

Figures 5.1, 5.2 and 5.3 show examples of two-dimensional trapping geometries.

Lax and Phillips [1967] considered the case $n = 3$ and stated the following conjecture, which in the meantime has become one of the pillar of acoustic scattering theory.

Conjecture 5.2. Trapping obstacles admit an infinite sequence of eigenvalues $(k_j)_j$ such that

$$\text{Im } k_j \longrightarrow 0, \quad \text{Re } k_j \longrightarrow +\infty \quad \text{as } j \to +\infty.$$

Since then, many authors contributed to the study of the connection between the geometry of the obstacle and the location of resonances for any dimension n. Ikawa [1983, 1985] showed that the conjecture is not correct in general, namely he showed two strictly convex objects for which there are no scattering poles k_j with Im $k_j \geq \alpha$ ($\alpha < 0$); yet he admitted that the conjecture remains correct for

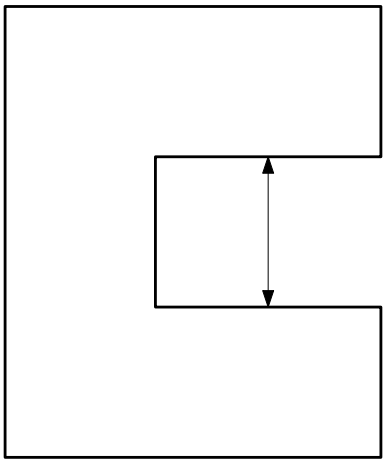

FIGURE 5.1: Two-dimensional rectangular cavity with a trapped ray.

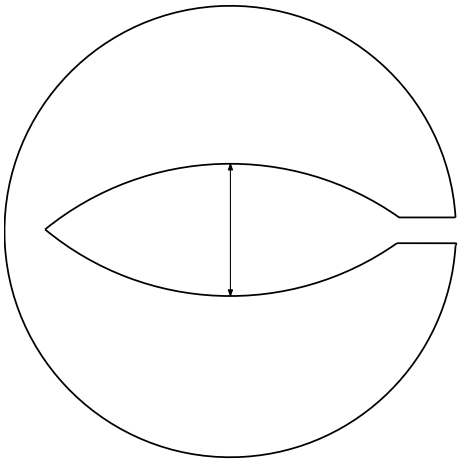

FIGURE 5.2: Two-dimensional elliptic cavity with a trapped ray.

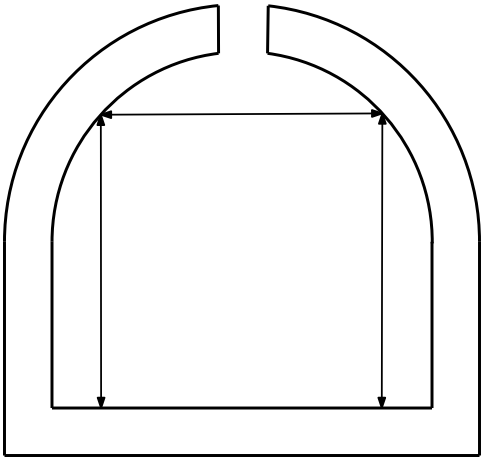

FIGURE 5.3: Two-dimensional dome with a trapped ray.

a great part of trapping obstacles and he was the first to prove for a particular obstacle K the existence of a sequence of resonances converging to the real axis. Stefanov and Vodev [1995, 1996] used the link between resonances and quasimodes to prove that the Lax-Phillips conjecture is true if one restricts attention to trapping domains that contain a trapped ray that is stable under perturbation - a so-called 'elliptic' trapped ray. In this case, there exist resonances close to the quasimodes [Stefanov, 1999, Tang and Zworski, 1998].

Interest in trapping obstacles has not faded in the last decades. Chandler-Wilde et al. [2009] considered the modified boundary integral operator

$$A_{k,\eta} := \mathcal{K}_k + 0.5\mathcal{I} - i\eta\mathcal{V}_k,$$

and showed that the condition number of $A_{k,\eta}$, which grows like $k^{1/3}$ as $k \to \infty$ when the scatterer is a sphere, grows as fast as $k^{7/5}$ for a class of trapping obstacles. Moreover, Betcke et al. [2011] proved that there exist trapping obstacles for which the condition numbers grow as fast as $\exp(\gamma k)$ ($\gamma > 0$) as $k \to \infty$ through some sequence. Again, Betcke and Spence [2011] considered a trapping domain to demonstrate that coercivity for a certain wavenumber k seems to be strongly dependent on the distance to the nearest resonance.

Far for being answered, the question about the link between the shape of an obstacle and the corresponding scattering poles, especially in the case of trapping geometries, is object of current research, and one of the main target of the present thesis is exactly providing more insight on the topic by using pseudospectra. In the following Section we analyse some three-dimensional geometries, whose inspiration comes from very different research areas, not only acoustic scattering but also civil engineering, mechanical engineering, and music.

5.2 A parallelepipedal cavity

The rectangular cavity in Figure 5.4a is already known in the acoustic scattering community. In Chandler-Wilde et al. [2009] the authors give a two-dimensional Lipschitz domain Ω with boundary Γ for which $\|A_{k,\eta}^{-1}\|$ grows as $k \to +\infty$. Such a

domain contains a square whose two parallel sides form part of Γ. Later, Betcke and Spence [2011] considered exactly the two-dimensional trapping domain in Figure 5.4a to demonstrate that coercivity for a certain wavenumber k seems to be strongly dependent on the distance to the nearest resonance. The two-dimensional rectangular cavity was used again in Betcke et al. [2011] to support evidence for some theoretical results on condition number estimates proved in the paper. We consider here the three-dimensional version of the same obstacle, i.e., a parallelepiped with edges of length $3\pi/5, 3\pi/5, \pi/2$ with a parallelepipedal cavity with edges of length $3\pi/10, \pi/5, \pi/5$. The section of such three-dimensional object is the two-dimensional rectangular cavity shown in Figure 5.4a.

Figure 5.4c shows the resolvent $L^2(\Gamma)$-norm and pseudospectra of the double-layer boundary integral operator $\mathcal{K}_k+0.5\mathcal{I}$ on the described scatterer for wavenumbers k in a complex neighbourhood of the real interval $2 < k < 8$. Such operator arises from the indirect formulation of exterior Dirichlet boundary value problems, and so Dirichlet resonances can be sought between its poles (cf. Table 1.2). Yet, the peaks appearing on the real line correspond to interior Neumann eigenvalues, as the same operator arises also in the direct formulation of such a boundary value problem. In the complex plane, a resonance $\tilde{k}$ appears approximately at $7.65 - i0.25$. Pseudospectra, which are shown in a logarithmic plot, appear to be disk centred in the interior Neumann eigenvalues on the left of the Figure, while on the right, that is, close to the resonance $\tilde{k}$, they are far from circular and protrude significantly towards the real line. This behaviour is typical of non-normal phenomena, and modifies the resolvent norm of real wavenumbers in the neighbourhood. Such an example highlights the effect of complex resonances close to real wave-numbers and shows the importance of detecting scattering poles by plotting pseudospectra.

Figure 5.4b shows the double-layer potential $\tilde{u}_k = \mathcal{D}_k\tilde{\phi}_k$ whose density is the eigenfunction $\tilde{\phi}_k$ corresponding to the resonance $\tilde{k}$, i.e., $(\mathcal{K}_{\tilde{k}} + 0.5\mathcal{I})\tilde{\phi}_{\tilde{k}} = 0$. In the physical domain $\Omega = \mathbb{R}^3 \setminus K$ the potential is 'trapped' inside the cavity, and it looks like a perturbation of a low-frequency potential for an interior Dirichlet problem in the corresponding closed cavity. The potential $\tilde{u}_k$ remains defined also inside the obstacle K but no physical meaning is to be attributed to this

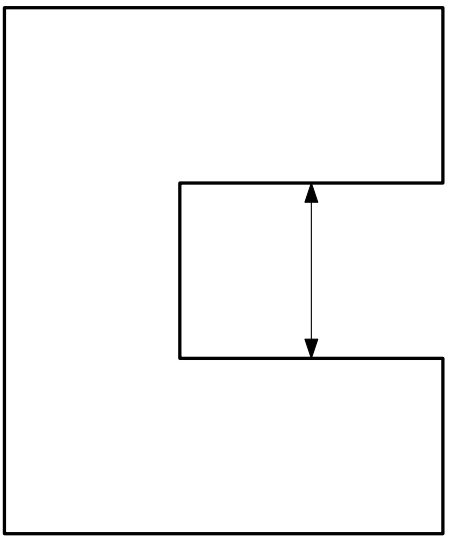

(A) Section of the scatterer with a trapped ray.

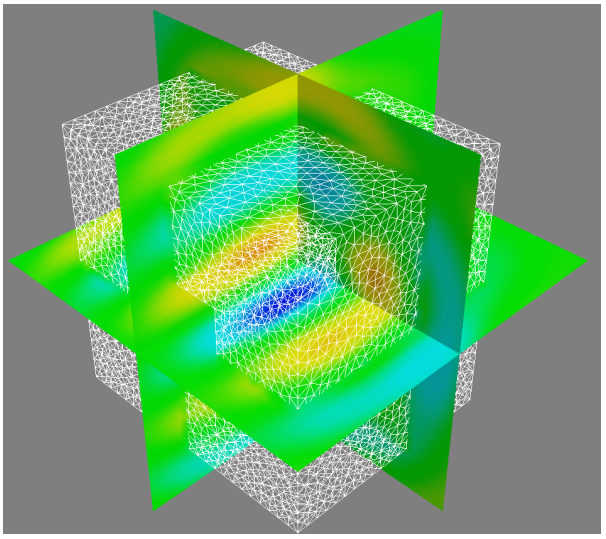

(B) Solution $\tilde{u}$ corresponding to $\tilde{k} = 7.65 - i0.25$.

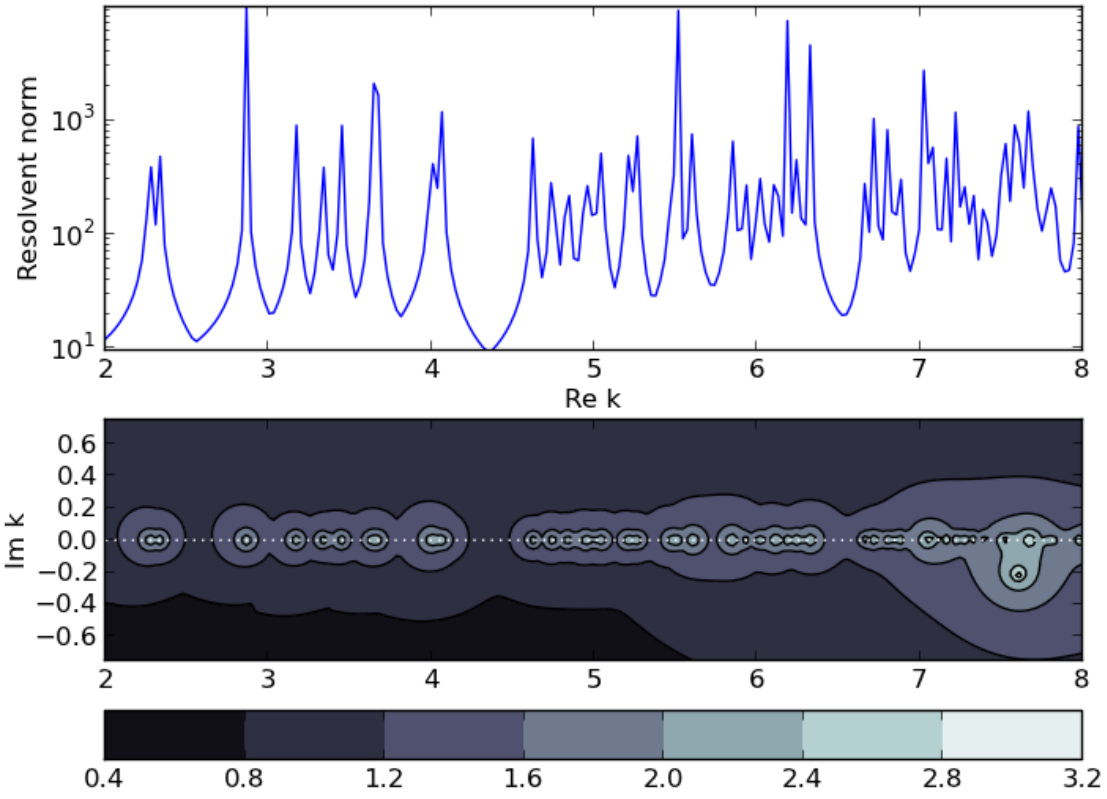

(C) Resolvent norm on the real line (top) and pseudospectra (bottom) of $\mathcal{K}_k + 0.5\mathcal{I}$.

FIGURE 5.4: Parallelepipedal cavity

when the exterior problem is considered (it is the Helmholtz solution of the interior Dirichlet problem with boundary data $-\tilde{\phi}_k$). Outside the cavity the potential $\tilde{u}_k$ visibly starts propagating to infinity, as one can expects from a resonant solution.

5.3 An ellipsoidal cavity

Acoustic scattering by elliptic cavities has been studied as well. Betcke et al. [2011] proved that for two-dimensional domains with an ellipse-shaped cavity, $\|A_{k,\eta}^{-1}\|$ grows exponentially as $k \to \infty$ through some sequence k_m, namely

$$\|A_{k_m,\eta}^{-1}\| \geq C e^{\gamma k_m} \left(1 + \frac{|\eta|}{k_m}\right)^{-1}.$$

We build a three-dimensional scatterer with an ellipsoidal cavity in the following way: inside the unit sphere centred in the origin we consider the solid of revolution generated by the arc with extremes $(.00, .00, \pm.75)$ on the circle centred in $(0, 1, 0)$ and we connect the interior cavity with the exterior sphere by a cylinder of diameter $d = 0.2$ and with the symmetry axis being the revolution axis of the cavity. The section of such a scatterer is shown in Figure 5.5a.

Figure 5.5c shows the resolvent $L^2(\Gamma)$ norm and pseudospectra of the boundary integral operator $\mathcal{K}_k + 0.5\mathcal{I}$ on the described obstacle in a complex neighbourhood of the real interval $10 < k < 12$. We have considered such a wavenumber range because no resonances have been detected close to lower frequencies. Most of the peaks of the resolvent norm correspond again to interior Neumann eigenvalues, which do not look perfectly aligned on the real line (also the pole $k_1^{(IN)} = 10.72 - i0.01$ is an interior Neumann eigenvalue). This effect is probably due to discretisation, although for the plot we used 13-15 elements per wavelength. Yet, among many interior Neumann eigenvalues, a few Dirichlet resonances appear, e.g.,

$$\tilde{k}_1^{(D)} = 10.05 - i0.0, \quad \tilde{k}_2^{(D)} = 11.4 - i0.01, \quad \tilde{k}_3^{(D)} = 11.63 - i0.02.$$

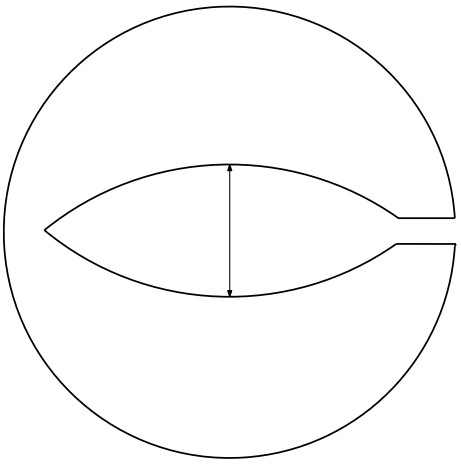

(A) Section of the scatterer with a trapped ray.

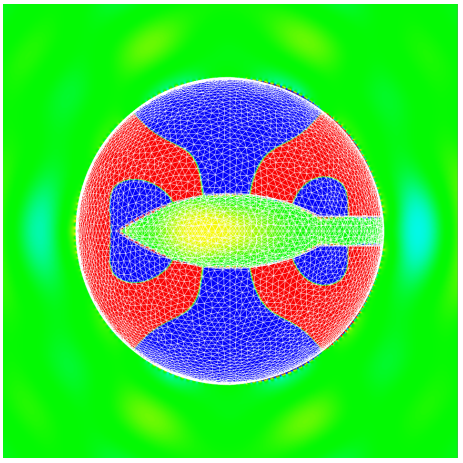

(B) Section of $\tilde{u}_k$ with $k = \tilde{k}_1^{(D)} = 10.05 - i0.01$.

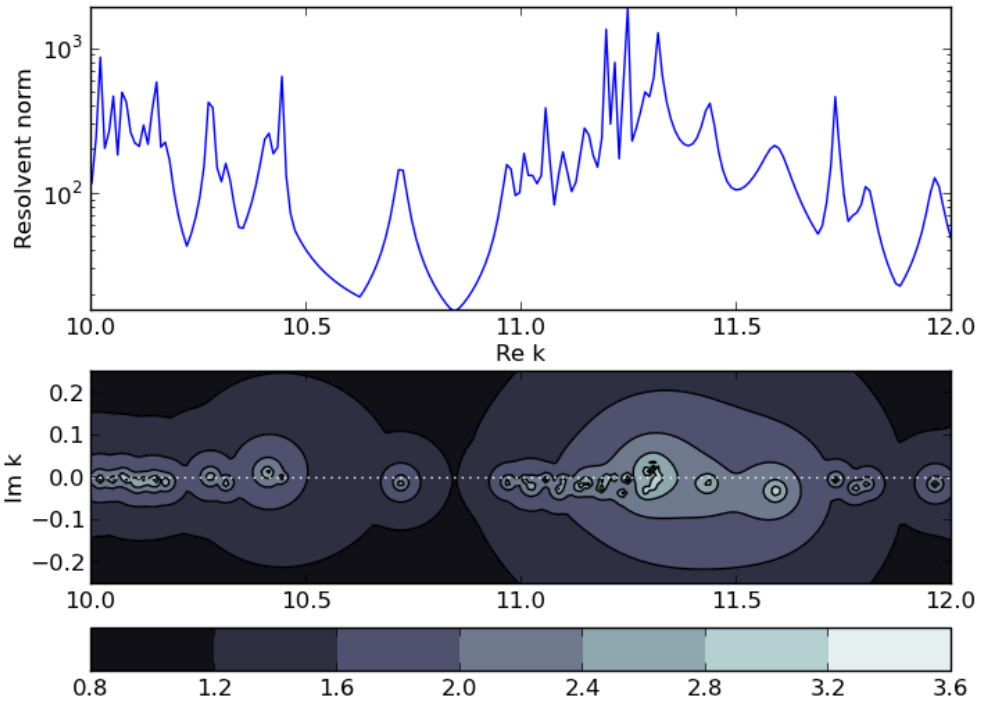

(C) Resolvent norm on the real line (top) and pseudospectra (bottom) of $\mathcal{K}_k + 0.5\mathcal{I}$.

FIGURE 5.5: Parallelepipedal cavity (Dirichlet problem)

The usual comments about the shape of pseudospectra, being circular around eigenvalues but having protruded shaped where resonances prevail, can be repeated for this setting as well.

Figure 5.5b shows the double-layer potential $\tilde{u}_k = \mathcal{D}_k\tilde{\phi}_k$ where the density $\tilde{\phi}_k$ is the eigenfunction of the double-layer boundary integral operator $\mathcal{K}_k + 0.5\mathcal{I}$ corresponding to $\tilde{k}_1^{(D)}$. In the exterior domain Ω, the potential $\tilde{u}_k$ is clearly 'trapped' inside the cavity and appear to be a perturbation of a corresponding interior Dirichlet boundary value problem in the closed elliptic cavity. In the interior domain K the potential corresponds to the Helmholtz solution of the interior Dirichlet problem with boundary data $-\tilde{\phi}_k$, and it is ignored as long as one is interested to exterior Dirichlet problem.

The interpretation of the different poles appearing in Figure 5.5c is not trivial. Crowded clusters of eigenvalues are difficult to analyse, and one cannot guess in advance the nature of a pole without computing either pseudospectra of the hypersingular boundary integral operator $\mathcal{T}_k$ or the potentials whose densities are the eigenfunctions corresponding to each pole. The hypersingular operator $\mathcal{T}_k$ arises in the direct formulation of both exterior and interior Neumann boundary value problem (cf. Table 1.2), and so both exterior Neumann resonances and interior Neumann eigenvalues can be sought between its poles.

Figure 5.6c shows resolvent $L^2(\Gamma)$ norm and pseudospectra of the hypersingular boundary integral operator $\mathcal{T}_k$ in a complex neighbourhood of the real interval $2 < k < 8$, where $\mathcal{K}_k + 0.5\mathcal{I}$ has no resonances. The poles correspond now to interior Neumann eigenvalues and exterior Neumann resonances. In particular, all the poles shown in the Figure are interior eigenvalues apart from the following exterior Neumann resonances:

$$\tilde{k}_1^{(N)} = 5.1 - i0.1, \quad \tilde{k}_2^{(N)} = 6.5 - i0.1.$$

Differently from what we have observed before, in the close neighbourhood of the resonances pseudospectra still look like balls centred in the poles; only large pseudospectra (e.g. look at the boundary of ϵ-pseudospectra with $\epsilon = 10^{0.3}$) cannot be seen as balls centred in the poles.

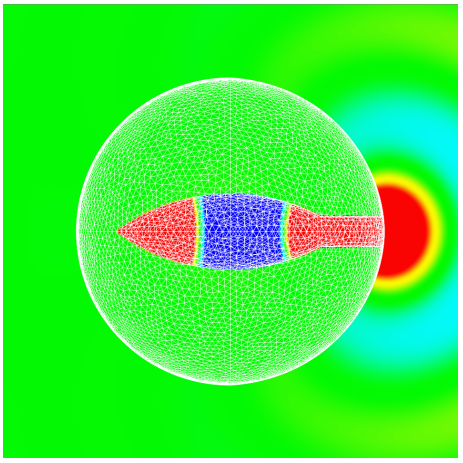

(A) Section of $\tilde{u}_k$ with $k = \tilde{k}_1^{(N)} = 5.1 - i0.1$.

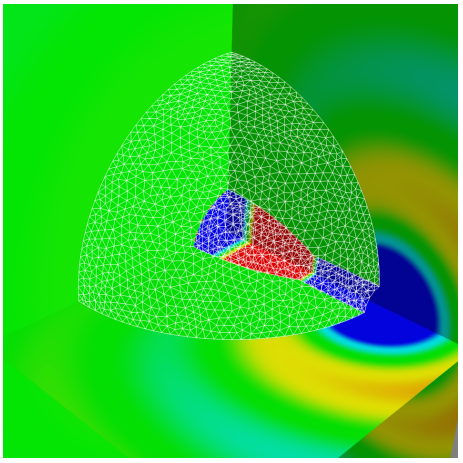

(B) Section of $\tilde{u}_k$ with $k = \tilde{k}_2^{(N)} = 6.5 - i0.1$.

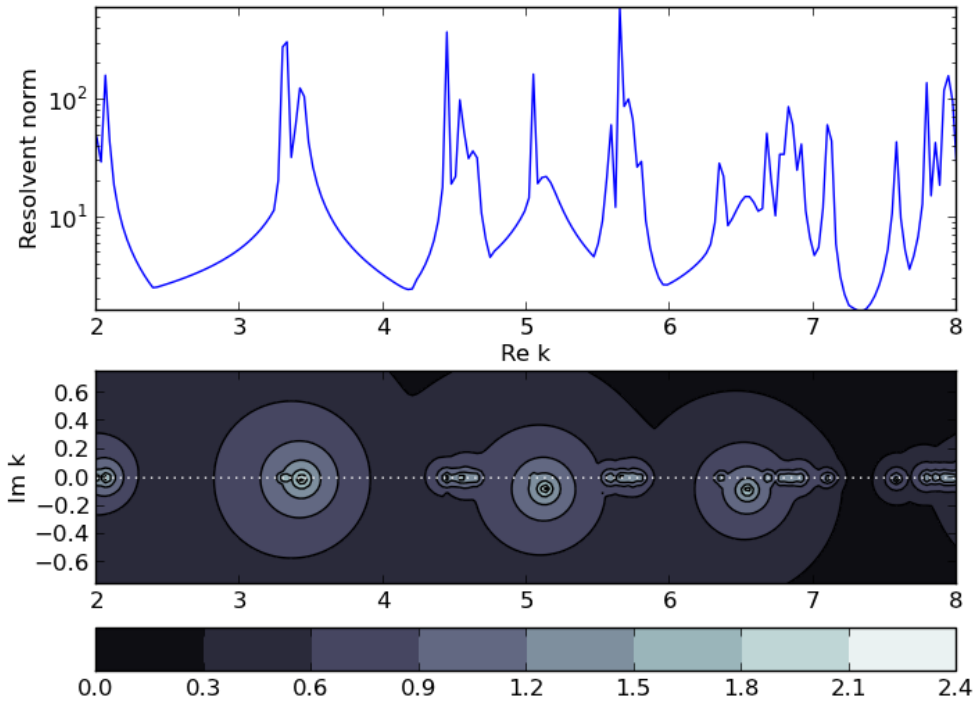

(C) Resolvent norm on the real line (top) and pseudospectra (bottom) of $\mathcal{T}_k$.

FIGURE 5.6: Parallelepipedal cavity (Neumann problem)

The double-layer potentials $\tilde{u} = \mathcal{D}_k\tilde{\phi}_k$, where the densities $\tilde{\phi}_k$ are the eigenfunctions of $\mathcal{T}_k$ corresponding respectively to $\tilde{k}_1^{(N)}$ and $\tilde{k}_2^{(N)}$, are shown in Figures 5.6a and 5.6b. In both the Figures, the potentials are localised inside the cavities and have zero Neumann boundary values. These Figures clearly show how the potentials shift through the conduct of the cavity and propagate in the exterior domain.

5.4 A Pantheon cavity

Acoustic scattering and resonances are not a topic of investigation only for mathematicians and physicists. Large attention to such phenomena is given for example in the field of civil engineering. Sounds and waves are object of investigation for civil engineers in many different context: e.g., noise control [Lacour et al., 2000] and high-speed railway traffic [Fiala et al., 2006]. Inspired from such a background, in the present Section we analyse the case of acoustic scattering by a Pantheon-like building.

We propose a new trapping geometry arising from architecture: the Pantheon-shaped scatterer whose section is shown in Figure 5.7a. As far as we know, no scatterer of this shape has been considered before in the acoustic scattering community. The Pantheon (cf. Figure 5.7b) is a circular-based building in Rome, Italy, of the 1st century AD and, almost two thousand years after it was built, its dome is still the world's largest unreinforced concrete dome. The dome has an oculus whose diameter measures 9.1 metres. The height to the oculus and the diameter of the interior circle are the same, 43.3 metres, so the whole interior would fit exactly within a cube (also, the interior could house a sphere 43.3 metres in diameter). Our model neglects the variable thickness of the dome, which varies from 6.4 metres at the base to 1.2 metres around the oculus, and it is normalised with respect to the inner radius such that the interior would perfectly house the unit sphere. All the other sizes are kept in scale.

Figure 5.7c shows again pseudospectra of the double-layer boundary integral operator $\mathcal{K}_k + 0.5\mathcal{I}$ on the Pantheon model for the usual complex neighbourhood of the real interval $1 < k < 4$. All the poles shown look to be perfectly on the

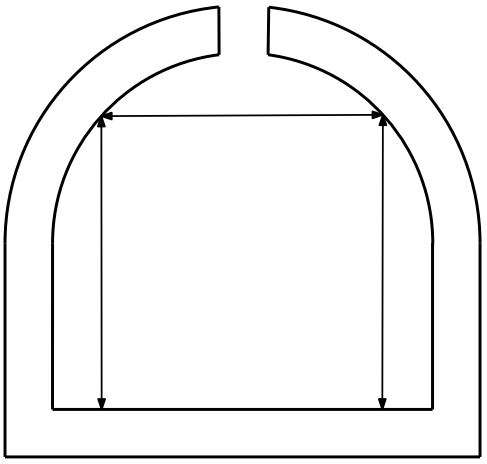

(A) Section of the scatterer with a trapped ray.

(B) Pantheon, Rome (from `mmdtkw.org/`).

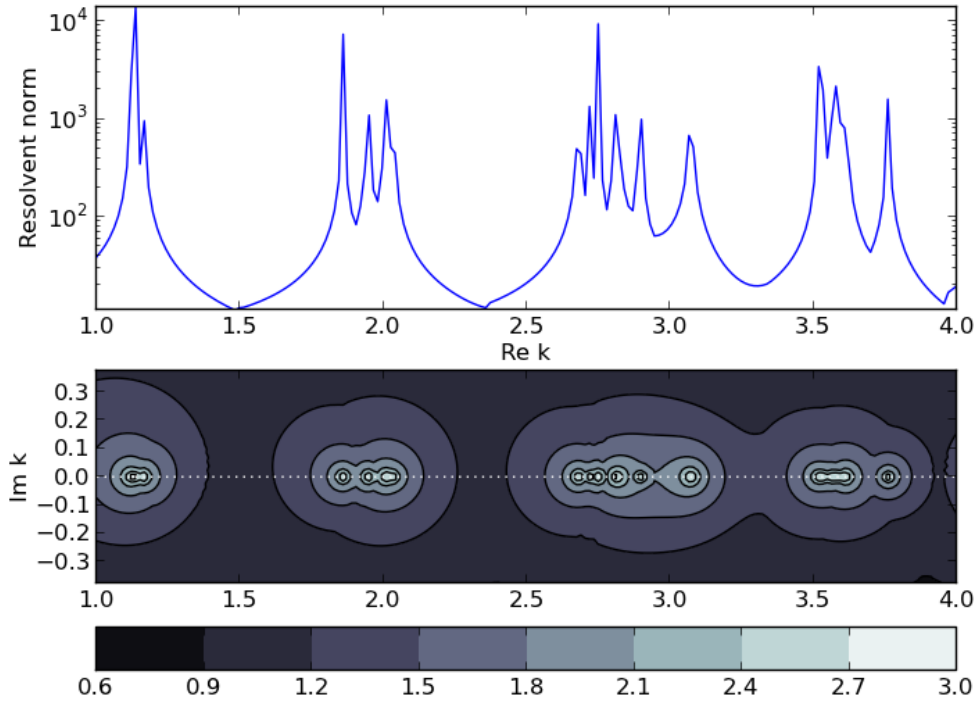

(C) Resolvent norm on the real line (top) and pseudospectra (bottom) of $\mathcal{K}_k + 0.5\mathcal{I}$.

FIGURE 5.7: Parallelepipedal cavity

real line and may be thought to be interior Neumann eigenvalues at first sight. By computing the corresponding eigenfunction, the value

$$k_1^{(D)} = 3.07$$

is revealed to be a resonance which lies exponentially close to the real line, as described by the Lax-Phillips conjecture. It is worth remarking the usual note about the shape of pseudospectra around resonances: while such sets appear to be balls centred in the interior Neumann eigenvalues, close to the exterior Dirichlet resonance pseudospectra appear to be strongly protruded to their left. The effect on real wave-number is evident from the upper part of the Figure: despite the distance between the peak corresponding to the resonance and its nearest left neighbourhood, the resolvent norm does not decrease as much as it does in narrower ranges (e.g. between 3.6 and 3.8). Figure 5.7c shows perfectly how resonances are responsible for non-normal behaviours.

As usual, Figure 5.8 shows the double-layer potential $\tilde{u}_k = \mathcal{D}_k\tilde{\phi}_k$ where the density $\tilde{\phi}_k$ is the eigenfunction of $\mathcal{K}_k + 0.5\mathcal{I}$ corresponding to $k_1^{(D)}$. The potential $\tilde{u}_k$ is perfectly 'trapped' inside the Pantheon cavity, looking almost like a low-frequency solution of the interior Dirichlet problem for the closed cavity. As we have seen before, the potential remains defined also inside the obstacle K but there it has no physical connection to the exterior Dirichlet problem we are considering.

5.5 A dumbbell cavity

Another applied field where acoustic scattering and resonances play a relevant role is mechanical engineering. Devices such as manufacturing plants, industrial equipments and machineries, heating and cooling systems, transport systems, aircrafts, watercrafts, robotics, medical devices and weapons, can be made only after a careful analysis of the acoustic phenomena happening inside and around them. Acoustic phenomena are an object of current investigation between mechanical engineers in different areas: from agricultural machineries cabins insulation [Desmet et al., 2003] to fluid mechanics [Ziada, 2006], from electronic

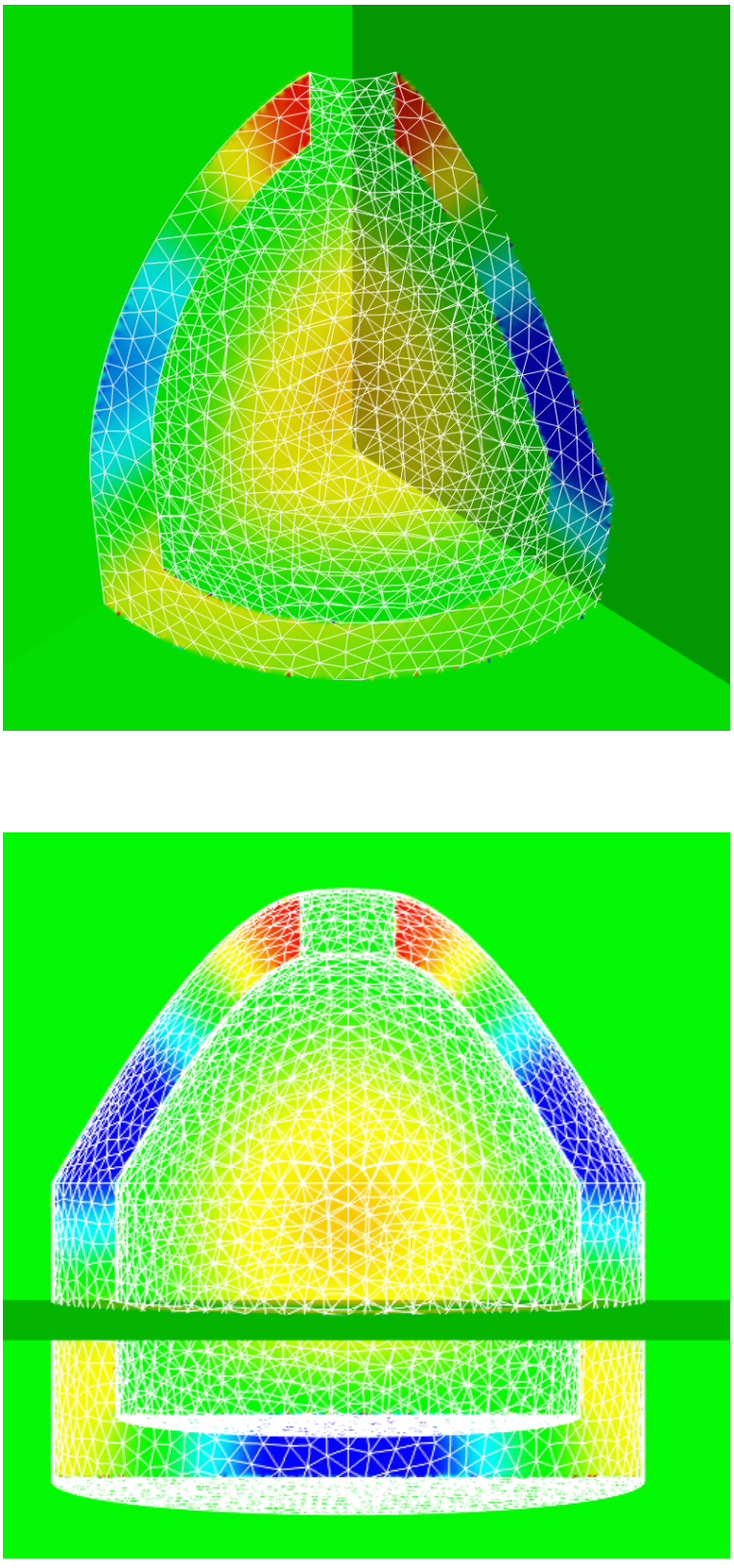

FIGURE 5.8: Double-layer potential corresponding to the resonance $k_1^{(D)} = 3.07$.

devices [Weinstein and Bhave, 2010] to eggshell crack detection [De Ketelaere et al., 2000]. Arising from these applications, in the present Section we analyse the case of acoustic scattering by a dumbbell-like object.

Figure 5.9a shows a two-dimensional section of the three-dimensional dumbbell we are going to analyse in the present Section. The scatterer is composed of two spherical shells connected by a cave cylinder whose surface presents an open vault. Each spherical shell is defined by the two spheres of radius equal to 0.9 and 1.0 respectively. The distance between the centres of the two spherical shells is equal to 5.0. The cave cylinder is defined by an internal cylinder, whose base is a circle of radius 0.4, and an external cylinder, whose base is a circle of radius 0.5; the length of the two cylinders is then approximately equal to 3.38 and 3.26 respectively. The internal cavity is connected to the exterior by a vault of length 1.0 and supporting angle equal to π.

Figure 5.9b shows once again pseudospectra of the double-layer boundary integral operator $\mathcal{K}_k + 0.5\mathcal{I}$ on the dumbbell for the usual complex neighbourhood of the real interval $1 < k < 4$. As in the case of the Pantheon, all the poles shown look to be perfectly on the real line and may be thought to be interior Neumann eigenvalues at first sight. It is only by plotting the corresponding eigenfunctions and potentials that one can verify that the value

$$k_1^{(D)} = 3.50$$

is a resonance laying exponentially close to the real line. No particular remarks are to be made in this case as far as shape is concerned: pseudospectra appear to be balls centred in the poles also in the case of such resonance, with no strong protrusion in any direction. Also by looking at the resolvent norm on the real line, no particular sign of non-normal behaviour can be observed around the resonance for this particular scatterer.

Figure 5.10 shows the double-layer potential $\tilde{u}_k = \mathcal{D}_k\tilde{\phi}_k$ where the density $\tilde{\phi}_k$ is the eigenfunction of $\mathcal{K}_k + 0.5\mathcal{I}$ corresponding to $k_1^{(D)}$. The potential $\tilde{u}_k$ is again perfectly 'trapped' inside the Pantheon cavity, almost looking like a low-frequency solution of the interior Dirichlet problem for the closed dumbbell. As

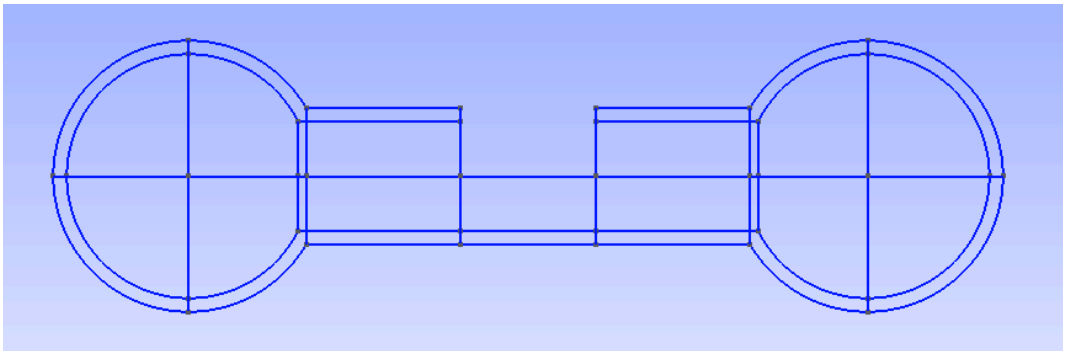

(A) Section of the scatterer.

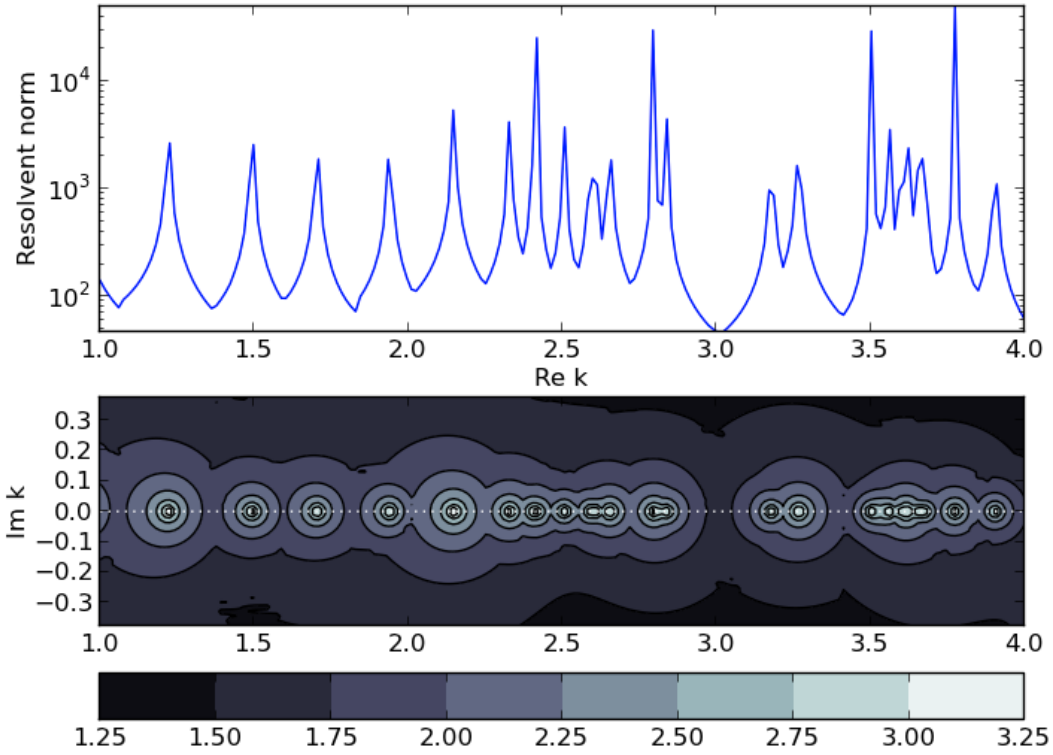

(B) Resolvent norm on the real line (top) and pseudospectra (bottom) of $\mathcal{K}_k + 0.5\mathcal{I}$.

FIGURE 5.9: Dumbbell cavity

we have seen before, the potential remains defined also inside the obstacle K but there it has no physical connection to the exterior Dirichlet problem we are considering.

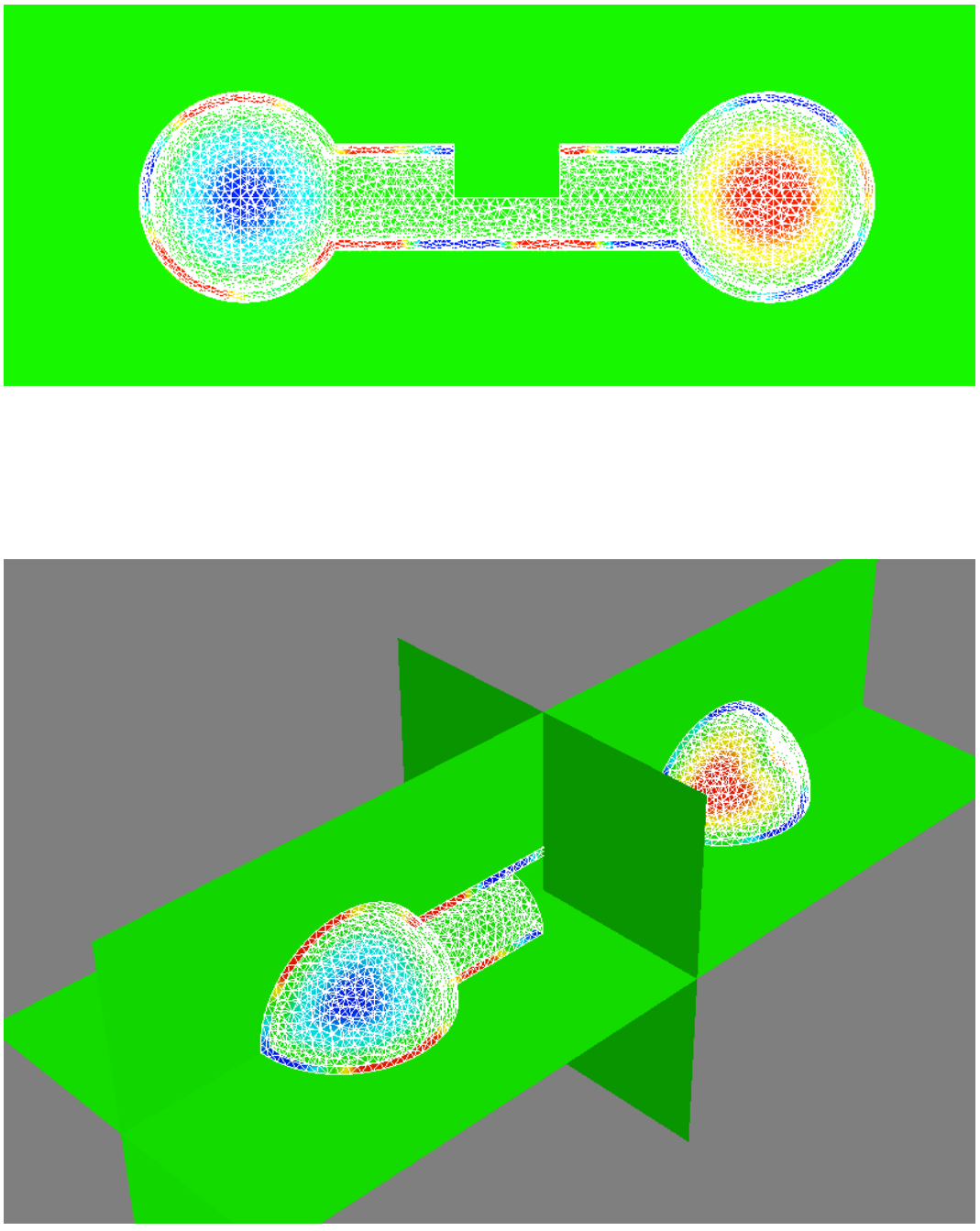

FIGURE 5.10: Double-layer potential corresponding to the Dirichlet resonance $k_1^{(D)} = 3.50$.

5.6 A guitar cavity

The enumeration of the fields where acoustic scattering and resonances have their effects would not be complete without mentioning what is probably the oldest of all of them: music. Sounds are nothing but acoustic waves whose frequency (i.e., wave number) is an audible range, and people have made musical instruments from cavities since prehistory. Despite being primarily artistic topics, music and voices are also the target of rigorous scientific investigations. There are academic papers addressing the subject of acoustic scattering and resonances in music in many different contexts: from classical guitar bodies [Curtu et al., 2009] to african tribal music [Rifkin, 2009], from theater vocal qualities [Bourne and Garnier, 2012] to bird songs [Palacios and Tubaro, 2000]. Inspired by the previous researches, in the present Section we analyse a guitar-shaped obstacle.

Figure 5.11a shows a two-dimensional section of the three-dimensional guitar we consider in the present Section (a three-dimensional mesh is shown in Figure 5.11b). The body of the scatterer is composed of two intersecting short cave cylinders. Each cylinder has an external and internal circular basis of radius 1.1 and 1.0 respectively, and an external and internal height of length 0.7 and 0.5 respectively. The two cave bodies lie on the same plane and intersect each other in such a way that the distance between the intersection points of the internal cylinders (i.e., the two cavities) is 1.0. The resulting cavity is connect with the exterior by a cylindrical cavity on one side of the scatterer; such cylinders has height equal to 0.1 (i.e. the thickness of the scatterer border) and its circular basis has a radius of 0.5. The resulting object simulates a rudimental guitar.

Figure 5.12a shows once again pseudospectra of the double-layer boundary integral operator $\mathcal{K}_k + 0.5\mathcal{I}$ on the described guitar-like scatterer for a complex neighbourhood of the real interval $3 < k < 7$. As we have seen before, all the poles shown look to be perfectly on the real line and may be thought to be all interior Neumann eigenvalues at first sight. It is only by plotting the corresponding eigenfunctions and potentials that one can verify the existence of multiple exterior resonances:

$$k_1^{(D)} = 6.42, \quad k_2^{(D)} = 6.55, \quad k_3^{(D)} = 6.75, \quad k_4^{(D)} = 6.85.$$

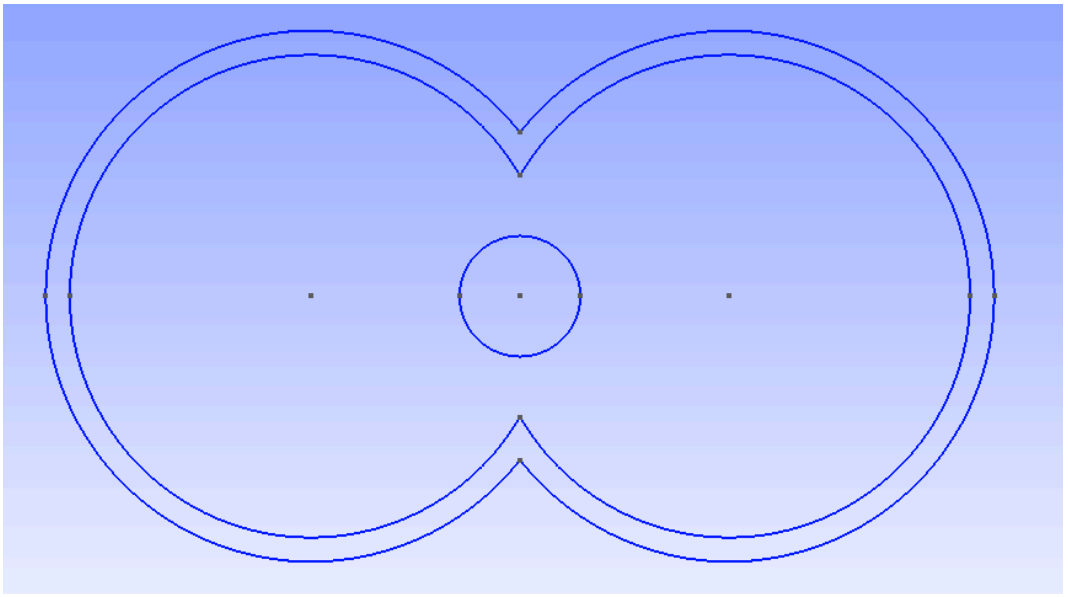

(A) Section of the scatterer.

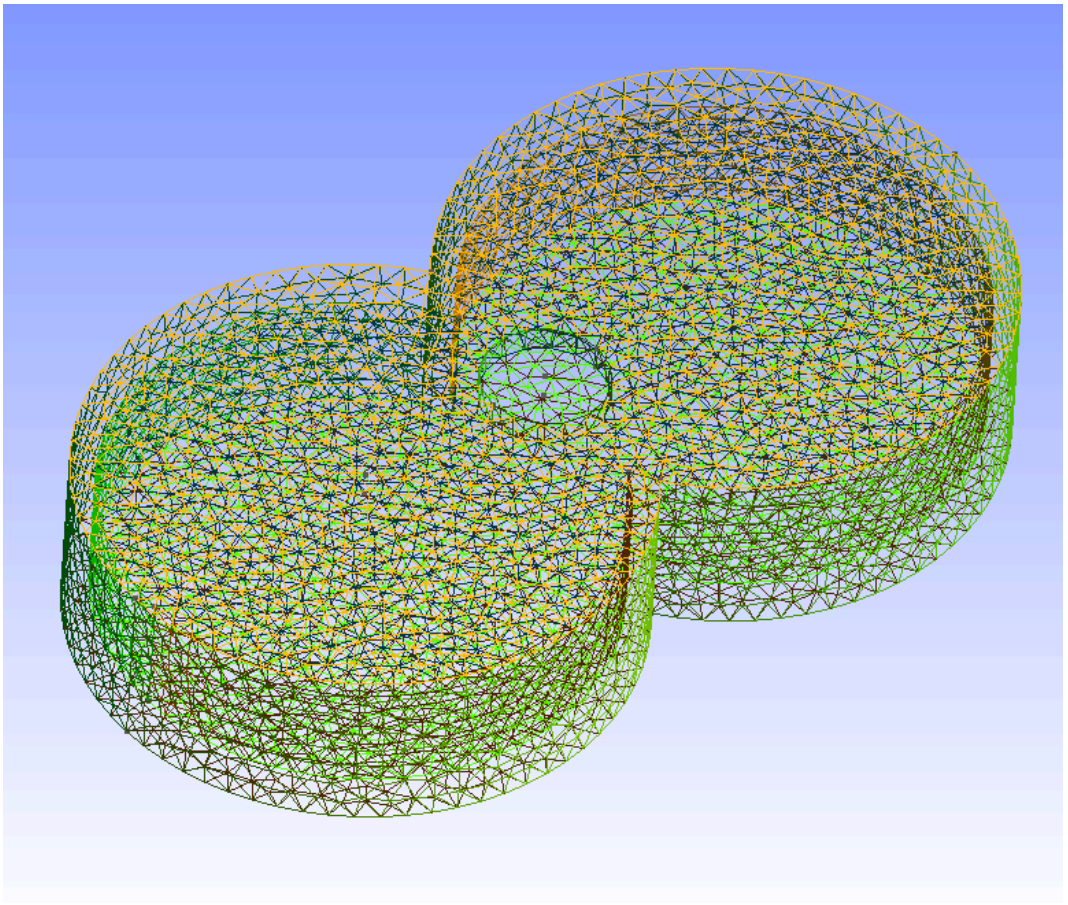

(B) 3d mesh of the scatterer.

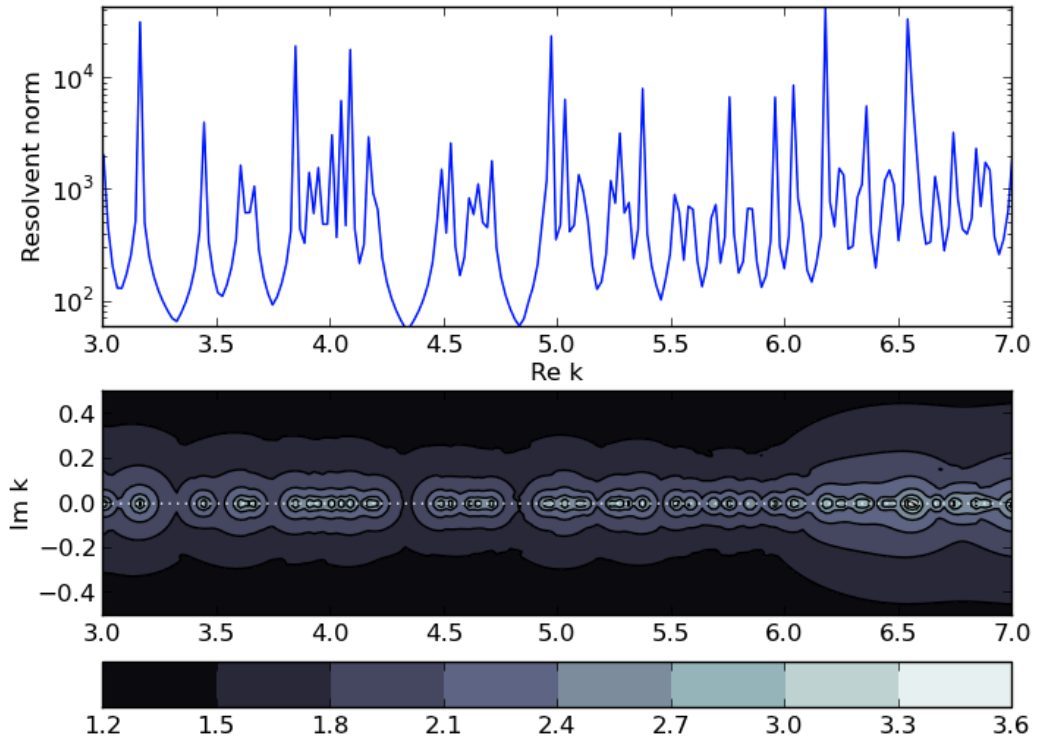

(A) Resolvent norm on the real line (top) and pseudospectra (bottom) of $\mathcal{K}_k + 0.5\mathcal{I}$.

FIGURE 5.12: Guitar cavity

Such resonances lay exponentially close to the real line. Due to the high number of crowded poles, it is difficult to analyse in details the shape of pseudospectra: they tend to appear as balls centred in the poles everywhere, even if it is possible to observe a less regular shape in the interval where resonances are located; in particular, the border of the $10^{-2.1}$-pseudospectra looks to be somehow wider in the $6 < k < 7$ area than in the rest of the spectral plot.

Figures 5.13-5.14 show the double-layer potential $\tilde{u}_k = \mathcal{D}_k\tilde{\phi}_k$ where the density $\tilde{\phi}_k$ is the eigenfunction of $\mathcal{K}_k + 0.5\mathcal{I}$ corresponding to $k_1^{(D)}$, $k_2^{(D)}$, $k_3^{(D)}$ and $k_4^{(D)}$ respectively. Again, the potentials $\tilde{u}_k$ are well 'trapped' inside the guitar, and they look like low-frequency solutions of the interior Dirichlet problem for the closed cavity sliding out to the exterior domain through the circle on the side of the scatterer. As usual, the potential remains defined also inside the obstacle K but there it has no physical connection to the exterior Dirichlet problem we are considering.

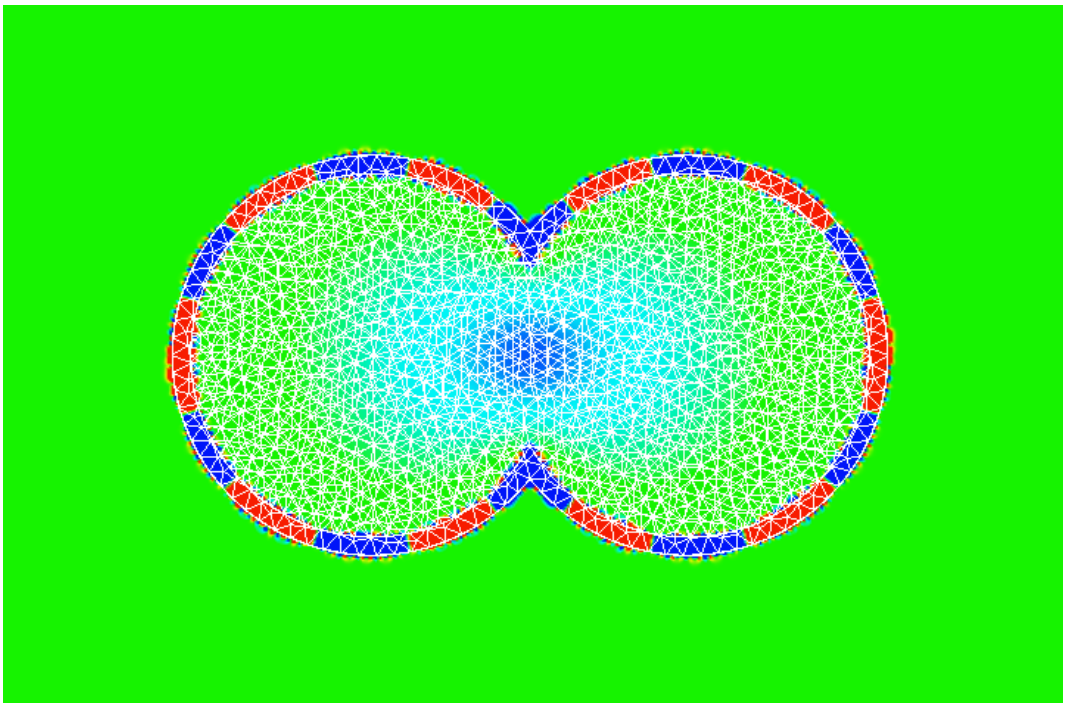

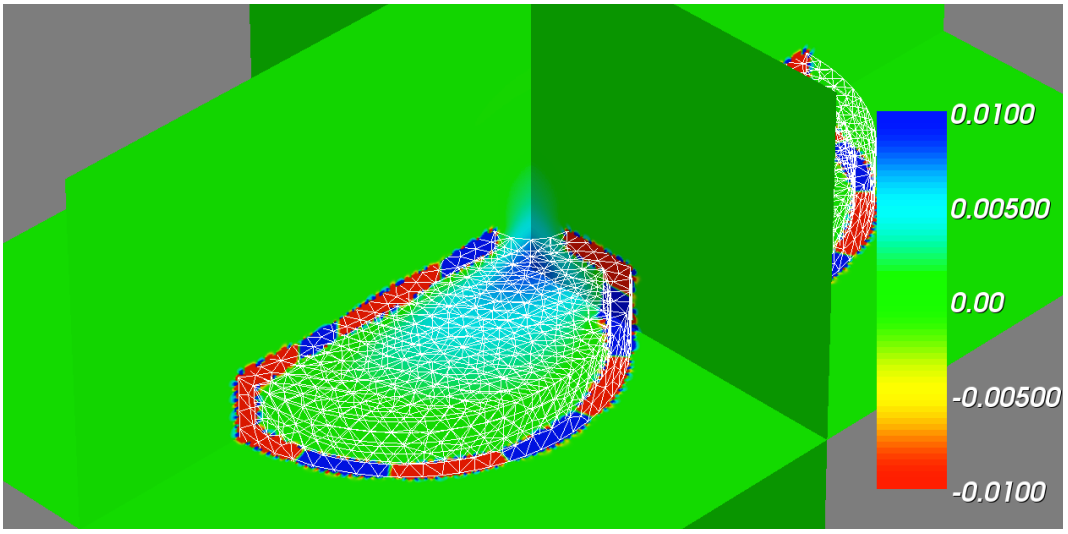

FIGURE 5.13: Double-layer potential corresponding to the Dirichlet resonance $k_1^{(D)} = 6.42$.

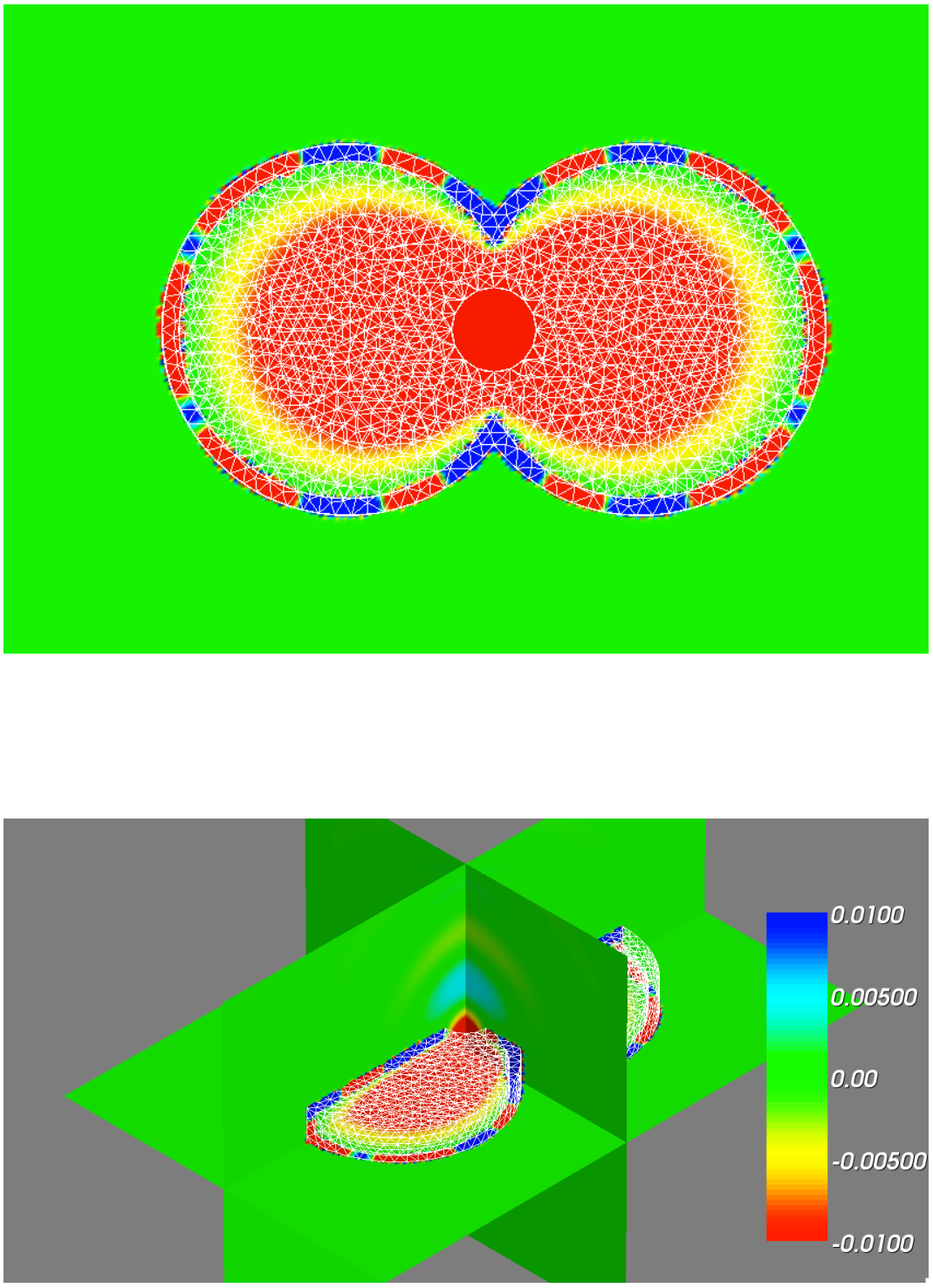

FIGURE 5.14: Double-layer potential corresponding to the Dirichlet resonance $k_1^{(D)} = 6.55$.

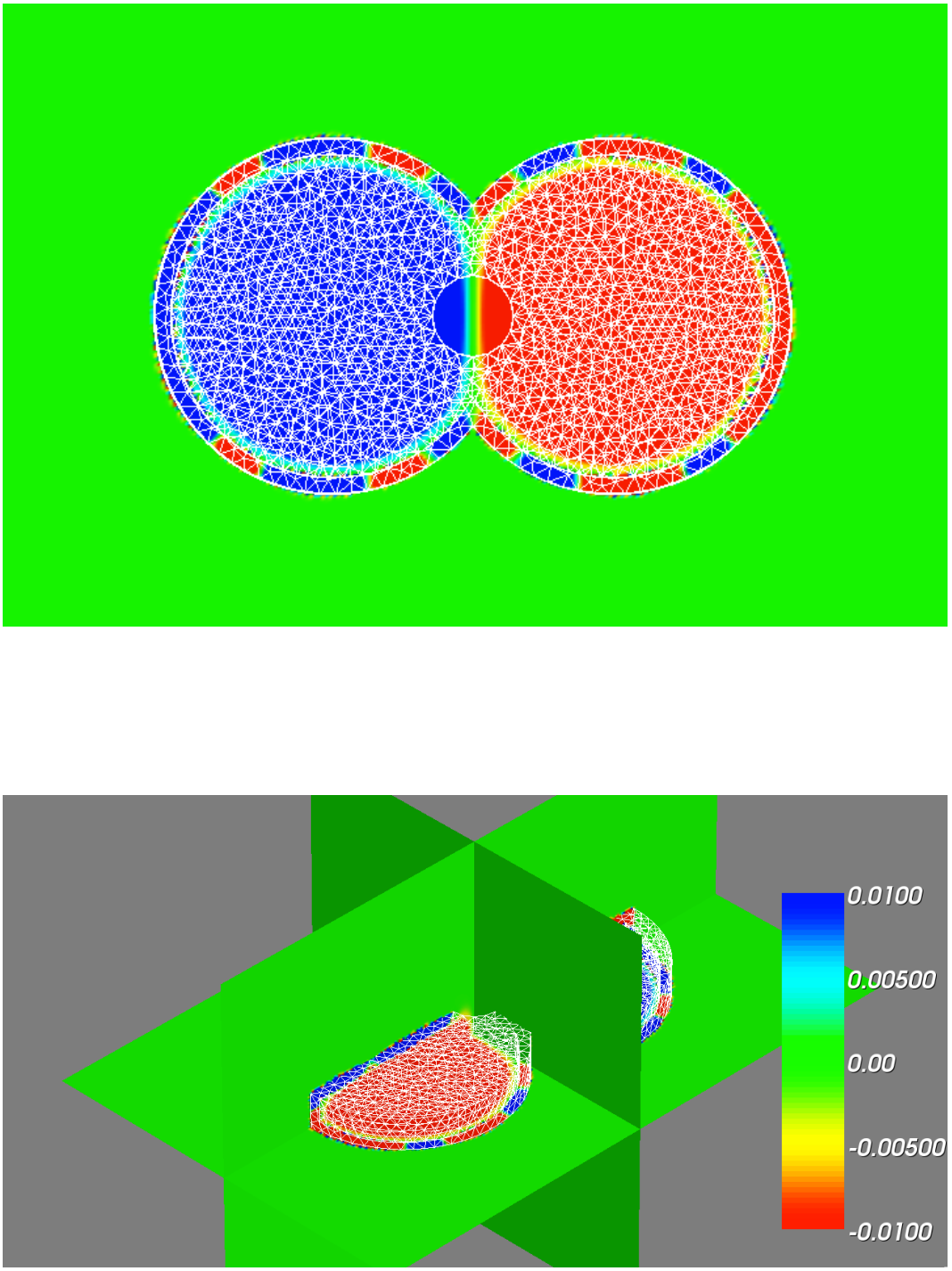

FIGURE 5.15: Double-layer potential corresponding to the Dirichlet resonance $k_1^{(D)} = 6.75$.

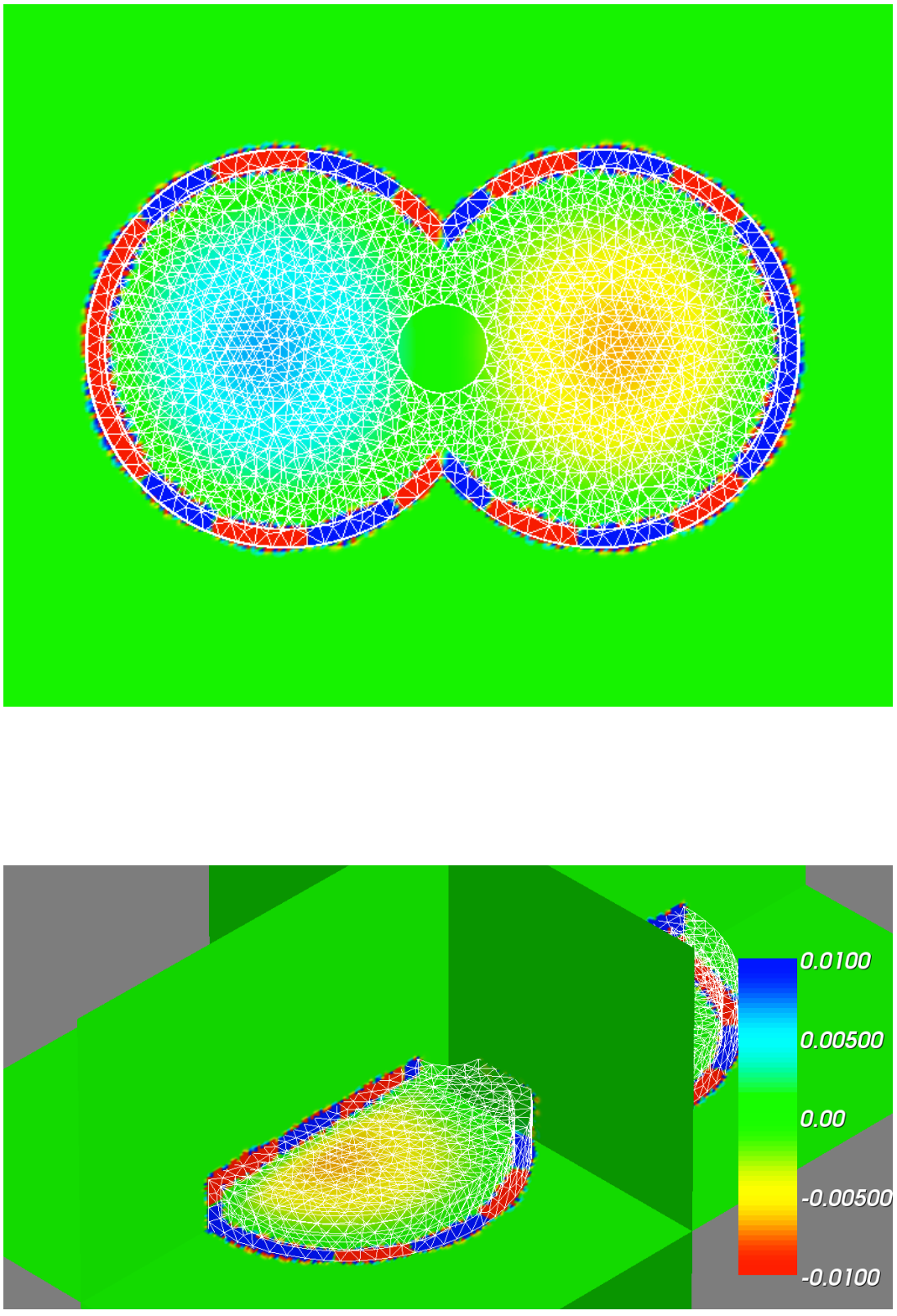

FIGURE 5.16: Double-layer potential corresponding to the Dirichlet resonance $k_1^{(D)} = 6.85$.

Chapter 6

Conclusion

In this last Chapter of the thesis, we draw a few conclusions from our research activity and we highlight its implications for future researches. Moreover, we analyse the limitations of our work and we suggest some possible developments for future investigations.

The present thesis has addressed the problem of the numerical computation of resonances and pseudospectra in the context of acoustic scattering. After having introduced the mathematical formulation of the problem in Chapter 1, we have described in Chapter 2 the notion of pseudospectra and we have investigated its role in describing non-normal behaviours and its extension to matrix pencils and analytic families. The connection between pseudospectra and non-normality in the linear case is one of the main reasons why we are interested in the numerical computation of pseudospectra; in the non-linear case, the target is the possibility of quantifying the influence of complex resonances over real wave-numbers through pseudospectra. Few are the plots of pseudospectra which have appeared so far in the acoustic scattering literature, and most of them comes from FEM discretizations; in Chapter 3 we have given an overview of the PML/FEM-based methods for such computations, and we have discussed some points which turn out to be useful also in BEM-based methods (e.g., weighted norms). Chapter 4 is instead original, and we consider it to be our main contribution to the acoustic scattering community; there, we propose numerical algorithms based on BEM for computing resonances and pseudospectra and we analyse their efficiency and

performance in depth. Such algorithms are based on integral equations methods and boundary element methods, and they benefit from the use of high performance numerical strategies as the Fast Multiple Method and the Adaptive Cross Approximation. We want to think of Chapter 4 as the kernel the present thesis. In Chapter 5 we have applied our BEM-based algorithms to half a dozen of physically relevant scatterers, inspired from different fields where acoustic scattering plays a relevant role, and we have highlighted the insight which can be given through the numerical computation of resonances and pseudospectra in the many different fields where acoustic scattering plays a key role. This is an implicit suggestion to extend the range of the fields where analytical tools such as resonances and pseudospectra are adopted to investigate different real-world phenomena.

We summarise the main implications of the work for future research in the following points:

- Pseudospectra have been proved to be a powerful tool to investigate the operators arising in acoustic scattering, and to quantify the influence of complex resonances on physical wave-numbers.
- BEM has been shown to be a valid alternative to FEM for the numerical investigation of eigenvalues and resonances arising in boundary value problems for acoustic scattering, and a couple of efficient and high-performance algorithms have been provided.
- Plotting pseudospectra can be a preliminary step to provide an insight into acoustic phenomena in many different fields where the location of resonances and the behaviour of resonant mode play a relevant role.

Aside to these results, we acknowledge many open problems in our work. Again, we summarise them as follows:

- In Chapter 3 we have considered only an eigenspace projection method to improve the FEM-based algorithm. Many other methods are available to reduce the size of the discretisation matrices and improve its performance.

- In Chapter 4 we have considered only approximate LU inverses as preconditioners for the iterative BEM-based algorithm. Many other preconditioners are available and can further improve the performance.

- The FMM has been used with default parameters, without calibrating their values to obtain optimal performances. Much may be gained by tuning the method for the particular application.

- The inner-outer strategy has been tested by using only IRAM as eigensolver. Many other iterative methods for eigenvalue computation are known, and an optimal choice can be sought between them.

- The computations shown in the present thesis concern only low wavenumber ranges. The problem of computing resonances and pseudospectra for high frequencies has not been treated at all.

- In Chapter 5 we have proposed scatterers deduced from fields where the author has limited or no knowledge at all. More appropriate applications could have been found after discussions with experts in each different field.

Each of the previous open problems suggests a possible hint for further investigations on the topic. Yet, there are other suggestions that we would like to point out, and which have been out of the scope of our research from the beginning. In Chapter 2 we have highlighted the connection between linear pseudospectra and non-normal behaviour, and we have introduced the extensions of pseudospectra to operators pencils and to analytic families. Yet, many results for linear pseudospectra still miss a counterpart for these extended notions. In particular, it would be very beneficial either to prove all the results about non-normality also in the case of non-linear pseudospectra, or to give consistent and global counterexamples. The research on this frontier is still ongoing. Moreover, a consistent comparison of FEM- and BEM-based algorithms for the numerical computation of resonances and pseudospectra would be interesting. In the present thesis we have only given an overview of FEM-based methods, showing a two-dimensional applications, while we have focused on BEM-based methods and on three-dimensional scatterers. It would be interesting to compare the properties

and the performances of different FEM- and BEM-based algorithms on the same two- or three-dimensional scatterers.

Appendix A

Aguilar-Balslev-Combes-Simon Theory of Quantum Resonances

In the present Appendix we give an overview of the Aguilar-Balslev-Combes-Simon theory of quantum resonances. The theory is interesting as includes PML as a special case but it is not necessary as far as the numerical computation of acoustic resonances is concerned. The Appendix is a self-contained rewriting of Section 16.2 in Hislop and Sigal [1996], where a more detailed exposition of quantum spectral theory can be found. The original results are contained in Aguilar and Combes [1971], Balslev and Combes [1971], Simon [1973].

Let us consider a Schrödinger operator

$$H := -\Delta + V$$

with the potential V such that H has essential spectrum $[0, \infty)$ and negative eigenvalues. The resolvent of H, $R_H(z)$, is known to be analytic in $\mathbb{C} \setminus \sigma(H)$ and its operator norm is bounded above by $1/|\text{Im } z|$ [Hislop and Sigal, 1996, Corollary 5.7]. Indeed, for $z \in \sigma(H)$ the resolvent is an unbounded operator on $L^2(\mathbb{R}^n)$. The resolvent of a Schrödinger operator (for suitable potentials V) remains bounded as $\text{Im } z \to 0$ if we replaces $L^2(\mathbb{R}^n)$ with appropriate weighted

Hilbert spaces. Another way in which the boundary values of the resolvent can be controlled is to consider matrix elements of the resolvent between vectors in $L^2(\mathbb{R}^n)$ with certain nice properties. In general, there is a discontinuity in the matrix elements $(f, R_H(z)g)_{L^2(\mathbb{R}^n)}$, for suitable $f, g \in L^2(\mathbb{R}^n)$, as we approach $\mathbb{R}^+$ from above and below.

As there is a discontinuity across the essential spectrum, we could construct a meromorphic continuation. This is one of the accomplishments of the Aguilar-Balslev-Combes theorem. Hence, we are interested in studying the meromorphic continuation of matrix element of $R_H(z)$ through the discontinuity along $\mathbb{R}^+$.

Definition A.1. The quantum resonances of a Schrödinger operator H associated with a dense set of vectors $\mathcal{A}$ in the Hilbert space $\mathcal{H}$ are the poles of the meromorphic continuations of all matrix elements

$$(f, R_H(x)g)_{L^2},$$

$f, g \in \mathcal{A}$, from $\{z \in \mathbb{C} \mid \text{Im } z > 0\}$ to $\{z \in \mathbb{C} \mid \text{Im } z \leq 0\}$.

The dependence of the resonances on $\mathcal{A}$ is disturbing but these poles can often be shown to be identical with the poles of the meromorphic continuation of Green's function for H in scattering situations. In these cases, the resonances are independent of $\mathcal{A}$ and intrinsic to the operator H.

The existence of the meromorphic continuations of matrix elements $(f, R_H(x)g)_{L^2}$, the association of the poles of these continuations with the eigenvalues of certain non-self-adjoint operators associated with H, and the identification of these eigenvalues as resonances, are the main and general results of the Aguilar-Balslev-Combes-Simon theory.

To present the Aguilar-Balslev-Combes-Simon theory, we need the following definitions and assumptions.

(A0) $H = -\Delta + V$ is a self-adjoint Schrödinger operator with domain $\mathcal{D}(H) \subset \mathcal{H}$, $\mathcal{H}$ being an Hilbert space, with essential spectrum $\sigma_{\text{ess}}(H) = \mathbb{R}_+$ and discrete spectrum $\sigma_d(H) \subset \mathbb{R}_-$.

(A1) There exists a family $\mathcal{U}$ of linear operators U_θ, $\theta \in D = \{z \in \mathbb{C} \mid |z| < 1\}$, such that for $\theta \in D \cap \mathbb{R}$, U_θ is unitary, $U_\theta D(H) = D(H)$ for all $\theta \in D$, and $U_0 = 1$. Furthermore, there exists a dense set of vectors $\mathcal{A} \subset \mathcal{H}$ such that

(i) the map $(\psi, \theta) \in \mathcal{A} \times D \to U_\theta \psi$ is analytic on D with values in $\mathcal{H}$;

(ii) for $\theta \in D$, $U(\theta)\mathcal{A}$ is dense in $\mathcal{A}$.

(A2) We define, for $\theta \in D \cap \mathbb{R}$, a family of unitary equivalent operators $H(\theta) = U_\theta H U_\theta^{-1}$. We assume that the map

$$\theta \in D \to H(\theta),$$

is analytic of type-A, i.e. $D(H(\theta))$ is independent of θ and, for each $u \in D(H)$, $H(\theta)u$ is analytic with respect to $\theta \in D$.

Definition A.2. The family $\mathcal{U}$ satisfying (A1) and (A2) is called a spectral deformation family for H. We call the dense set of vectors $\mathcal{A}$ the analytic vectors for U_θ.

Let us now assume that (A0)-(A2) are satisfied by H, and we consider $\sigma(H(\theta))$. When $\theta \in D \cap \mathbb{R}$, the operators $H(\theta)$ are unitarily equivalent to H by (A2), and so $\sigma(H) = \sigma(H(\theta))$. For general $\theta \in D$, $\sigma(H(\theta))$ is a closed subset of $\mathbb{C}$ that may even have a nonempty interior. Furthermore, $H(\theta)$ may have complex eigenvalues that have no counterpart in $\sigma(H)$. To say more about $\sigma(H(\theta))$, we make the following assumption:

(A3) There exists an open, connected set $\Omega \subset \{z \in \mathbb{C} \mid \text{Re } z > 0\}$ such that $\Omega^+ = \Omega \cap \mathbb{C}^+ \neq \emptyset$, $\Omega^- = \Omega \cap \mathbb{C}^- \neq \emptyset$, and for all $\theta \in D^+ = D \cap \mathbb{C}^+$, $\sigma_{\text{ess}}(H(\theta)) \cap \Omega^+ = \emptyset$. For each $\epsilon > 0$, there exists a subset $\Omega_\epsilon^- \subset \overline{\Omega^-}$ such that for some $\theta \in D_\epsilon^+ = \{z \in D \mid \text{Im } z > \epsilon\}$, we have $\sigma_{\text{ess}}(H(\theta)) \cap \Omega_\epsilon^- = \emptyset$.

The notion of deformation family is the overlapping point with the definition of PML and the reason for the present Appendix. It is indeed the most important example of deformation family, the dilation analyticity group, that looks very similar to Bérenger's PML. Let $H_0 = -\Delta$ on $L^2(\mathbb{R}^n)$. Let U_θ, $\theta \in \mathbb{R}$, be the

implementation on $L^2(\mathbb{R}^n)$ of the group of dilations on $\mathbb{R}^n$, $x \to e^\theta x$. For $f \in L^2(\mathbb{R}^n)$, U_θ is defined by

$$(U_\theta f)(x) = e^{\frac{n\theta}{2}} f(e^\theta x).$$

The one-parameter unitary group $\mathcal{U} = \{U_\theta \mid \theta \in \mathbb{R}\}$ implements a shift of the coordinate, which is what the PML does (cf. Equation (3.6)). Then $H(\theta)$ corresponds to the PML operator $-\tilde{\Delta}$ with θ being the variety of damping function $\tilde{\sigma}$ we can possibly choose (cf. Equation (3.4)). With the set of analytic vectors $\mathcal{A}$

$$\psi(z) = p(z)e^{-\alpha z^2},$$

for $\alpha > 0$, $z \in \mathbb{C}^n$, and any polynomial p, we have that the family $\mathcal{U}$ is a spectral deformation family for H_0 and $\mathcal{A}$ are analytic vectors for U_θ [Hislop and Sigal, 1996].

Given assumptions (A0)-(A3), we can now state the Aguilar-Balslev-Combes-Simon theorem concerning meromorphic continuations.

Theorem A.3. Let H be a self-adjoint Schrödinger operator with spectral deformation family $\mathcal{U}$ and analytic vectors $\mathcal{A}$ such that (A0)-(A3) are satisfied.

(1) For $f, g \in \mathcal{A}$, the function

$$F_{fg}(z) = (f, R_H(z)g)_{L^2(\mathbb{R}^n)}, \tag{A.1}$$

defined for Im $z > 0$, has a meromorphic continuation across $\sigma_{\text{ess}}(H) = \overline{\mathbb{R}^+}$ into Ω_ϵ^-, for any $\epsilon > 0$.

(2) The poles of the continuation of $F_{fg}(z)$ into Ω_ϵ^- are eigenvalues of all the operators $H(\theta)$, $\theta \in D_\epsilon^+$, such that $\sigma_{\text{ess}}(H(\theta)) \cap \Omega_\epsilon^- = \emptyset$.

(3) These poles are independent of $\mathcal{U}$ in the following sense. If $\mathcal{V}$ is another spectral deformation family for H with a set of analytic vectors $\mathcal{A}_\mathcal{V}$ such that (A1)-(A3) are satisfied and $\mathcal{A} \cap \mathcal{A}_\mathcal{V}$ is dense, then the eigenvalues of $\tilde{H}(\theta) = V_\theta H V_\theta^{-1}$, $\theta \in D_\epsilon^+$, in $\overline{\Omega_\epsilon^-}$ are the same as those of $H(\theta)$ in this region.

The Aguilar-Balslev-Combes-Simon theory identifies quantum resonances as the eigenvalues of the spectrally deformed operator $H(\theta)$ in the lower half-plane. This is exactly what we implicitly did looking for the generalized eigenvalues of $-\tilde{\Delta}-k^2 n$ and interpreting them as resonances for the original Helmholtz operator $-\Delta - k^2$. The price to pay for such a description, in both the cases, is that we must work with non-self-adjoint operators. Despite this, the theory is a powerful tool for investigation of resonances in quantum mechanical system and for the numerical computations of resonances. Yet, the communication between this two communities has not been as frequent as the similarity of the researches would ask, with very few papers on quantum resonances with numerical computations and very few papers on numerical computations of resonances with a clear frame in the deeper Aguilar-Balslev-Combes-Simon theory of quantum resonances.

Bibliography

J. Aguilar and J.M. Combes. A class of analytic perturbations for one-body Schrödinger Hamiltonians. *Comm. Math. Phys.*, 22:269–279, 1971.

W. E. Arnoldi. The principle of minimized iteration in the solution of the matrix eigenvalue problem. *Quart. Appl. Math.*, 9:17–29, 1951.

A. H. Baker, E. R. Jessup, and T. Manteuffel. A technique for accelerating the convergence of restarted GMRES. *SIAM J. Matrix Anal. Appl.*, 26(4): 962–984, 2005.

E. Balslev and J.M. Combes. Spectral properties of many body Schrödinger operators with dilation analytic interactions. *Comm. Math. Phys.*, 22:280–294, 1971.

M. Bebendorf. Approximation of boundary element matrices. *Numer. Math.*, 86 (565-589), 2000.

M. Bebendorf. Hierarchical LU decomposition-based preconditioners for BEM. *Computing*, 74:225–247, 2005.

M. Bebendorf. *Hierarchical matrices: a means to efficiently solve elliptic boundary value problems*, volume 63 of *Lecture Notes in Computational Science and Engineering*. Springer-Verlag, 2008.

M. Bebendorf and S. Rjasanow. Adaptive low-rank approximation of collocation matrices. *Computing*, 70:1–24, 2003.

M. Bebendorf, S. Rjasanow, and E. Tyrtyshnikov. Approximation using diagonal-plus-skeleton matrices. In Chapman and Hall/CRC Res. Notes

Math., editors, *Mathematical aspects of boundary element methods (Palaiseau, 1998)*, volume 414, pages 45–52, 2000.

J. Berenger. A perfectly matched layer for the absorption of electromagnetic waves. *J. Comput. Physics*, 114:185–200, 1994.

J. Berenger. Perfectly matched layers for the FDTD solution of wave-structure interaction problems. *IEEE Trans. Antennas Propagat.*, 44(110-117), 1996.

T. Betcke and E. Spence. Numerical estimation of coercivity constants for boundary integral operators in acoustic scattering. *SIAM J. Numer. Anal.*, 49(4): 1572–1601, 2011.

T. Betcke, S N Chandler-Wilde, I G Graham, S Langdon, and M Lindner. Condition number estimates for combined potential operators in acoustics and their boundary element discretisation. *Numerical Methods for PDEs*, 27(1):31–69, 2011.

T. Betcke, J. Phillips, and E. Spence. Spectral decompositions and nonnormality of boundary integral operators in acoustic scattering. *IMA J. Numer. Anal.*, 34(2):700–731, 2014.

D. Bindel and A. Hood. Localization theorems for nonlinear eigenvalue problem. *SIAM J. Matrix Anal. Appl.*, 34(4):1728–1749, 2013.

T. Bourne and M. Garnier. Physiological and acoustic characteristics of the female music theater voice. *J. Acoust. Soc. Am.*, 131(2):1586–1594, February 2012.

S. C. Brenner and L. R. Scott. *The Mathematical Theory of Finite Element Methods*. Number 15 in Texts in Applied Mathematics. Springer, third edition, 2008.

D. Brunner, M. Junge, P. Rapp, M. Bebendorf, and L. Gaul. Comparison of the fast multipole method with hierarchical matrices for the Helmholtz-BEM. *CMES*, 58(2):131–158, 2010.

S. N. Chandler-Wilde, I. G. Graham, S. Langdon, and M. Lindner. Condition number estimates for combined potential boundary integral operators in acoustic scattering. *J. of Int. Eq. and Appl.*, 21(2):229–279, 2009.

H. Cheng, W. Crutchfield, Z. Gimbutas, L. Greengard, F. Ethridge, J. Huang, V. Rokhlin, N. Yarvin, and J. Zhao. A wideband fast multipole method for the helmholtz equation in three dimensions. *J. Comput. Physics*, 216:300–325, 2006.

P. G. Ciarlet. *The Finite Element Method for Elliptic Problems*, volume 40 of *Classics in Applied Mathematics*. SIAM, 2002.

F. Collino and P. Monk. The perfectly matched layer in curvilinear coordinates. *SIAM J. Sci. Comput.*, 19(6):2061–2090, 1998.

D. Colton and R. Kress. *Integral equation methods in scattering theory*, volume 72 of *Classics in Applied Mathematics*. SIAM, reprint of 1983 edition, 2013a.

D. Colton and R. Kress. *Inverse Acoustic and Electromagnetic Scattering Theory*, volume 93 of *Applied Mathematical Sciences*. Springer-Verlag, third edition edition, 2013b.

M. Costabel. Boundary integral operators on Lipschitz domains: Elementary results. *SIAM J. Mathem. Anal.*, 19(3):613–262, 1988.

J. K. Cullum and A. E. Ruehli. Pseudospectra analysis, nonlinear eigenvalue problems, and studying linear systems with delays. *BIT*, 41(2):265–281, 2001.

I. Curtu, M. Stanciu, N. Cretu, and C. Rosca. Modal analysis of different types of classical guitar bodies. *10th WSEAS International Conference on Acoustics and Music: Theory and Applications*, 2009.

B. De Ketelaere, P. Coucke, and J. De Baerdemaeker. Eggshell crack detection based on acoustic resonance frequency analysis. *J. Agric. Engineering Res.*, 76:157–163, 2000.

W. Desmet, B. Pluymers, and P. Sas. Vibro-acoustic analysis procedures for the evaluation of the sound insulation characteristics of agricultural machinery cabins. *Journal of Sound and Vibration*, 266(3):407–441, 2003.

P. Fiala, G. Degrande, J. Granat, and F. Augusztinovicz. Structural and acoustic response of buildings in the higher frequency range due to surface rail traffic. Technical report, ICSV13 - Vienna, Vienna, Austria, July 2006.

V. Frayssé, M. Gueury, F. Nicoud, and V. Toumazou. Spectral portraits for matrix pencils. Technical report, CERFACS, Toulouse, August 1996.

M. Freitag. *Inner-outer Iterative Methods for Eigenvalue Problems - Convergence and Preconditioning.* PhD thesis, University of Bath, 2007.

G. Golub and C. Van Loan. *Matrix Computations.* The John Hopkins University Press, 3rd edition, 1996.

K. Green and T. Wagenknecht. Pseudospectra and delay differential equations. *J. of Comp. and Applied Math.*, 196:567–578, 2006.

R. R. Greengard and V. Rokhlin. A fast algorithm for particle simulations. *J. Comput. Physics*, 73:325–348, 1987.

N. Gumerov and R. Duraiswami. *Fast Multipole Methods for the Helmholtz Equation in Three Dimensions.* Elsevier, 2005.

W. Hackbush. A sparse matrix arithmetic based on h-matrices I. introductio to H-matrices. *Computing*, 62(2):89–108, 1999.

N. Higham. *Accuracy and Stability of Numerical Algorithms.* SIAM, 1996.

E. Hille and R. S. Phillips. *Functional Analysis and Semi-Groups.* American Mathematical Society, 1957.

P. D. Hislop and I. M. Sigal. *Introduction to Spectral Theory, With Applications to Schrödinger Operators*, volume 113 of *Applied Mathematical Sciences.* Springer-Verlag, 1996.

F. Ihlenburg. *Finite Element Analysis of Acoustic Scattering.* Number 132 in Applied Mathematical Sciences. Springer, 1998.

M. Ikawa. On the poles of the scattering matrix for two strictly convex obstacles. *J. Math. Kyoto Univ.*, 23:127–194, 1983.

M. Ikawa. Trapping obstacles with a sequence of poles of the scattering matrix converging to the real axis. *Osaka J. Math.*, 22:657–689, 1985.

S. Kim and J. Pasciak. The computation of resonances in open systems using a perfectly matched layer. *Mathematics of Computation*, 78:1375–1398, 2009.

R. Kirby. From functional analysis to iterative methods. *SIAM Review*, 52(52): 269–293, 2010.

R. E. Kleinman and G. F. Roach. Boundary integral equations for the three-dimensional Helmholtz equation. *SIAM Review*, 16:214–236, 1973.

D. Kressner and B. Vandereycken. Subspace methods for computing the pseudospectral abscissa and the stability radius. *SIAM. J. Matrix Anal. & Appl.*, 35(1):292–313, 2014.

W. D. Kupradse. Existence and uniqueness theorems in diffraction theory. *Doklady. Akad. Nauk. USSR*, 5:1–5, 1934a.

W. D. Kupradse. Integral equations for electromagnetic waves. *Doklady. Akad. Nauk. USSR*, 4:1–5, 1934b.

W. D. Kupradse. *Randwertaufgaben der Schwingungstheorie und Integralgleichungen.* Deutscher Verlag der Wissenschaften, Berlin, 1956.

O. Lacour, M.A. Galland, and D. Thenail. Preliminary experiments on noise reduction in cavities using active impedance changes. *Journal of Sound and Vibration*, 230(1):69–99, 2000.

P. D. Lax and R. S. Phillips. *Scattering theory.* Academic Press, 1967.

A. Logg, K.-A. Mardal, and G. Wells. *Automated Solution of Differential Equations by the Finite Element Method. The FEniCS Book*, volume 84 of *Lecture Notes in Computational Science and Engineering.* Springer-Verlag, 2012.

S. H. Lui. Computation of pseudospectra by continuation. *SIAM J. Sci. Comput.*, 18:565–573, 1997.

W. C. H. McLean. *Strongly Elliptic Systems and Boundary Integral Equations.* Cambridge University Press, 2000.

W. Michiels and S.-I. Niculescu. *Stability and stabilization of time-delay systems: an eigenvalue-based approach.* SIAM, 2007.

W. Michiels, K. Green, Thomas Wagenknecht, and S.-I. Niculescu. Pseudospectra and stability radii for analytic matrix functions with application to time-delay systems. *Lin. Alg. Appl.*, 418:315–335, 2006.

J. C. Nedelec. *Acoustic and Electromagnetic Equations: Integral Representations for Harmonic Problems*, volume 144 of *Applied Mathematical Sciences*. Springer-Verlag, 2001.

NIST. Nist digital library of mathematical functions. http://dlmf.nist.gov/, 2014.

M. Palacios and P. Tubaro. Does beak size affect acoustic frequencies in woodcreepers? *The Condor*, 102:553:560, 2000.

S. C. Reddy, P. J. Schmid, and D. S. Henningson. Pseudospectra of the Orr-Sommerfeld operator. *SIAM J. Appl. Math.*, 53:15–47, 1993.

M. Reed and B. Simon. *Methods of modern mathematical physics. Vol. 1 Functional analysis*. Academic Press, 1980.

K. S. Riedel. Generalized epsilon-pseudospectra. *SIAM J. Numer. Anal.*, 31: 1219–1225, 1994.

R. Rifkin. Engraved art and acoustic resonance: exploring ritual and sound in north-western south africa. *Antiquity*, 83:585–601, 2009.

S. Rjasanow and O. Steinbach. *The Fast Solution of Boundary Integral Equations*. Springer, New York, 2007.

V. Rokhlin. Rapid solution of integral equations of classic potential theory. *J. Comput. Physics*, 60:187–207, 1985.

V. Rokhlin. Diagonal forms of translation operators for the Helmholtz equation in three dimensions. *Applied and Computation Harmonic Analysis*, 1:82–93, 1993.

Y. Saad and M. H. Schultz. GMRES: A generalized minimal residual algorithm for solving nonsymmetric linear systems. *SIAM J. Sci. Stat. Comput.*, 7:856–869, 1986.

S. Sauter and C. Schwab. *Boundary Element Methods*, volume 39 of *Springer Series in Computational Mathematics*. Springer, 2011.

B. Simon. The theory of resonances for dilation analytic potentials and the foundations of time dependent perturbation theory. *Ann. Math.*, 97:247–274, 1973.

V. Simoncini and D. Szyld. Recent computational developments in Krylov subspace methods for linear systems. *Numerical Linear Algebra with Applications*, 14(1):1–59, 2007.

W. Śmigaj, S. Arridge, T. Betcke, J. Phillips, and M. Schweiger. Solving boundary integral problems with BEM++. *ACM Trans. Math. Software*, 2015.

P. Sonneveld. CGS, a fast Lanczos-type solver for nonsymmetric linear systems. *SIAM J. Sci. Stat. Comput.*, 10:36–52, 1989.

E. Spence. Boundary acoustic layer potentials via oscillatory integral techniques. *BIT*, 55(1):279–318, 2015.

P. Stefanov. Quasimodes and resonances: sharp lower bounds. *Duke Math. J.*, 99(1):1–178, 1999.

P. Stefanov and G. Vodev. Distribution of resonances for the neumann problem in linear elasticity outside a strictly convex body. *Duke Math. J.*, 78(3):677–714, 1995.

P. Stefanov and G. Vodev. Neumann resonances in linear elasticity for an arbitrary body. *Comm. Math. Phys.*, 176:645–659, 1996.

O. Steinbach. *Numerical Approximation Methods for Elliptic Boundary Value Problems*. Springer, 2008.

S.-H. Tang and M. Zworski. From quasimodes to resonances. *Math. Res. Lett.*, 5(3):261–272, 1998.

M. Taylor. *Partial differential equations II, qualitative studies of linear equations*. Springer-Verlag, 1996.

F. Tisseur and N. Higham. Structured pseudospectra for polynomial eigenvalue problems, with applications. *SIAM J. Numer. Anal.*, 23(1):187–208, 2001.

K.-C. Toh and L. N. Trefethen. Calculation of pseudospectra by the Arnoldi iteration. *SIAM J. Sci. Comput.*, 17:1–15, 1996.

L-N. Trefethen. Pseudospectra of linear operators. *SIAM Review*, 39(3):383–406, September 1997.

L. N. Trefethen and D. Bau. *Numerical Linear Algebra*. SIAM, 1997.

L. N. Trefethen and M. Embree. *Spectra and pseudospectra. The behavior of nonnormal matrices and operators*. Princeton University Press, 2005.

E. Tyrtyshnikov. Mosaic-skeleton approximations. *Calcolo*, 33:47–57, 1998.

H. A. Van der Vorst. Bi-CGSTAB: A fast and smoothly converging variant of Bi-CG for the solution of nonsymmetric linear systems. *SIAM J. Sci. Stat. Comput.*, 13(2):631–644, 1992.

J. L. M. van Dorsselaer. Pseudospectra for matrix pencils and stability of equilibria. *BIT*, 37(4):833–845, December 1997.

J. L. M. van Dorsselaer. Several concepts to investigate stronly nonnormal eigenvalue problems. *SIAM J. Sci. Comput.*, 24(3):1031–1053, 2003.

T. Wagenknecht, W. Michiels, and K. Green. Structured pseudospectra for nonlinear eigenvalue problems. *J. Comput. Appl. Math.*, 211:245–259, 2008.

D. Weinstein and S. Bhave. Acoustic resonance in an independent-gate FinFET. *Hilton Head*, pages 459–462, 2010.

S. Ziada. Vorticity shedding and acoustic resonance in tube bundles. *J. Braz. Soc. Mech. Sci. and Eng.*, 28(2):186–189, 2006.